This is to certify that the
dissertation entitled

A CRYSTALLOGRAPHIC INVESTIGATION OF LIGAND BINDING TO OVINE PROSTAGLANDIN ENDOPEROXIDE H SYNTHASE-1

presented by

Christine A. Harman

has been accepted towards fulfillment
of the requirements for the

Doctoral degree in Biochemistry and Molecular Biology

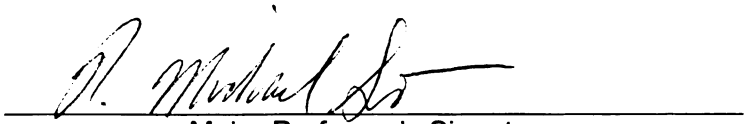

Major Professor's Signature

12/13/05

Date

MSU is an Affirmative Action/Equal Opportunity Institution

A CRYSTALLOGRAPHIC INVESTIGATION OF LIGAND BINDING TO OVINE PROSTAGLANDIN ENDOPEROXIDE H SYNTHASE-1

By

Christine A. Harman

A DISSERTATION

Submitted to
Michigan State University
in partial fulfillment of the requirements
for the degree of

DOCTOR OF PHILOSOPHY

Department of Biochemistry and Molecular Biology

2005

ABSTRACT

A CRYSTALLOGRAPHIC INVESTIGATION OF LIGAND BINDING TO OVINE PROSTAGLANDIN ENDOPEROXIDE H SYNTHASE-1

By

Christine A. Harman

Prostaglandin Endoperoxide H Synthase-1 (PGHS-1) and -2 (PGHS-2) also known as Cyclooxygenase-1 (COX-1) and -2 (COX-2) catalyze the committed step in the formation of prostaglandins and thromboxanes, in which two molecules of oxygen are incorporated into AA forming PGH_2. Past kinetic studies have indicated that arachidonic acid (AA) can exist in at least three catalytically competent conformations within the COX active site each of which lead to either PGG_2, the productive product, 11-HETE and 15-HETE (abortive products). Two single mutations V349A and W387F were found to create almost equal amounts of PGG_2 and 11-HETE. Results discussed in Chapter II show that a V349A/W387F mutant of ovine PGHS-1 produced predominantly 11-HETE. The crystal structure of AA bound to V349A/W387F oPGHS-1 was determined to 3.1 Å. The conformation of AA in this double mutant was observed to be distinctively different than the conformation of AA observed in the native enzyme, providing structural evidence that the conformation of AA occurring at the moment of hydrogen abstraction pre-determines the product of the COX reaction. Further, the roles of residues V349 and W387 were found to be crucial in the properly positioning atoms C9 and C11 of AA for endoperoxide formation.

We also investigated the binding of Mead acid, a non-essential fatty acid, to PGHS-1. Although Mead acid was found to be a poor substrate for PGHS-1, products are formed and resemble abortive COX products indicating that Mead acid may undergo

a similar mechanism in which the C13 pro*S* hydrogen is removed, the rate limiting step. A crystal structure of Mead acid bound to PGHS-1 was determined to 2.85 Å; but only weak density was observed for Mead acid in the COX active site. Simulated annealing experiments were used to observe a series of Mead acid conformers. Two binding populations, the "catalytically possible" and inhibitory conformations, were observed. Six of ten Mead acid conformers were observed in "catalytically possible" conformations suggesting that Mead acid is capable of binding in a conformation that would support catalysis. However, the inhibitory conformers demonstrated that Mead acid binds in manner that would not support catalysis suggesting that the missing ω6 double bond in Mead acid is important for positioning the pro*S* hydrogen of C13 for potential abstraction. The ability of Mead acid to act as an inhibitor for PGHS-1 was tested and the *Ki* of Mead acid was determined to be ~62 μM indicating that Mead acid is not an efficient inhibitor of PGHS. The combination of these studies demonstrate that the ω6 double bond plays an important role in facilitating binding and positioning of 20-carbon fatty acids.

PGHS-1 is inhibited ~ten times more efficiently by the (*S*)-enantiomers of the α-substituted indomethacin ethanolamides. Crystal structures of an enantiomeric pair of these inhibitors were determined to 2.7-2.85 Å, in an effort to understand the structural basis of this enantiomeric selectivity of PGHS-1. Comparisons of the structures reveal there are two different binding modes of these inhibitors, in which the (*S*)-enantiomer is able to utilize the side pocket region PGHS-1 while the *R*-enantiomer cannot because of the R-stereochemistry. In addition, the binding of the *R*-enantiomer appears to confer local strain to the protein suggesting this enantiomer may have a faster dissociation rate.

A dedication in memory of my beautiful mother, Felipa Ann (Naya) Zucker

ACKNOWLEGEMENTS

First round of thanks goes to my advisors Dr. Bill Smith and Dr. Michael Garavito in which their guidance has been invaluable. I am so grateful to Dr. Smith for his support and encouragement as well as for sharing his vast knowledge of eicosanoids and fatty acid metabolism, and I admire him greatly for his excellent editing ability. Dr. Garavito was a wonderful mentor and I have learned so much from our conversations about crystallography and science. I cannot thank him enough for what he has done for me over the years, and I feel extremely fortunate to have worked for such a brilliant and creative individual.

Much thanks goes out to Mike Malkowski and Anne Mulichak, past members of the Garavito lab, for taking me on my first synchrotron trip and for giving me my first lesson on crystallography. I will never forget them. I would also like to thank other members of the Garavito lab including Amy, Mike D, Nicole and Rachel for their friendship, laughs and for making my experience a wonderful one. Members of the Smith lab whom I would like to thank include Jill, Cindy, Jiayan, and Yeon-Joo for their friendship and advice over the years. I also owe thanks to Dr. Dave DeWitt for keeping it real (and for his stock pile of gummy bears) as well as past and present members of his lab particularly Jeff Leipprandt for the many, many bioreactors he grew up and harvested for me.

Of course, I would like to thank my family for their love and faith in me. And lastly, I would like to thank my loving and supportive husband Ben and our sweet daughter Mia both of whom I love with all my heart and could not have done this without them.

TABLE OF CONTENTS

LIST OF TABLES

LIST OF FIGURES

LIST OF ABBREVIATIONS

PGHS	prostaglandin endoperoxide H synthase
oPGHS-1	ovine prostaglandin endoperoxide H synthase-1
hPGHS-2	human prostaglandin endoperoxide H synthase-2
COX	cyclooxygenase
POX	peroxidase
AA	arachidonic acid
$cPLA_2$	cytosolic 85kDa phospholipase A_2
$sPLA_2$	secretory phospholipase A_2
ω3 or (n-3)	designation in which double bond present three carbons in from acyl end of fatty acid
ω6 or (n-6)	designation in which double bond present six carbons in from acyl end of fatty acid
20:4, ω6	arachidonic acid
18:2, ω6	linolenic acid
20:5, ω6	eicosapentonic acid
20:3, ω6	dihomo-γ-linolenic acid
20:3, ω9	mead acid
11-HETE	11-hydroxy-5,8,12.14-eicosatetraenoic acid
11-HPETE	11-hydroperoxy-5,8,12,14-eicosatetraenoic acid
15-HETE	15-hydroxy-5,8,11,13-eicosatetraenoic acid
15-HPETE	15-hydroperoxy-5,8,11,13-eicosatetraenoic acid
12-HHTre	12-hydroxy-5,8,10-hepadecatrienoic acid
9-HODE	9-hydroxy-10-,12-octadecadienoic acid
13-HODE	13-hydroxy-9,11-octadecadienoic acid
EGF	epidermal growth factor
MBD	membrane binding domain
NSAID	non-steroidal anti-inflammatory
β-OG	n-ocyl-β-D-glucopyranoside
$C_{10}E_6$	polyoxyethylene(6)decyl ether
Compound 8	indomethacin-(*R*)-α-ethyl-ethanolamide
Compound 9	indomethacin-(*S*)-α-ethyl-ethanolamide
TLC	thin layer chromatography
PG	prostaglandin
Tx	thromboxane
V_{max}	maximum velocity of a reaction
K_m	Michaelis-Menton constant
K_i	dissociation constant for enzymes-inhibitor complex
IC_{50}	inhibitor concentration for 50% inhibition
EDTA	ethylenediamine tetraacetic acid
PBS	phosphate buffered saline

CHAPTER I

LITERATURE REVIEW

Introduction

Prostaglandin endoperoxide H synthases-1 and -2 (PGHS-1 and -2) also known as cyclooxygenases (COXs) are bifunctional, heme-containing and membrane-bound enzymes that catalyze the conversion of arachidonic acid (AA) to PGH_2, the committed step of prostanoid biosynthesis [1-3]. Prostanoids, which include prostaglandins and thromboxanes belong to a large class of bioactive, oxygenated C_{18}-C_{22} compounds called eicosanoids. Eicosanoids comprising the prostanoids, the leukotrienes, and the epoxy eicosatrienoic acids, are formed from ω3(n-3) and ω6(n-6) fatty acids through three major pathways in which each path is named after the enzyme that catalyzes the committed step of that pathway (Figure 1) [4]. In mammals, the predominant fatty acid precursor for the synthesis of prostanoids is AA, a 20 carbon ω-6 fatty acid, and thus eicosanoids derived from AA are formed through the arachidonic cascade .

Prostaglandins, which are formed via the cyclooxygenase (PGHS) pathway (Figure 1), are local acting, hormones that regulate a broad range of normal physiological functions including blood pressure and body temperature regulation, renal retention, smooth muscle contraction, vascular homeostasis, platelet aggregation and inflammation [5-7]. In addition to these normal physiological functions, prostaglandins have also been associated with various inflammatory and blood-clotting diseases [8], and other pathologies such as colon and ovarian cancer [9, 10] and Alzheimer's disease [8].

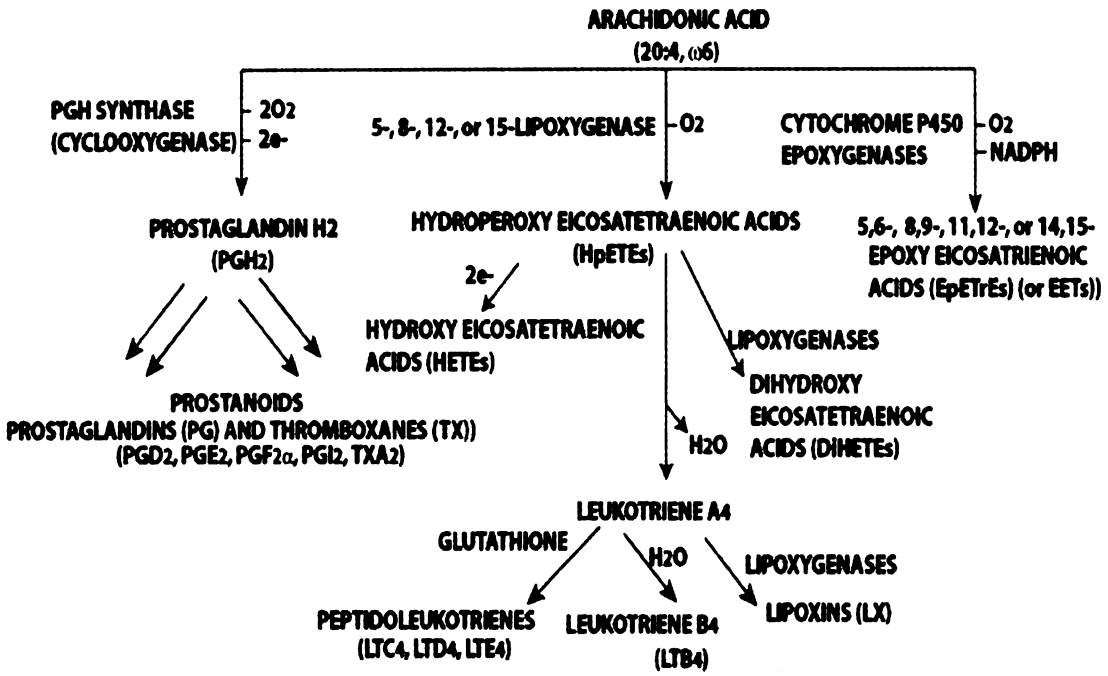

Figure 1 The arachidonic acid cascade. Arachidonic acid is metabolized by three separate enzyme systems, which include the cyclooxygenase, lipoxygenase, and P450 epoxygenase pathways.

As prostaglandins are generally unstable, they are not stored by cells, but rather are synthesized in response to an extracellular stimulus. For example, when a hormone interacts with its receptor, a series of events is activated that in turn activates one or more phosholipases A_2, that then cleave AA from the phospholipids of the cellular membranes. Free AA is then acted upon by PGHS producing, PGH_2, the common precursor of prostaglandins and thromboxanes.

In the early 1990's, a second isoform of PGHS was discovered [11]. Both isoforms, termed PGHS-1 and PGHS-2 catalyze the two reactions involved in converting

AA to PGH_2. These activities include a cyclooxyenase activity, which catalysis a bis-oxygenation of AA to form the intermediate hydroxperoxide, PGG_2 and a peroxidase activity catalyzing a two-electron reduction of PGG_2 to form the final product of the enzyme, PGH_2 (Figure 2). These reactions occur at two distinct sites in the enzymes; however, they are functional coupled through a requirement of heme for both activities [12, 13]. Through the action of specific terminal synthases, PGH_2 is converted into an array of biologically diverse lipids mediators, the series-2 prostanoids that include (PG) E_2, $F_2\alpha$, D_2, I_2, and thromboxane $(Tx)A_2$.

Despite numerous similarities in structure and function, PGHS-1 and PGHS-2 differ in their patterns of expression, regulation, substrate utilization, and inhibition. PGHS-1 is constitutively expressed in most tissues, and its activity is mainly associated with producing prostaglandins needed for maintaining homeostasis or "housekeeping" functions such as renal water retention, blood pressure regulation, gastric intestinal motility. Expression of PGHS-2 is rapidly induced in response to mitogens, cytokines and growth factors [14]. Other notable disparities between the isoforms include variations in glycosylation, an 18-amino acid cassette present in PGHS-2 but not PGHS-1, and other subtle structural differences within the COX active site that contribute to differences in substrate utilization and inhibition between the isoforms.

The PGHS enzymes are the target of non-steroidal anti-inflammatory drugs (NSAIDs), which include compounds like aspirin, ibuprofen and naproxen. All NSAIDs, classified by their ability to reduce pain, fever and inflammation are known to inhibit the cyclooxygenase activity by interacting with the cyclooxgenase site thereby preventing the

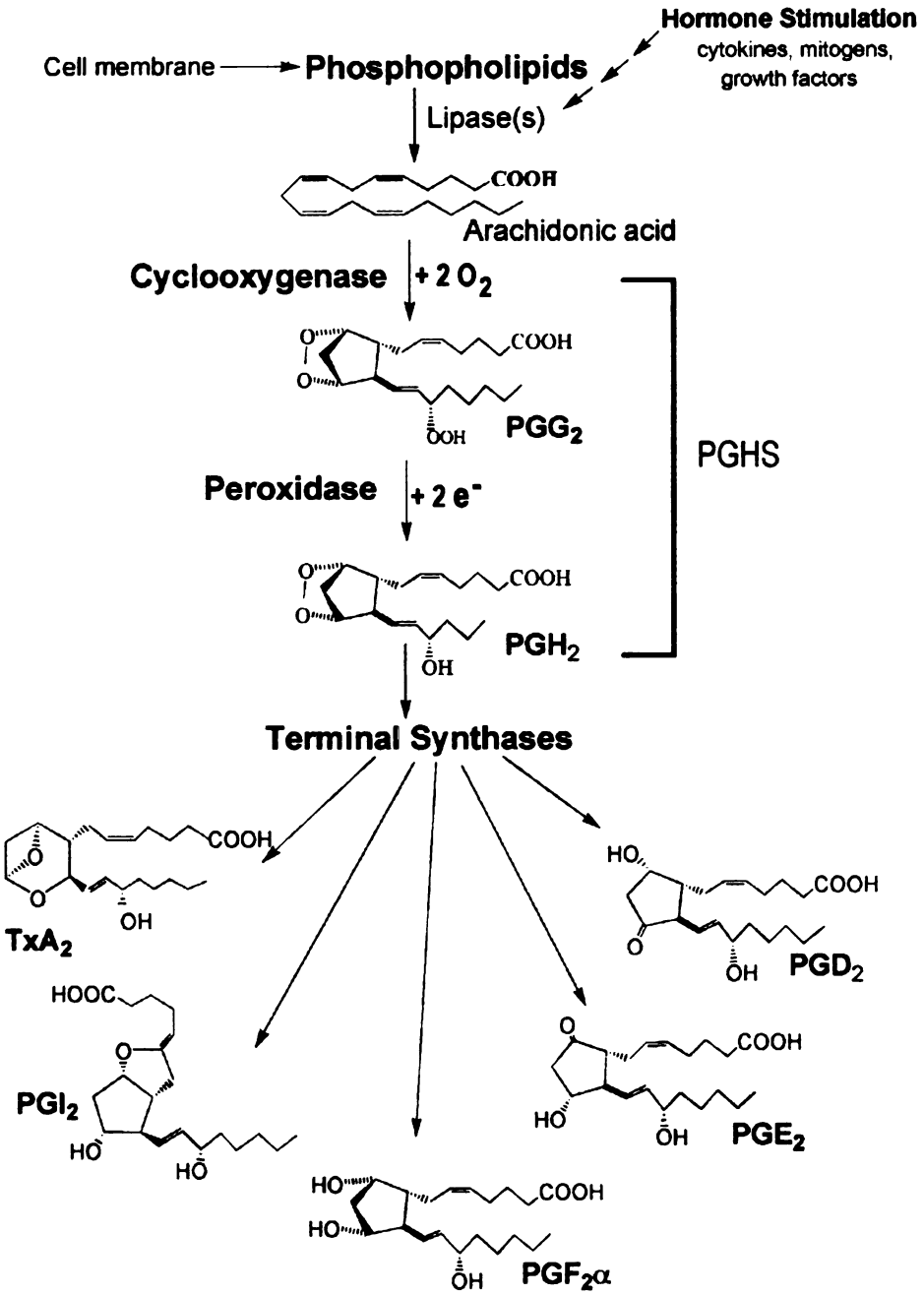

Figure 2 Biosynthetic pathway of prostanoids derived from arachidonic acid catalyzed by PGHS.

binding of AA. However, inhibition by aspirin occurs through a different mechanism: the COX active site in PGHS-1 and PGHS-2 is chemically modified whereupon the hydroxyl group of Ser530 is acetylated. The effect of aspirin acetylation differs between the enzymes, bringing attention to subtle structural differences demonstrating that PGHS-2 has a slightly larger active site. Crystal structures of both PGHS-1 and PGHS-2 in complexes with various inhibitors and ligands have been determined and have further contributed to our understanding of inhibition of the PGHS enzymes. The understanding of the pharmacological differences between the isoforms is what led to the development of the PGHS-2 selective inhibitors.

Prostaglandin Biosynthesis

The biosynthesis of prostaglandins and thromboxanes occurs through a three step process in which AA is released from cellular membranes, converted to PGH_2 by the PGHS-1 and -2 and then acted upon by specific synthases that convert PGH_2 into an array of prostaglandins or thromboxanes [3, 4]. AA is the major precursor for prostaglandins and thromboxanes and is stored at the *sn*2 position of the glycerophospholipids of the cellular membranes.

AA is liberated from the membrane phospholipids by the action of phospholipases. There are several groups of phospholipases that participate in releasing AA from the cellular membranes; these include the Ca^{+2}-independent phospholipase ($iPLA_2$), Ca^{+2}-dependent cytosolic phospholipase ($cPLA_2$) and the inducible, secretory phospholipases ($sPLA_2$); however, $cPLA_2$ and the secretory PLA_2s are regarded as the principal phopholipases involved in a coordinated action to release AA for utilization by

the PGHS enzymes [15-17]. The Ca^{+2}-independent PLA_2 is mainly involved in cell membrane remodeling [16].

The mobilization of AA destined for PG synthesis is initiated when various hormones interact with their receptors (e.g. bradykinin, angiotensin II, thrombin). This triggers an increase in intracellular Ca^{+2} that activates $cPLA_2$, a Ca^{+2} dependent phospholipase. The activation of $cPLA_2$ by Ca^{+2} leads to the translocation of $cPLA_2$ to the endoplasmic reticulcum (ER) and nuclear envelope (NE) where it cleaves AA from the *sn*2 position of the phospholipids on the cytosolic surface of the membrane. $cPLA_2$ is the dominant phospholipase involved in liberating AA from the cellular membranes; however, when the stimulus is enduring and intense the inducible, secreted $sPLA_2$ begins to contribute providing an additional release of AA for utilization by the PGHS enzymes, particularly for utilization by PGHS-2, the inducible form [16]. Thus the combined action of these phospholipases is believed to be one mechanism for providing AA for immediate and prolonged stimulation for utilization by either constitutive PGHS-1 via $cPLA_2$ releasing AA during immediate stimulation or inducible PGHS-2 via $sPLA_2$ releasing additional AA after prolonged stimulation [4, 16, 17]. The $cPLA_2$ phopholipases are specific in cleaving AA from the membranes; however, the secretory forms of PLA_2 lack any specificity for either the phospholipid head group or the acyl group at the *sn*2 position [4]; therefore, under some conditions during a stimulus it is possible that PGHS is exposed to mixed pool of fatty acids other than AA. This mixed fatty acid pool effect the type of prostanoids produced from these substrates by the PGHS enzymes [4].

Once AA is released from the cytosolic surface of the ER and NE via $cPLA_2$, it traverses the membrane becoming available as a substrate for the PGHS enzymes converting AA to PGH_2. The product PGH_2 is further converted to a specific prostanoid depending on the presence of specific terminal synthases within the cell. The prostanoids are secreted from the cells via some carrier-mediated transporter [18, 19] [20] where they interact in an autocrine or paracrine fashion with specific prostaglandin receptors that are in turn linked to heterotrimeric G-protein coupled receptors [21, 22]. The binding of prostanoids to their specific G-protein linked receptor, in turn, activates a cascade of intracellular signaling events characterized by increasing cellular levels of cAMP, Ca^{+2}, and phosphatidyl inositol [23, 24].

The Two Activities of PGHS

The cyclooxygenase of PGHS binds AA and incorporates two molecules of oxygen in a regio- and stereo-specific fashion forming the intermediate, PGG_2, while the peroxidase catalyses a two-electron reduction of PGG_2 to form PGH_2, the final product [25, 26]. Although the two reactions occur at physically separate sites, the two activities are functionally coupled. A model for the functional link between the COX and POX activity initially proposed by Ruf and coworkers (Figure 3) involves a branched chain mechanistic model in which the heme within the peroxidase site must first undergo a two-electron oxidation by a hydroperoxide (a single POX turnover) in order to initiate catalysis at the COX site [12]. During the first POX turnover an oxyferryl heme/protoporphyrin radical cation species (Compound I) is formed, which creates a

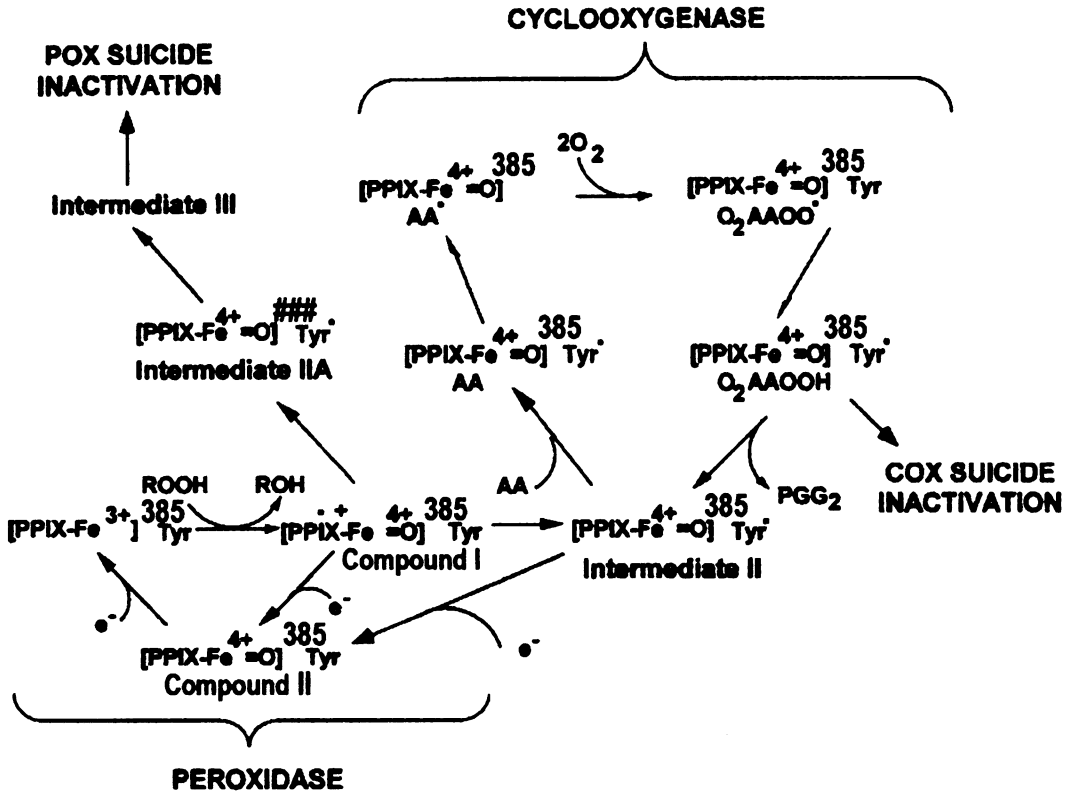

Figure 3 Interdependence of the peroxidase and cyclooxygenase activities. Ruf model [12] of the peroxidase-dependent activation of the cyclooxygenase activity of PGH synthase via formation of an intermediate tyrosyl radical (Tyr385). Fe^{3+} PPIX, ferric iron protoporphyrin IX (heme); ROOH, alkyl hydroperoxide; ROH, alcohol; AA, arachidonic acid; Fe^{4+}=O PPIX, oxyferryl heme. Compound I, an oxyferryl group (Fe(IV)=O) plus a protoporphyrin IX radical cation; Intermediate II, an oxyferryl plus a neutral protoporhyrin IX plus a Tyr385 tyrosyl radical; Compound II, an oxyferryl group plus a neutral protoporphyrin IX.

tyrosyl radical on residue Y385 (Intermediate II) located within the COX site of PGHS [13]. The Y385 tyrosyl radical is required to initiate the COX reaction. Thus, once a tyrosyl radical is formed and AA is bound within COX site, the COX reaction begins [27, 28].

The COX reaction begins by abstraction of the 13 pro*S* hydrogen atom of AA by Tyr385 radical producing an arachidonyl radical, the rate-limiting step [25, 29] (Figure 4). The radical migrates to position C11 of AA and is subsequently attacked by O_2 forming an 11R-peroxyl radical. The peroxyl radical on C11 attacks the double bond at C9 forming an endoperoxide between C9 and C11. Formation of the endoperoxide and radical migration to C8 leads to cyclopentane ring formation between C8 and C12, requiring a reconfiguration of the substrate. The radical migrates to C15 and leads to an attack by a second molecule of oxygen at C15 forming a C15 peroxyl radical. The C15 peroxyl radical then abstracts the hydrogen from Y385 to yield PGG_2 while simultaneously regenerating the tyrosyl radical for another cycle of COX catalysis. PGG_2 diffuses from the COX site and migrates to the peroxidase site and undergoes a two electron reduction yielding PGH_2, which is then utilized by downstream synthases to produce a variety of prostanoids including PGE_2, PGI_2, PGD_2, and $PGF2_{\alpha}$ and thromboxanes each of which are responsible for a variety of biological functions.

Suicide Inactivation

An interesting and not very well understood characteristic of PGHS catalysis is that of suicide inactivation. Each PGHS monomer exhibits a limited number of turnovers ranging from 10 to 1300 depending on the conditions before COX activity disappears [30]. The observed loss of activity is not due to total consumption of substrate or product inhibition, but most likely involves formation of an active radical species that irreversibly inactivates the enzyme [31, 32]. Both the COX and POX activities of PGHS were found to undergo suicide inactivation; however, the relationship between POX inactivation and COX inactivation remains unclear [33, 34]. Kinetic and spectral studies have provided

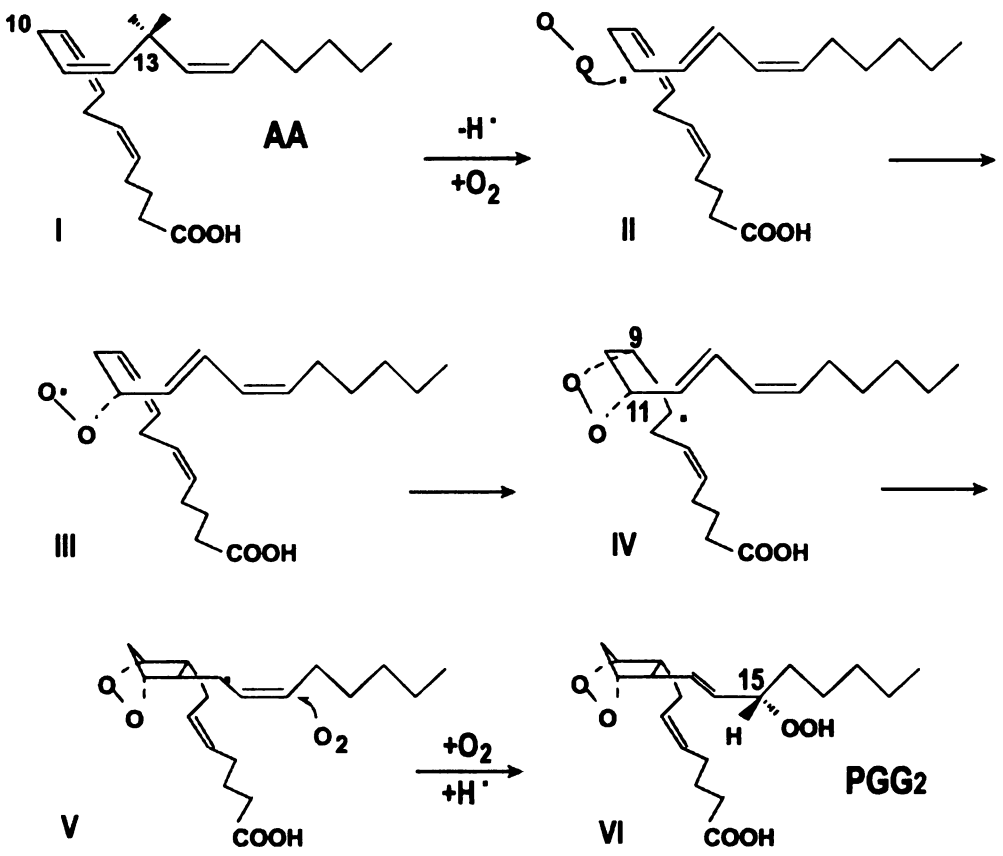

Figure 4 The mechanism for conversion of arachidonic acid to PGG_2 by the cyclooxygenase activity of PGHS. Arachidonic acid (AA) is converted to PGG_2 through sequence of steps I-VI by the cyclooxygenase activity of PGHS. The C15 peroxyl group (-OOH) of PGG_2 (VI) is reduced to –OH by the activity of the peroxidase of PGHS to form the final product PGH_2 [25].

evidence that POX inactivation originates from Intermediate II characterized as Fe(IV)=O and a protein tyrosyl radical, which is the intermediate that links POX activity to COX activity (Figure 3) [30]. Another spectral intermediate termed Intermediate III was isolated during the POX self-inactivation process and appeared to be produced from Intermediate II [30]. Intermediate III is believed to be the species, which leads to

inactivation; however, the chemical mechanism remains a mystery, but is believed to involve a radical mediated process that possibly cross-links the enzyme and eliminates activity.

Other studies have shown that COX and POX inactivation are distinct events and that each process originates from different intermediates [35]. A Y385F mutant, which cannot form Intermediate II is able to undergo POX inactivation at the same rate as native; therefore, residue Y385 is not required for POX inactivation; however, is presumed to be required for COX inactivation. Studies with the Y385F mutant suggest that COX inactivation results from a different intermediate (Figure 3) [35]. This intermediate is suggested to be like Intermediate III containing an oxylferryl heme and a protein tyrosyl radical; however, the radical would be centered on a tyrosine other than Y385 [35]. Although there are still many unanswered questions into the nature of the intermediates responsible for inactivation of POX and COX, nonetheless, these radical intermediates lead to irreversible loss of activity of the enzyme.

Biochemical Comparisons of PGHS-1 and PGHS-2

The primary sequence of PGHS-1 and PGHS-2 are very similar having 60-65% sequence identity between them, and between the individual isoforms of different species, which have approximately 80-85% identity [36]. Both PGHS-1 and PGHS-2 have a signal sequence at the N-terminus, which is removed during processing to mature enzyme, thus PGHS-1 and PGHS-2 when in mature form contain 576 and 587 amino acids, respectively [36].

Although, PGHS-1 and PGHS-2 are similar in primary structure, there are several major differences within several regions of the primary sequence (Figure 5). At the N-terminus of PGHS-2, the signal peptide sequence is truncated in comparison to PGHS-1, thus to account for this 15 is added to the numbering of PGHS-2 for comparing to equivalent residues within the isoforms since numbering starts at the N-terminus of nascent protein. Additionally, there is an 18-amino acid insertion at the C-terminus of PGHS-2, which is not present in PGHS-1. The function of this 18 residue insertion is not yet known; however, it had been speculated that is might be involved in protein turnover and protein-protein interactions [36]. Significant sequence differences exist within the membrane-binding region of PGHS-1 and PGHS-2, which only share 38% identity between the isoforms. However, in regions that involve catalysis there is significant conservation of residues with a few exceptions being within the COX active site. Lastly, PGHS-1 and PGHS-2 are differentially glycosylated in that PGHS-1 is uniformly N-glycoylated at three sites that include Asn68, Asn144, and Asn410. These sites are also N-glycosylated in PGHS-2; however, there is a forth site that is variably glycoslylated at Asn580 [37]. The variable glycosylation of PGHS-2 is readily observed as a doublet on SDS-PAGE, representing multiple molecular weight species whereas PGHS-1 appears as a singlet [37, 38]. For expression of active protein both PGHS-1 and PGHS-2 require glycosylation only at site Asn410. Since activity of purified PGHS-1 and PGHS-2 is retained when sugars are removed, glycosylation at Asn410 appears to be mainly involved in proper folding of the protein [37]. Glycosylation at the variable fourth site in PGHS-2 does not seem be as important in protein folding since an Asn580 mutant of PGHS-2 yield fully active protein [37]. The role of the fourth glycosylation site is

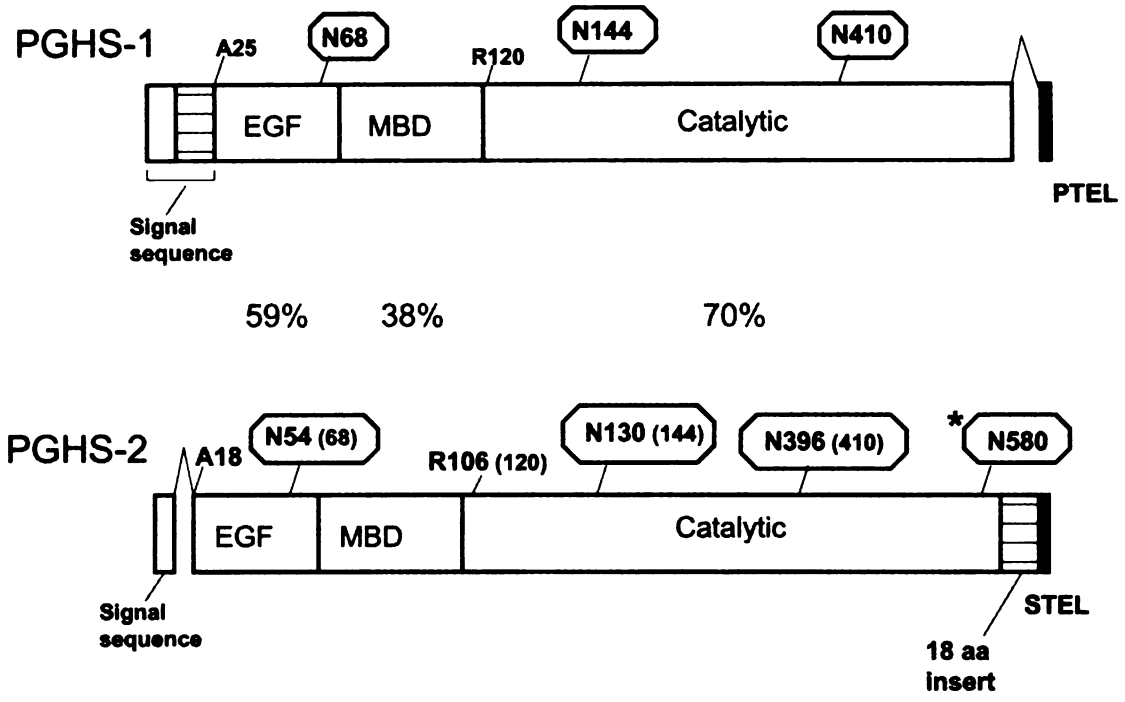

Figure 5 Comparison of the PGHS-1 and PGHS-2 proteins. The three structural domains of the PGHS enzymes are shown as EGF (epidermal growth factor domain), MBD (membrane binding domain), and the Catalytic domain, which contains the two active sites of PGHS. The percentages represent the similarity within the individual domains between the isoforms. In addition, the lined boxes represent insertions within PGHS-1 and PGHS-2 that are not present in the other isozyme. The glycosylation sites within each of the proteins are represented by circled residue numbers. PGHS-1 numbering for the glycosylated residues in PGHS-2 are shown in ()'s.

not known; however, it might play a role in PGHS-2 expression in the baculovirus system in which PGHS-2 is expressed more successfully as compared to PGHS-1.

Other differences between the isoforms include some significant sequence differences within the membrane binding domain and some minor differences within the

COX active site. Despite these differences, crystal structures of each isoform show that the three-dimensional structure of the two isoforms is nearly superimposable [36, 39-42].

There are also similarities and differences between the isoforms with respect to cellular localization and expression patterns. Both enzymes have been localized to the lumenal surface of the endoplasmic reticulum and the inner and outer membranes of the nuclear envelope with PGHS-2 being found to be more highly concentrated in the nuclear envelope as compared to PGHS-1 [43]. Although the isoforms are generally localized in similar membranes, they differ substantially in their patterns of expression. PGHS-1 is expressed constitutively and the prostaglandins produced via PGHS-1 are mostly involved in housekeeping functions such as blood pressure regulation, and gastric intestinal motility and protection. PGHS-2, however, is predominantly expressed by induction via growth factors, cytokines and mitogens; however, with some exceptions being in the brain and kidney where PGHS-2 has been found to be constitutively expressed. The prostaglandins produced via PGHS-2 are known to be involved in inflammation, pain and fever, in addition to being implicated in pathological conditions that include rheumatoid arthritis, colon cancer [8, 9] and neurological disorders such Alzheimer's disease [44], thus PGHS-2 has been the isoform of much focus as a drug target because of its association with these various pathologies. Interestingly, recent studies have found that PGHS-1 rather than PGHS-2 appears to be a major regulator of PGE_2 production in ovarian cancer cells lines [10], demonstrating that PGHS-1 may also play a role in various cancers. PGHS-1, however, is more commonly associated with blood clotting diseases, and has been the primary target of aspirin in providing anti-thrombogenic and cardioprotective therapy [45, 46].

Despite significant differences in patterns of expression and physiological and pathological roles, on a basic functional level the two isoforms are similar. Both bind one molecule of iron (FeIII) heme (protoporphyrin IX) per monomer, which is required for catalysis. Additionally, both utilize the same substrate with similar affinity (K_m ~5-10 μM), and carry out the same catalytic mechanism to produce the same product [3]. There are some exceptions that involve substrate affinity and rate of product formation under conditions in which AA and lipid peroxide concentrations are low. *In vitro* studies have shown that at concentrations of AA below 2 μM, PGHS-1 appears to have a higher apparent K_m than that of PGHS-2 [15, 17, 47]. Other studies have demonstrated that activation of COX activity in PGHS-1 requires ten times the concentration of lipid peroxide than that of PGHS-2 at conditions of low AA concentrations [48]. Therefore, under conditions of low peroxide and AA concentration activity of PGHS-2 would be favored over PGHS-1 [17] providing one mechanism in which PGHS-1 and PGHS-2 can independently function in the same cell.

Structure of PGHS-1 and PGHS-2

The first crystal structure of ovine PGHS-1 complexed with the NSAID flurbiprofen was published in 1994 by Picot et al [39], and since then has been followed by many other structure complexes with various inhibitors [40, 41] and AA [42], and other fatty acid substrates [49, 50]. PGHS-1 and PGHS-2 exist structurally and function as homodimers. All published crystal structures show that the PGHS monomer consists of three structural domains: the N-terminal EGF domain, a membrane binding domain

(MBD) and a large C-terminal globular catalytic domain housing the cyclooxygenase site and the peroxidase site where heme binds (Figure 6).

The EGF domain consisting of the first 40 amino acids at the N-terminus is mainly involved in dimerization of PGHS in that portions of this domain between two monomers create a substantial region of the subunit interface of the PGHS homodimer. However, being a common domain in several families of membrane proteins, the EGF domain of PGHS has been speculated to perhaps also serve a role in membrane integration of the membrane binding domain of PGHS [36]. The membrane binding domain of PGHS, continuing from the EGF domain, consists of approximately 48 amino acids that fold into four amphipathic α helices. The helices lie in slightly angled orientations relative to each other with one helix protruding up into the catalytic domain creating a portion of the entrance to the COX active site. The outside portions of the helices are composed of hydrophobic residues providing a hydrophobic surface that can interact with the first leaflet of the membrane bilayer. The monotopic nature of PGHS has functional significance for substrate binding in that when substrate is released from the membrane phospholipids it transverses from the hydrophobic compartment of the bilayer through a direct route to the COX site provided by the membrane binding domain which anchors PGHS in the membrane.

Just above the membrane binding domain sits the large catalytic domain of PGHS, which contains the two active sites (Figure 6). The cylcooxygenase site, where AA binds, exists as a long, hydrophobic channel originating from the membrane binding domain and tunnels up into the core of the catalytic domain. The crystal structure of

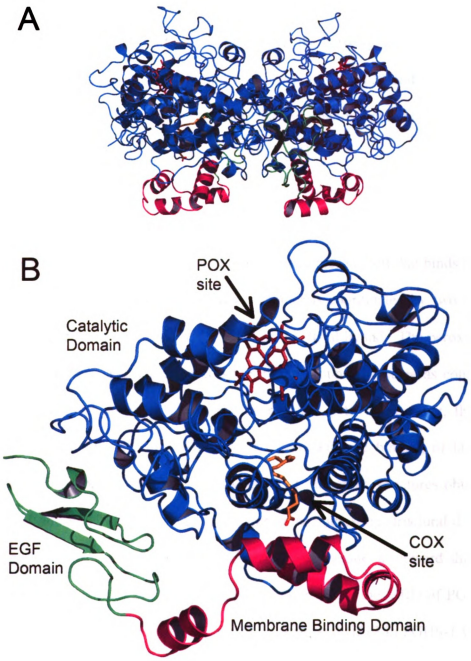

Figure 6 Crystal Structure of Ovine PGHS-1. Panel A shows PGHS as a dimer. Panel B shows the monomer structure, which is composed of three structural domains. The N-terminal EGF (epidermal growth factor) domain, and the membrane binding domain are shown in *green* and *magenta*. The large catalytic domain (*blue*) posses the two active sites. The COX site is shown with AA bound while the Co^{3+}-proptoporphyrin is bound within the POX site where heme would normally bind. Images in this dissertation are presented in color.

Co^{+3}–protoporphyrin IX oPGHS-1/AA complex shows that AA binds within the COX active site in an "L-shaped" configuration in which the carboxylate is anchored at the mouth of the site through ionic interactions with residues Arg120 and Y355 while the acyl portion of AA weaves up inside the channel making numerous hydrophobic interactions with various residues along the channel [42].

At the top of the COX channel, the catalytic residue Tyr385 resides and is ~12.5 Å from the heme bound within the peroxidase site (Figure 7). The peroxidase site, which sits just above the cyclooxygenase channel is a solvent exposed cleft that binds one heme per monomer of PGHS. The heme in each monomer is coordinated by two histidines with His388 as the proximal ligand and His207 as the distal ligand. The peroxidase site of PGHS is more open and solvent accessible in and around the heme as compared to other peroxidases such as mammalian myeloperoxidase (MPO); however, this is not unusual considering this site in PGHS must accommodate the binding of large alkyl peroxide substrates like PGG_2 [36]. Comparisons of numerous structures obtained for both PGHS-1 and PGHS-2 have revealed the impact of interesting structural differences between the isoforms. Some major structural differences include an upward shift of one end of helix D of the MBD providing a larger opening within the MBD of PGHS-2. In addition, a substitution of three amino acids (I523, I434, and H513 in PGHS-1 vs. V523, V434, and R513 in PGHS-2) located within and near the active site of PGHS bestows PGHS-2 with a 20% larger active site. This is the major structural difference that has been exploited in the development of PGHS-2 selective inhibitors such as Vioxx and Celebrex.

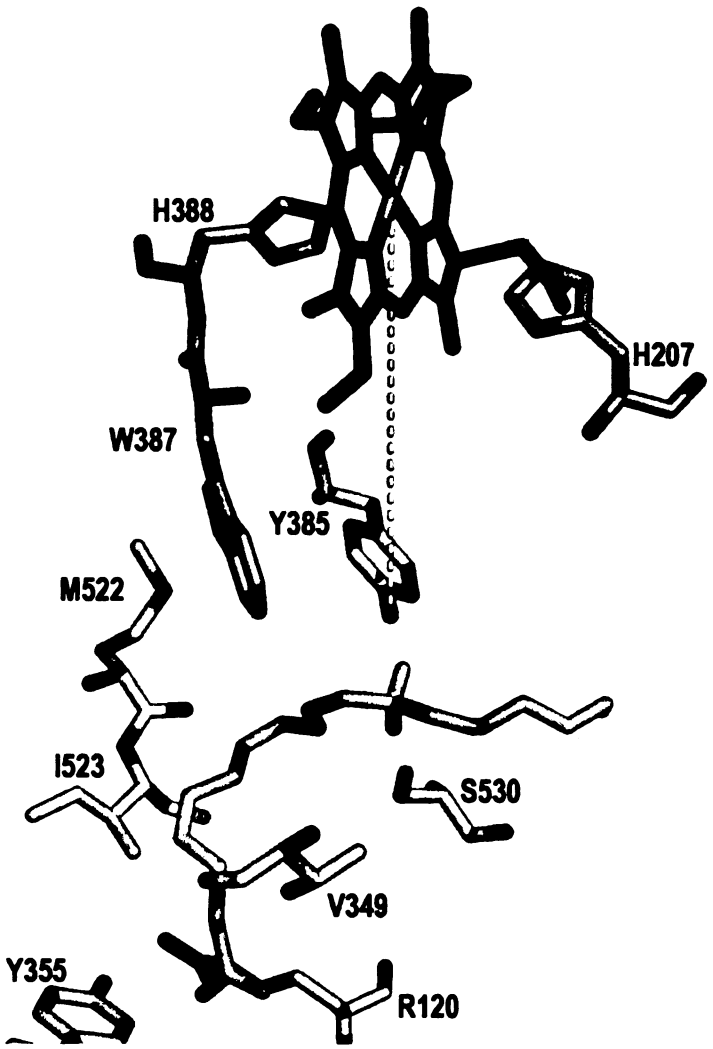

Figure 7 Orientation of POX site relative to the COX active site of PGHS. Co^{3+}-protoporhyrin (shown with protoporhyrin *purple* and Co^{3+} ion *pink*) represents the heme position in the POX site. Dashed line represents a distance of ~12.5 Å between the Co^{3+} ion and the hydroxyl group of Tyr 385 located within the COX active site. AA (*orange*) is shown bound in the COX active site.

Arachidonic Acid Binding to the COX Active Site

The conversion of AA to PGG_2, the product of the COX site, involves a series of regio- and stereo-specific reactions. Since AA can assume up to 10^7 low energy conformations [51], the binding conformation of AA is not only of interest in understanding the feasibility of catalysis, but also for understanding how the proper regio- and stereo-specific additions of oxygen and ring formations are achieved. Many kinetic and structural studies with mutants of PGHS-1 and PGHS-2 have focused on understanding the interactions between active site residues and AA and how these interactions play a role in binding and positioning of AA, in addition to catalysis. The crystal structure of the oPGHS-1/AA complex, in which Co^{+3}–protoporphyrin IX replaces heme, provided the first look at how AA binds within the COX active site. This protein/ligand complex revealed significant hydrophobic contacts between AA and the residues lining the COX active site (Figure 8) further elucidating the results obtained from kinetic analysis of native and mutant forms of PGHS.

The role of various residues of the PGHS-1 COX active site have been classified according to their involvement in the binding and positioning of AA, in addition to catalysis. The classifications were derived from differences observed in kinetic parameters and product formation ratios between native oPGHS-1 and various mutants of PGHS-1 [52, 53]. Mutation studies of Tyr385, which is positioned near C13 of AA in the Co^{3+}-protoporphyrin PGHS-1/AA crystal structure (Figure 8), have clearly shown Tyr385 to be involved as the tyrosyl radical that abstracts the hydrogen from C13. Tyr348 and

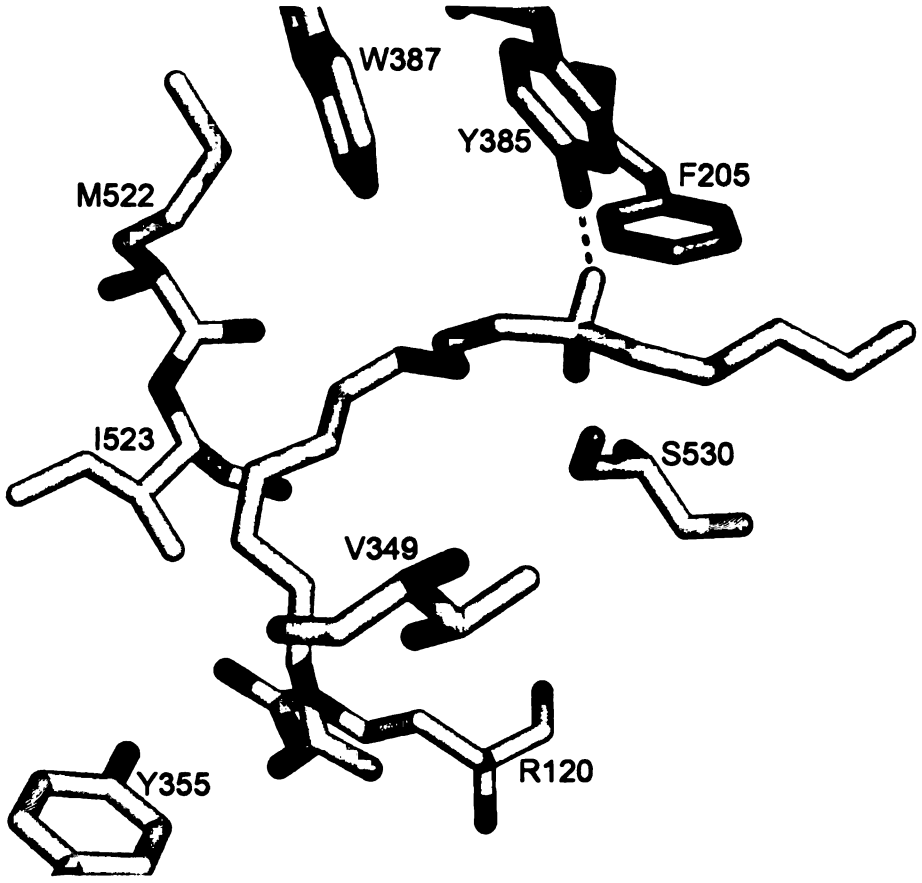

Figure 8 Arachidonic acid bound within the COX active site of Co^{3+}-protoporphyrin oPGHS-1 structure (PDB bank 1diy). Dashed line represents approximately 2.9Å distance from the C13 pro*S* hydrogen of AA. Arachidonic acid binds with an extending "L-shaped" configuration with carboxylate group making several ionic interactions with R120 and Y355 and hydrophobic interactions with various residues lining the COX channel.

Gly533, which are not involved directly in catalysis, appear to be important in positioning C13 of AA for hydrogen abstraction by Tyr385. In particular, Gly533, which contacts the carbons C19 and C20 of AA as observed in the crystal structure, is speculated to be significant in maintaining the position of the ω-end of AA so as to support catalysis.

Other residues shown to be significant in positioning AA include residues V349 and W387. Studies with various mutants of V349 including V349A and V349L

demonstrated that AA could exist in at least three distinct and catalytically competent conformations occurring at the moment of hydrogen abstraction, the rate-limiting step of the COX reaction [52]. Thus, the conformation of AA at the moment of hydrogen abstraction, would dictate what product would be formed. In the case of native enzyme, greater than 95% of PGG_2 would be formed; however, mutant enzymes such as V349A and V349L produced significant amounts of 11R-hydroxy-5Z, 8Z, 12E, 14Z-eicosatetraenoic acid (11-HETE), and 15R-hydroxy-5Z, 8Z, 11Z, 13E or 15S- hydroxy-5Z, 8Z, 11Z, 13E (15-HETE) being abortive products in which only one molecule of oxygen was inserted before the reaction aborted [52]. Various mutants of PGHS-1 and PGHS-2 resulted in a significantly altered shift in the ratio of products formed as compared to the native enzyme, thus demonstrating the important role of the residues lining the COX active site in maintaining an optimal conformation of AA to produce PGG_2. Mutants of PGHS-1 such as V349A and W387F were of particular interest because each mutation alone displayed a similar product profile in which approximately 30-50% of both 11R-HETE and PGG_2 were formed and no detectable amount of 15-HETE was formed [52, 53].

Interestingly these various mutants of PGHS remain relatively active in metabolizing AA; however, mutations of residues such as V349 and W387 result in aberrant forms of PGHS, which drastically change the course of the reaction and therefore, the products that are formed from AA. It was speculated from the crystal structure of the Co^{3+}-protoporphyrin oPGHS-1/AA complex that mutations at V349 and W387 were somehow resulting in a conformation of AA (at the moment of hydrogen abstraction) approximately half of the time that would prevent the formation of an

endoperoxide bridge between atoms C9 and C11 of AA. As a consequence, the reaction would abort thus yield almost equal ratios of 11R-HETE and PGG_2. Chapter II discusses in detail the structural roles of residues V349 and W387 and how they influence the conformation of AA bound within the COX site as well as how these residues play a role in the formation of the endoperoxide group.

Substrate Specificity of PGHS-1 and PGHS-2

Arachidonic acid is the preferred substrate for the PGHS enzymes and is the prostanoid precursor that is converted into 2-series prostaglandins, the predominant series of prostanoids found in blood plasma [54]. However, the 1-series prostaglandins are the most abundant form of prostanoids found in seminal fluid indicating that PGHS can utilize dihomo-γ-linolenic acid (DHLA; 20:3*n*-6) as a substrate [25, 26], which is found at higher levels than AA in vesicular gland tissue (Figure 9) [55]. Other fatty acids in addition to DHLA have been found to be oxygenated by PGHS some of which include linoleic acid (LA; 18-2*n*-6) α-linolenic acid (18:3*n*-3) and eicosapentaenoic acid (EPA; 20:5*n*-3) [56], and some less common fatty acids such as adrenic acid (22:4*n*-6) [57], columbinic acid (5E, 9Z, 12Z-octadecatrienoic acid), and Mead acid (5Z, 8Z, 11Z-eicosatrienoic acid) [58].

The ability of COX to oxygenate a variety of fatty acids would not be unusual given that there is the possibility that PGHS can be exposed to a mixed pool of free fatty acids taking into account that there are varying abundances of fatty acids within different tissues and that during a stimulus various fatty acids can be cleaved from the cellular membranes by forms of secretory PLA_2 that lack specificity for a particular fatty acid [4].

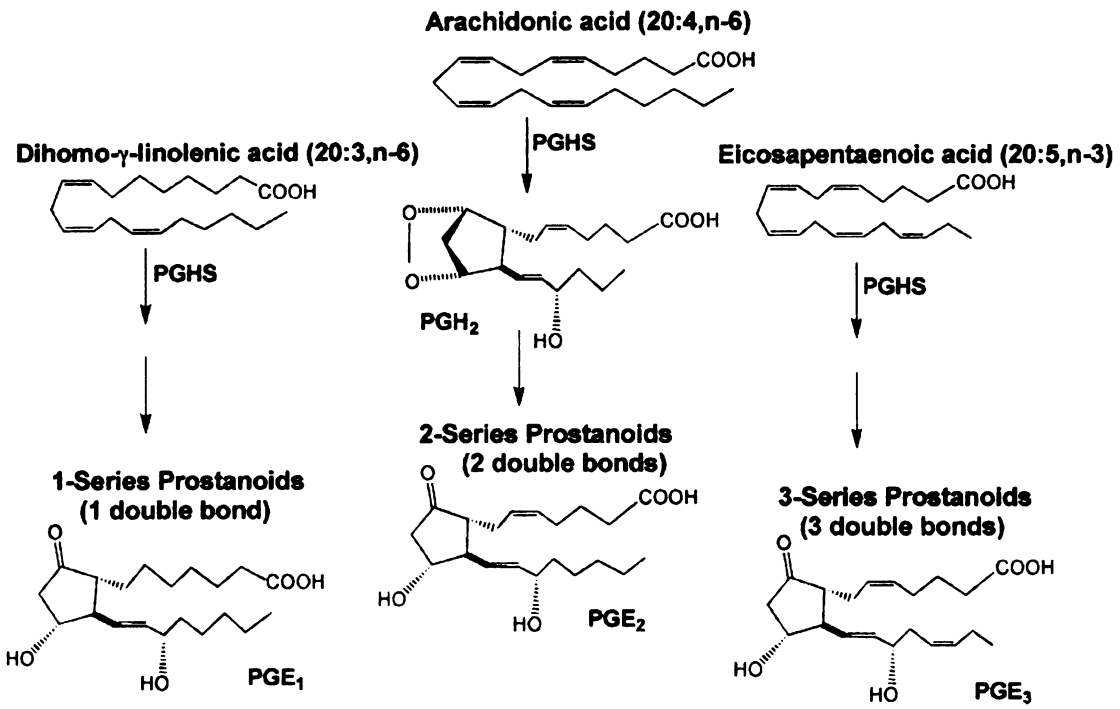

Figure 9 Conversion of various fatty acids to 1,2,3-series prostanoids.

EPA, for instance, is stored at the *sn*2 position like AA, and can be cleaved upon activation of phosholipases A_2 [3, 49, 59, 60]. Subsequently, EPA can then be converted to PGH_3, which can further isomerize to various prostanoids such thromboxane A_3 and PGD_3 [3, 59] (Figure 9).

Although these fatty acids substrates are utilized at lower efficiency as compared to AA, they can compete with AA and in some cases act as inhibitors preventing the formation of the 2-series prostanoids being derived from AA. As previously mentioned, EPA can be converted into 3-series prostanoids through PGHS pathway; however, it acts more as a potent inhibitor of AA oxygenation rather than being an efficient substrate [3, 56, 59]. The inhibitory effects of EPA can serve the same benefit as aspirin by reducing

the formation of the pro-thrombogenic thromboxane A_2 by platelet PGHS. Similarly, linoleic acid, like EPA, is a poor substrate for PGHS that can also effectively compete with AA in binding to PGHS, in addition, it can be oxygenated by PGHS forming the monohydroxy acids 9-HODE and 13-HODE [56, 61]. Other fatty acids that act as competitive inhibitors of PGHS include 18:1,n-9 and 22:6, n-3; however, unlike EPA and linoleic acid are not oxygenated by PGHS [34, 56, 62].

Several crystal structures of PGHS-1 complexed with various fatty acid substrate including DHLA, EPA and linolenic acid have been published and help elucidate the structural basis of substrate specificity observed from mutagenic studies by highlighting active site residues which contribute to substrate binding and positioning for utilization by PGHS-1. All structures to date with fatty acid bound to PGHS-1 show a similar overall "L-shaped" binding orientation similar to what is observed for AA bound to PGHS-1 where the carboxyate (atom C1) is anchored at R120 and Y355 and the ω-end weaves up into the channel [42]. However, each fatty acid having slight differences in flexibility of the substrate due to differences in the number of carbons and double bonds as well as double bond positions can have a major influence on the binding orientation which in turn affects the ability of the fatty acid to be utilized as a substrate (Figure 10) [42, 49, 50]. DHLA, a close analog of AA having only one less double bond, is utilized most efficiently by PGHS-1 and PGHS-2 and binds within the COX site of PGHS-1 very similarly to AA; however, the positions of carbons C2-C10 differ significantly particularly, the position of the C8-C9 double bond. This altered position is a result of increased flexibility due to a missing double bond between carbons C5-C6. Despite these binding differences, atom C13 of AA remains properly positioned for hydrogen

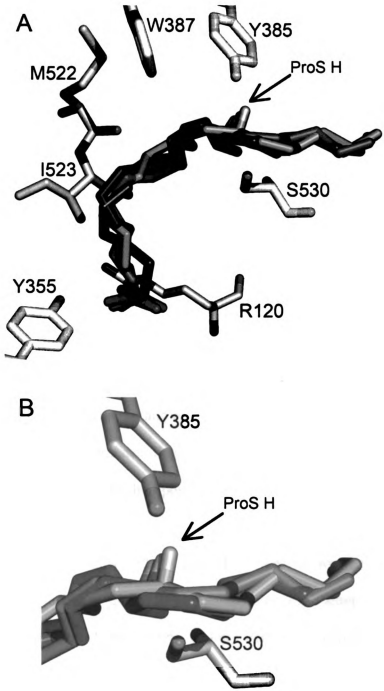

Figure 10 Superposition of various fatty acid bound within the COX active site of PGHS-1. Arachidonic acid, DHLA, linoleic acid, and EPA are shown in orange, green, magenta, and blue. The pro*S* hydrogens of AA, DHLA, and LA are shown and labeled with arrow. EPA is bound an inhibitory mode in that the pro*S* hydrogen of EPA is positioned in an opposite direction as compared to the other fatty acids shown.

abstraction and atoms C8-C10 are still positioned to support endoperoxide formation and cyclopentane ring closure [50]. The structure of DHLA represents a catalytically productive conformation of substrate bound; however, oPGHS-1/EPA complex revealed more of an inhibitory binding mode. EPA, like DHLA, binds with an L-shaped conformation having the carboxylate interacting with Arg120; however, the ω-end of EPA having an extra double bond (C17-C18) is more inflexible, thus binding within the hydrophobic pocket is accommodated by compression near the carbonyl end. Consequently, EPA binds with a strained orientation where atoms C3-C10 pack more closely to one side of the COX channel (V349) resulting in a mispositioning of C13 with respect to Tyr385, the catalytic residue of the COX site (Figure 10) [49]. Linoleic acid which is used more efficiently than EPA but less than DHLA binds to PGHS-1 in a less strained and catalytically competent binding mode despite having two fewer carbons than AA, DHLA, and EPA, thus demonstrating further that slight differences in carbon number, number of double bonds and their positions effect flexibility in turn changing the ability to be used as a substrate or act as an inhibitor.

Substrate specificity studies with PGHS-2 have also shown that PGHS-2 can utilize a variety of fatty acids to similar and in some cases with better efficiency than PGHS-1. Our understanding of the binding of fatty acids to PGHS-2 is not as well established as for PGHS-1. Most structure complexes of PGHS-2 are with various inhibitors, which have tremendously increased our understanding of subtle differences between PGHS-1 and PGHS-2, namely, particularly the larger active site of PGHS-2 and how it may be utilized in binding of ligands as compared to PGHS-1. Some of these structural differences have presented more questions in relation to the reason there are

two isoforms of PGHS. Recently, it was shown that PGHS-2 was capable of oxygenating the endocannabinoid, 2-arachionylglyerol with similar efficiency, as AA while PGHS-1 could not [63]. In addition, PGHS-2 was able to convert 2-AG to PGH_2-glycerol, which can be further converted to series 2-prostanyl-glycerol derivatives *in vitro* and *in vivo* [64, 65] creating a unique group of prostaglandins possibly having different roles from prostaglandins derived from AA. The ability of PGHS-2 to utilize 2-AG while PGHS-1 does not is of major interest and is thought to involve the larger active site of PGHS-2, which is able to accommodate the binding of this larger fatty acid.

Inhibition of PGHSs

The PGHS enzymes are inhibited through the action of NSAIDs, which bind to the COX active site preventing the binding of substrate while leaving the peroxidase activity unaffected. The NSAIDs are a structurally diverse group of compounds that inhibit the enzymes nonselectively, selectively or through chemical modification. The largest group of the nonselective NSAIDs is the acidic cyclooxygenase inhibitors some of which include ibuprofen, flurbiprofen, naproxen, indomethacin, diclofenate, and aspirin. These "classical " NSAIDs are structurally similar in that they are composed of either a mono or bi-cyclic aromatic ring system and all possess a free carboxylate group.

Although these compounds are similar in structure they display markedly different dynamics in inhibition of PGHS, and can be divided into groups based on their ability to undergo either simple competitive or time-dependent inhibition. Inhibitors such as ibuprofen and naproxen are characterized as freely reversible competitive inhibitors of PGHS; however, other NSAIDs like flurbiprofen and indomethacin inhibit PGHS

through a time-dependent manner characterized by increased potency of inhibition as preincubation time of enzyme with inhibitor increases, thus inhibition is only slowly reversible [66]. Various studies hinted that the structural requirements for time-dependent inhibition in the case of some of these inhibitors is attributed to a combined presence of a halogen and a free carboxylate group [66, 67].

Crystal structures of various NSAIDs bound to PGHS-1 and PGHS-2 demonstrated that the carboyxlate group of acidic NSAIDs interacts with the guanidinium group of Arg120. This interaction was not only shown to be involved in time-dependent inhibition in PGHS-1, but was also shown to be essential for high affinity binding of acidic NSAIDs and AA. Mutations of Arg120 to smaller more neutral residues have rendered PGHS-1 resistant to inhibition by NSAIDs and abolished binding of AA to PGHS-1 [67]. However, comparative mutation studies in PGHS-2 have shown that an ionic interaction between Arg120 and a free carboxylate group was not as crucial for binding of NSAIDs and AA [68]. Although most classical NSAIDs are non-selective inhibitors, in general they seem to bind more tightly to PGHS-1 as compared to PGHS-2 possibly because of the importance of the ionic interaction between the carboxylate group of the inhibitor and Arg120 of PGHS-1.

Aspirin, unlike other NSAIDs, irreversibly inhibits PGHS-1 by chemically modifying the enzyme through aceylation of Ser530, a residue located within the COX site near Tyr385, the catalytic residue. Aspirin acetylates Ser530 in both PGHS-1 and PGHS-2 and causes a complete loss in the production of prostaglandins; however, the effects of acetylation are different between the enzymes. Aspirin acetylation in PGHS-1 completely blocks AA from accessing the COX site, thus PGHS-1 cannot oxidize AA

and is rendered completely inactive. However, acetylated PGHS-2 is able to bind and oxidize AA, only producing 15*R*-HETE as the major product with no detectable prostaglandin products [69, 70]. The ability of PGHS-2 to still accommodate the binding and utilization AA even after aspirin acetylation suggested that there were some slight structural differences in the form of a larger binding pocket in PGHS-2.

Past studies have documented that the PGHS isozymes do differ in their sensitivities to inhbition by NSAIDs, in addition, structural studies have clearly identified subtle structural differences between the isoforms, which led to the development of series of PGHS-2 selective inhibitors. The most distinctive structural feature between the isoforms are several amino acid differences within the COX active site in which residues Ile434 and Ile523 are replaced with smaller valines and His513 in PGHS-1 is replaced with arginine in PGHS-2. These differences not only increased the size, but also the chemical environment of the PGHS-2 COX active site. The most structurally diverse class of PGHS-2 selective inhibitors are the diarylheterocycles, which are characterized as having a *cis*-stilbene frame fused to a variety of heterocyclic rings being of 4,5 or 6-membered rings. The most critical feature of this class of inhibitors was found to be the presence of a sulfonamide or methysulfonamide group on one of the phenyl rings of the stilbene framework, making this class of inhibitors larger than the "classical" NSAIDs [71]. The diarylheterocycles were shown to bind to both PGHS-1 and PGHS-2; however, the selectivity towards PGHS-2 is a result of time-dependent inhibition while in PGHS-1 there was competitive binding, but being freely reversible. The structural basis of this selectivity and time-dependent inhibition towards PGHS-2 was found to be residue 523 where mutations of Val523 to isoleucine in PGHS-2 caused a loss in selectivity by

PGHS-2 selective inhibitors [72]. In addition, x-ray structure studies demonstrated that the sulfonamide group of these inhibitors interacts with the side pocket region of PGHS-2, and that having an extra methyl group on residue 523 prevented access to this side pocket region [41].

Recently, modification of the classical NSAID, indomethacin, produced an interesting series of inhibitors, the indomethacin ethanolamides. Inhibition studies of PGHS-1 and PGHS-2 with these variously modified inhibitors led to an interesting observation of enantioselective inhibition of PGHS-1, which was not observed in PGHS-2. The structural basis of this inhibition will be discussed in detail in Chapter IV.

CHAPTER II

CRYSTAL STRUTURE OF ARACHIDONIC ACID BOUND TO A MUTANT OF PROSTAGLANDIN ENDOPEROXIDE H SYNTHASE-1 THAT FORMS PREDOMINANTLY 11-HPETE[1]

Introduction

Prostaglandin endoperoxide H synthase (PGHS) is a heme-containing, bi-functional enzyme that catalyzes the conversion of arachidonic acid (AA) to prostaglandin (PG) H_2 (Figure 2), the immediate precursor to prostaglandins, thromboxanes and prostacyclin. In mammalian tissues, there are two isoforms of PGHS [3, 73]. PGHS-1 is constitutively expressed and produces prostaglandins in response to hormone stimulation mainly for regulating housekeeping functions. PGHS-2, the inducible form, is expressed in response to mitogens, growth factors, tumor promoters, and/or cytokines and produces prostaglandins associated with pain, fever, and inflammation[3, 73].

Despite the differences in patterns of expression, PGHS-1 and PGHS-2 are quite similar both structurally [39-41] and mechanistically[74]. Both isoforms function as dimers with each monomer having an epidermal growth factor domain, a membrane binding domain, and a large catalytic domain. The catalytic domain of PGHS possesses two distinct, but functionally connected active sites [34, 39-41]. These two sites include the cyclooxygenase (COX) site, which exists as a long hydrophobic channel within the core of the protein and binds AA [42] and nonsteroidal anti-inflammatory drugs [39-41],

and a more solvent exposed peroxidase (POX) site containing a heme moiety, which is involved in reducing PGG_2 formed at the COX site to PGH_2, the final enzymatic product.

The crystal structure of native Co^{+3} -protoporphyrin IX oPGHS-1 in a complex with AA shows that AA binds within the COX active site having the carboxylate group anchored at the mouth of the hydrophobic channel via electrostatic interactions with Arg120 and Tyr355 [42]. The carbons of the AA chain weave into the COX active site making forty-eight hydrophobic contacts with residues lining this channel. Based on the crystal structure and knowledge of the stereochemical requirements of the COX reaction [25], a structural sequence of catalytic events was proposed (Figure 11) [42]. The COX reaction begins with the abstraction of the 13pro*S* hydrogen of AA by a tyrosyl radical formed at Tyr385 creating an arachidonyl radical centered at C13 [74]. Following a rearrangement centering the radical on C11, an attack of molecular oxygen occurs to form an 11*R*-hydroperoxyl radical (Figure 11). At this point it is proposed that rotation about the C10-C11 bond moves the 11*R*-hydroperoxyl radical in close proximity to C9 to form the 9, 11-endoperoxide group; concurrently, rotation about the C10-C11 bond additionally brings C8 near to C12 to form the cyclopentane ring. Repositioning of C12 closer to C8 for ring formation also repositions atoms C13 to C20. The result is an optimal positioning of C15 for a second attack by molecular oxygen. Additionally, with the 15-hydroperoxyl radical now positioned in proximity to Tyr385, Tyr385 is poised to donate a hydrogen to form the product of the COX site, PGG_2, thus, simultaneously reforming the Tyr385 radical and regenerating the enzyme for another round of catalysis.

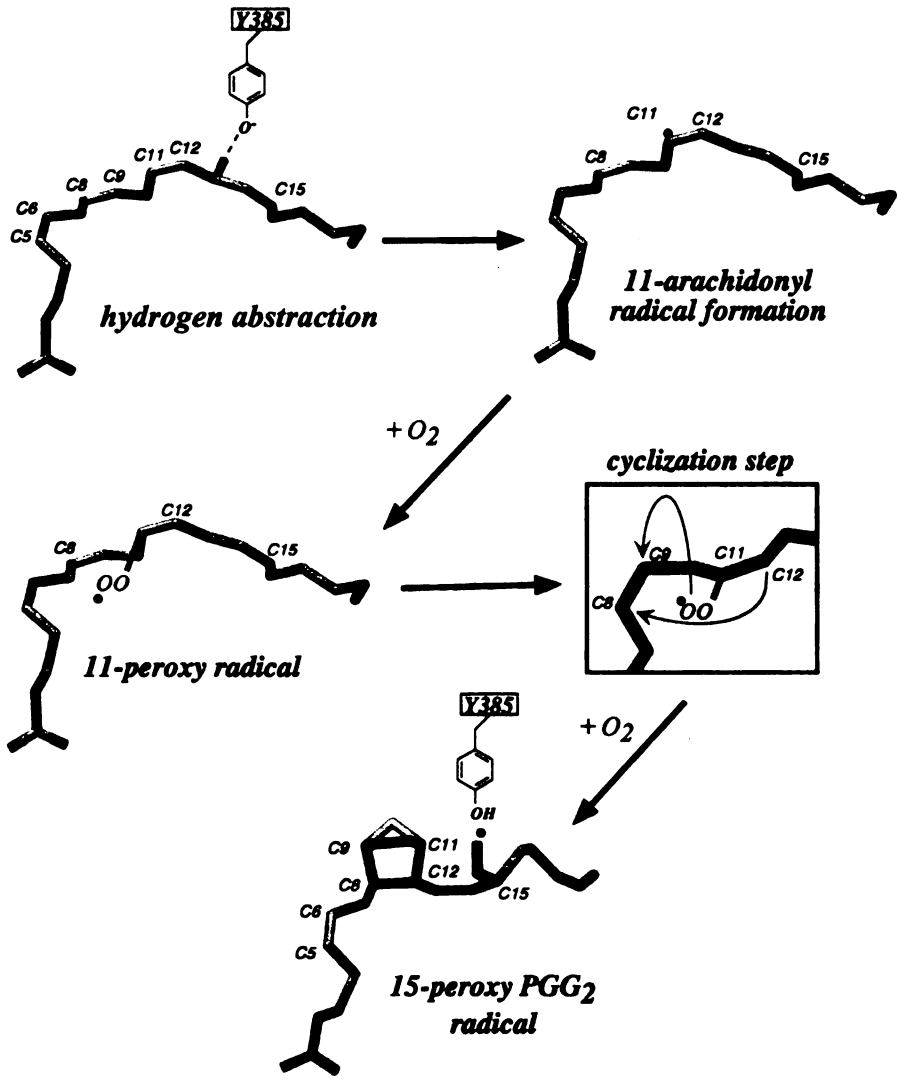

Figure 11 Cyclooxygenase mechanism based on the crystal structure of arachidonic acid bound to native ovine PGHS-1. Figure shown is from a published modified version [75] of the originally published scheme [42].

Both PGHS isoforms exhibit some lipoxygenase activity. Small amounts of 11-hydroperoxy-8Z, 12E, 14Z,-eicosatrienoic acid and 15-hydroperoxy-8Z, 11Z, 13E-eicosatrienoic are formed from dihomo-γ-linolenic acid [25], and the corresponding 11- and 15-HETEs are produced from AA [50, 52, 70]. Thus, the native enzyme is not 100% efficient in converting AA to PGG_2. Additionally, with native enzyme the K_m values for

AA in forming 11-HPETE, 15-HPETEs and PGG_2 are different for each product [52]. This suggests that AA can exist in the COX site in at least three catalytically competent arrangements at the time of hydrogen abstraction to yield either PGG_2, 11*R*-HETE, or 15*R/S*-HETE [52].

Extensive kinetic and product analysis of numerous mutants of the COX active site have identified several residues that influence the relative proportions of PGG_2 and monohydroperoxide products formed from AA [52, 53, 76]. Two single amino acid substitutions, V349A and W387F were of particular interest to us because relatively more 11*R*-HPETE is formed (35-50% of total products) without substantially altering the kinetics of oxygenation [53]. Because each single mutation favors the formation of 11*R*-HPETE approximately 50% of the time, we constructed and analyzed a V349A/W387F oPGHS-1 mutant. As described in this chapter, this double mutant produces predominantly 11*R*-HPETE. To investigate why this double mutant produces predominantly 11*R*-HPETE from AA, we determined the crystal structure of Co^{3+}-protoporhyrin V349A/W387F oPGHS-1 with AA bound in the COX active site. Significant differences in the conformations of AA bound to native oPGHS-1 vs. V349A/W387F oPGHS-1 mutant enzyme were observed. Our results provide insight into how Val349 and Trp387 influence the conformation of AA and how these residues are involved in directing the formation of the endoperoxide group.

Experimental Procedures

Materials

Arachidonic acid, 11*R*-HETE and 15*S*-HETE were purchased from Cayman Chemical Co. (Ann Arbor, MI), [1-^{14}C]-Arachidonic acid (40-60 mCi/mmol) was from

NEN Life Science Products (Boston, MA). Sf21 insect cells and 100X Antibiotic-Antimycotic were purchased from Invitrogen. Fetal bovine serum and HyQ-SFX insect medium used for cell growth and protein expression were purchased from HyClone (Logan, UT). Ni-NTA superflow resin was purchased from Qiagen, tween-20 used for solubilization and purification was from Pierce Chemical Co., and n-octyl-β-D-glucopyranoside (β-OG) used for crystallization was from Anatrace (Maumee, OH). Flurbiprofen and hemin were purchased from Sigma (St. Louis, MO) and Co^{3+}-protoporphyrin IX from Porphyrin Products (Provo, UT). Oligonucleotides used as primers for mutagenesis and for sequencing were prepared by the Michigan State University Macromolecular Structure and Sequencing Facility.

Preparation of V349A/W387F oPGHS-1

Site-directed mutants were prepared with a pFastbac vector containing a cDNA encoding native oPGHS-1 with a hexahistidine tag [77] and mutagenic oligonucleotides using the Stratagene QuikChange Kit (Stratagene, La Jolla, CA). Mutations were confirmed with sequence analysis performed by the DNA Sequencing Facility at Michigan State University.

Generation of Recombinant Baculovirus and Expression of oPGHS-1 Mutants

DH10Bac cells were transformed with pFastbac containing cDNA for either V349A oPGHS-1 or V349A/W387F oPGHS-1 to obtain baculoviral DNA, which was then isolated and used to transfect sf21 insect cells to produce recombinant baculovirus. The recombinant baculovirus was amplified, and supernatants of amplifications were used as inoculum stocks. Sf21 insect cells grown in a 17 L bioreactor to an approximate

density of 1.7-2.0 x10^6 cells/mL in medium with 1% antibiotic and antimycotic were infected with recombinant baculovirus at a multiplicity of infection of 0.01 at 27°C. Three to four days after infection, cells were harvested by centrifugation.

Purification oPGHS-1 Mutants from Sf21 Insect Cells

Cell pellets from three bioreactors were resuspended in 1X Phosphate Buffer Saline (PBS), pH 8.0 containing 20 mM imidazole and were lyzed by sonication. To solubilize PGHS from the membranes, Tween-20 was added to the lysate up to 1% (v/v) which was then incubated at 4° C for 45 min with gentle agitation. Solubilized lysate was centrifuged at 10,000 rpm at 4° C for 20 min, followed by ultracentrifugation at 45,000 rpm at 4°C for 90 min. The supernatant was carefully removed and incubated for at least 3 hrs at 4°C with Ni-NTA resin equilibrated in 1X PBS, pH 8.0, 20 mM imidazole, and 0.1% Tween-20. After this incubation period, the mixture of Ni-NTA resin plus supernatant was poured into a column which was washed with four column volumes each of 1X PBS, pH 8.0, 20 mM imidazole, 0.1% Tween-20 and 1X PBS, pH 8.0, 300 mM NaCl, 20 mM imidazole, 0.1% Tween-20. Hexa-histidine-tagged PGHS was eluted with 1X PBS, pH 8.0, 200 mM imidazole, and 0.1% Tween-20. Fractions with the highest specific peroxidase activity [42] were pooled and concentrated using a Millipore Ultrafree -15 spin concentrator (30-kDa molecular weight cut off) to a protein concentration of 8-10 mg/ml. Detergent exchange and desalting of the concentrated protein was performed by spinning protein over 5 mL of packed G-25 sephadex (Amersham Pharmacia) equilibrated in 20 mM HEPES, pH 7.0, 20 mM NaCl, 1mM NaN_3, and 0.5 % β-OG. Protein concentrations were determined using BCA protein assays (Pierce, Rockford, IL).

Analysis of Products formed from Arachidonic Acid

Aliquots (equivalent to 150 COX units, where one unit is defined as 1 nmol of O_2 consumed/min) of purified oPGHS-1 native and/or mutants were incubated for 1 min at 37° C with 35 μM [1-^{14}C]-arachidonic acid with and without 200 μM flurbiprofen in a reaction volume of 200 μl. Radioactive products were extracted and separated by thin layer chromatography as previously described [53]. Products were visualized by autoradiography and quantified by liquid scintillation counting. Negative controls from samples containing flurbiprofen were subtracted from values measured from the corresponding samples not containing flurbiprofen.

Characterization of V349A/W387F oPGHS-1

Kinetic parameters for V349A/W387F oPGHS-1 were measured with a cyclooxygenase assay by monitoring the initial rate of O_2 uptake at 37° C using an oxygen electrode [53]. A typical assay consisted of 3 mL of 100 mM Tris-HCl, pH 8.0, 1 mM phenol, 1 mM hemin, and 2-100 μM AA. Reactions were initiated by adding a volume of enzyme equivalent to 150 units of Ni-NTA purified V349A/W387F oPGHS-1.

Crystallization and Data Collection

Purified apo-V349A/W387F oPGHS-1 at approximately 8 mg/mL (0.11 mM) was reconstituted with a two-fold molar excess of Co^{3+}-protoporphyrin IX. Prior to setting up sitting drop crystallization experiments, the protein was incubated in the presence of AA at a five-fold molar excess over the protein concentration [78]. Protein was mixed 1:1 with buffer containing 0.68 M sodium citrate, 0.6-0.9 M LiCl, 1 mM NaN_3 and 0.3% β-OG and equilibrated within a reservoir containing 0.68-0.9 M sodium citrate, 0.60-0.90 M LiCl and 1 mM NaN_3. Crystals appeared after four weeks to several months. Crystals

were harvested with a nylon loop and transferred briefly into a cryo solution containing 0.9 M sodium citrate, 1.0 M LiCl, 0.15% β-OG, 1 mM NaN_3 and 24% (w/v) sucrose. Crystals were immediately flash frozen in liquid propane at -165°C. Data were collected at beamline 19ID of the Structural Biology Center (Advance Photon Source, Argonne IL). The data from a single crystal was indexed and integrated using HKL2000 [79] and then scaled together using SCALEPACK [79] (Table 1).

Structure Determination and Refinement

The crystals of V349A/W387F oPGHS-1 with AA were essentially isomorphous with crystals of oPGHS-1 complexed with AA. Thus, the structure of V349A/W387F oPGHS-1 was determined by using the protein atoms of native oPGHS-1/AA (Protein Data Bank code 1DIY) as a phasing model for simple rigid body refinement utilizing CNS version 1.1 [80], in order to correct for small changes in lattice parameters. After an initial round of simulated annealing, positional and group B-factor refinement, the resulting R and R free factors were 25.4% and 31.2%. Inspection of the initial 2Fo-Fc (contoured at 1σ) and Fo-Fc (contoured at 2.5σ) electron density maps using the program CHAIN [81] allowed the placement of Co^{+3}-protoporphyrin IX, seven carbohydrate residues, and three β-OG detergent molecules. Strong electron density was observed for AA starting from the carboxylate group up to carbon C4. With subsequent rounds of refinement, the improved phases led to the appearance of further electron density, which allowed the additional placement of atoms C5-C12 of AA. No further electron density was observed for AA. Although no density was observed for C13, the position of C13 was modeled based on the limited orientations it can adopt due to the stereochemical

Table 1 Data collection and refinement statistics for the Co^{3+}-protoporphyrin V349A/W387F oPGHS-1/AA cocyrstal structure.

Item		AA Model building	AA Simulated annealing
Spacegroup		$P6_522$	$P6_522$
a (Å)		181.88	181.88
b (Å)		181.88	181.88
c (Å)		103.37	103.37
Resolution (Å)		20-3.1	20-3.1
No. of unique reflections (F>0σ)		20640	20640
Completeness (%)		99.1 (99.8)[a]	99.1 (99.8)[a]
R merge, all data (%;I>0σ)		7.6 (32.0)[a]	7.6 (32.0)[a]
No. of atoms in refinement		4573	4571
R factor (%; reflections >2σ on F)		23.3	23.8
Free-R factor (%; reflections >2σ on F)		30.8	31.1
Mean positional error (Å)		0.43	0.43
r.m.s.d in bond length (Å)[b]		0.009	0.009
r.m.s.d in bond angle (°)		1.6	1.6
r.m.s.d in improper angle (°)		1.1	0.92
r.m.s.d in dihedral angle (°)		22.6	22.3
Average B factor	all atoms	44.9	41.1
	Protein	40.1	40.2
	Arachidonic Acid	55.6	56.7

[a]The values in parentheses represent the values in the last shell (3.2-3.1Å)
[b]r.m.s.d., root mean square deviation

restrictions of the C11-C12 double bond and was included in the refinement, thus C1 (including the carboxylate) to C13 of AA was included in the refinement of the model. Further refinement included the addition of 22 water molecules at positions that were within 2.4-3.6 Å of a hydrogen bond donor/acceptor and an electron density peak of 3σ or greater. The R and R free values of the final model are at 23.2% and 30.8% (Table 1). Evaluation with PROCHECK [82] showed that all non-pro and non-gly residues lay within the most favored or allowed regions of the Ramachandran plot.

Since medium resolution diffraction data were used in this analysis, the following two tests were performed to verify that changes observed in the AA conformation between the structures of native and V349A/W387F oPGHS-1 were significant. In the first test, Fo-Fc difference electron density maps were calculated using the observed structure factors and modified phase sets. As the crystals of native and mutant oPGHS-1 were isomorphous, a calculated phase set was created by combining the Co^{3+}-protoporphyrin V349A/W387F oPGHS-1, excluding the observed AA atoms, with atoms from the AA conformer observed in the refined model of native Co^{3+}-protoporphyrin oPGHS-1/AA complex (Protein Data Bank code IDIY). A similar method has been utilized previously to verify observed differences between AA and several other fatty acid substrates bound within the COX site [49, 50]. In areas where the carbon positions differ between the two observed conformations of AA, we would expect to observe the appropriate positive and negative difference density peaks, indicating a shift in atoms positions.

The second test addressed the possibility that other conformations of AA could exist and be represented by the density, given the broad extent of the electron density

observed at this resolution. A parallel series of simulated annealing refinements were performed, using the observed structure factors and the V349A/W387F oPGHS-1 coordinates. Each series of simulated annealing refinements were done four times in order to generate a family of structures from each starting point. The starting conformation of bound AA differed, however, between the two parallel series of refinement. In the first series, the AA conformer found in native oPGHS-1 [42], was used, while in the second series, the AA conformer derived from the refined V349A/W387F oPGHS-1 structure was used. If the contributions from the X-ray data for the mutant were significant, it was expected that the AA conformer seen in the mutant would be recovered in the first case and retained in the second. If not, both series of refinements would yield a wide range of unrelated AA conformers. As expected, the simulated annealing refinement starting from the AA conformer derived from the refined V349A/W387F oPGHS-1 structure generated a family of AA conformations which were very similar to the starting conformer. In contrast, all four AA conformers generated by using the native AA conformer as the starting point for refinement looked remarkably similar to the AA conformation found in the V349A/W387F mutant. Of these four conformers, one fit the observed electron density quite well and was used for further structure refinement. Statistics of the refinement of the final model using the conformer from simulated annealing are shown in (Table 1).

Results

Comparison of Products Formed from Arachidonic Acid by Native and Mutant oPGHS-1.

There are considerable differences in the proportions of oxygenated products formed from [1-^{14}C]-arachidonic acid by native oPGHS-1, V349A oPGHS-1 and

V349A/W387F oPGHS-1 (Figure 12). Native enzyme produces predominantly products derived from PGG_2 (~95% including HHT and various prostaglandins), and small amounts of 11-HETE (~2.5%) derived from 11-HPETE and 15-HETE (~2.5%).

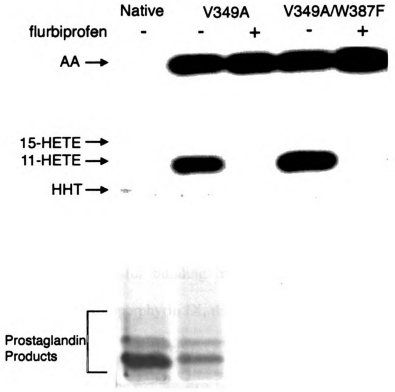

Figure 12 Thin layer chromatogram comparing the products formed from [1-^{14}C]AA by native, V349A oPGHS-1, or V349A/W387F oPGHS-1. [1-^{14}C]AA was incubated for 1 min at 37°C in the presence or absence of the cyclooxygenase inhibitor flurbiprofen with 150 cycloxygenase units of native, V349A, or V349A/W387F oPGHS-1 purified by chromatography on Ni-NTA. The samples were extracted, and the radioactive products were separated by thin layer chromatography and quantified by liquid scintillation counting as described under "Experimental Procedures". The locations of AA, monohydroxy fatty acid, and PG standards are noted. *HHT*, 12-hydroxy-5c,8c,10t-heptadecatrienoic acid.

In comparison, the V349/W387F double mutant produces predominantly 11-HETE (>84%) and correspondingly. less PGG_2 derived products (~12%) than native enzyme. V349A oPGHS-1 forms about 50% 11-HETE [53].

Kinetic Analysis of V349A/W387F oPGHS-1

To determine if AA is utilized with similar efficiencies as native and V349A/W387F oPGHS-1, the K_m value for the oxygenation of AA was determined using a cyclooxygenase assay. The K_m for AA of V349A/W387F oPGHS-1 was determined to be 5 μM, a value very similar to that previously reported for native enzyme under similar assay conditions [52, 53].

Arachidonic Acid Bound in the COX site of Co^{3+}-protoporphyrin V349A/W387F oPGHS-1

The electron density of the Co^{3+}-protoporphyrin V349A/W387F oPGHS-1/AA complex was of good quality for building in considerable amounts of non-protein substructure (i.e. the Co^{3+}-protoporphyrin IX, the carbohydrate groups linked to residues Asn68, Asn144, and Asn 410, and three β-OG detergent molecules bound within the membrane binding domain). The overall structure which includes the epidermal growth factor, the membrane binding and the catalytic domains of the Co^{3+}-protoporphyrin V349A/W387F oPGHS-1/AA complex is virtually identical to that of Co^{3+}-protoporphyrin oPGHS-1/AA complex having an r.m.s deviation of 0.3 Å over all Cα atoms. This indicates that the overall structure is relatively unchanged by the two mutations (V349A and W387F) in the COX active site.

The Fo-Fc electron density map allowed the placement of carbons C1 to C12 into the electron density with some degree of confidence although no electron density was

observed for carbons C13-C20. Given the broad extent of the electron density observed at this medium resolution, it was essential to verify that the observed differences in conformation of bound AA between native and V349A/W387F oPGHS-1 were significant. In a test using Fo-Fc difference electron density map analysis (see "Experimental Procedures" of this chapter), inspection of the electron density maps calculated with AA from the native oPGHS-1/AA complex within the V349A/W387F oPGHS-1 active site showed a significant positive peak contoured at 3σ representing the correct position of atoms C3-C7 of AA bound within the mutant active site (data not shown). In addition, a smaller negative peak contoured at 3σ was observed representing the misplaced positions of C2-C4 of the conformation of AA observed in the oPGHS-1/AA complex (Protein Data Bank entry 1DIY). The results of this test indicate that the data are of good quality at this limited resolution and show that conformation of AA bound within the V349A/W387F oPGHS-1 mutant differs from that seen in the native enzyme.

A second validity test, using a series of simulated annealing refinement (see "Experimental Procedures of this chapter), generated a family of AA conformers that were indistinguishable from the conformation of AA bound within the V349A/W387F mutant. All conformers from this refinement series fit the observed density well. The conformer, which best fit the electron density is shown in Figure 13 along with the conformer of AA obtained by model building. Both conformers are bound in the COX channel of the mutant enzyme with the carboxylate group oriented and stabilized at the mouth of the channel by two ionic interactions with the guanidinium group of Arg120 and one with the phenolic oxygen of Tyr355 (Figure 13). From the carboxylate at C1, the

carbons of AA weave through the COX active site making hydrophobic contacts with various side chains along the path to Tyr385. Continuous density was observed from the carboxylate of AA to C12; however; no density was observed past C12. The placement of C13, the site of initiation of catalysis via hydrogen abstraction, was based on the stereochemical constraints imposed by C12 and the C11-C12 double bond. Although there are minor shifts in the position of the C8-C9 and C11-C12 double bonds, both conformers are strikingly similar particularly when comparing the carbon positions of the carboxylate group up to C7.

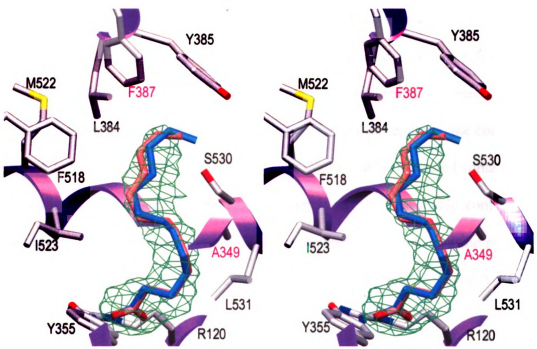

Figure 13 Stereo view of AA bound within the active site of V349A/W387F oPGHS-1. The simulated annealing omit map F_o-F_c density is contoured at 4.0 σ is shown in *green*. Carbon atoms of AA, which were originally built into the electron density, are shown in *pink* (atoms C-1-C12). Carbon atoms of AA obtained from simulated annealing are shown in *blue*. Side chains of various amino acids that line the COX active site and contact the substrate are shown in a color scheme where carbons are *gray*, oxygens are *red*, nitrogens are *dark blue*, and sulfur is *yellow*. Figures presented in Chapter II were created in part using the program SETOR [83].

The family of conformers, including the conformer shown in Figure 13 obtained from the simulated annealing experiments described in experimental procedures section, is shown in Figure 14. Aside from minor differences in atom positions, the four conformations obtained from the simulated annealing refinement starting from the AA bound to native enzyme are all markedly similar to that obtained by model building (Figure 13). The simulated annealing experiments show that the carbon chain weaves up into the active site with the same trajectory for all eight conformers. The results of simulated annealing tests strongly suggest that the X-ray data contain a sufficient amount of information to derive a unique family of AA conformers that differ in conformation from that seen in the native oPGHS-1/AA complex. The conformers in Figure 14A are shown with their ω ends (C13-C20). While there is no observable density for this portion of the substrate, the positioning of these atoms from simulated annealing refinement was entirely guided by the non-bonded energy terms of the molecular dynamics. Although there are no experimental data to validate the positions of these atoms, the conformation of the AA in this region is constrained by energy minimized, non-bonded contacts. Thus, the ω ends of the AA conformers are in stereochemically reasonable conformations. While having a limited level of confidence, it is interesting to note that the positions of the *proS* hydrogens are generally found to cluster in a group near to that of AA found in native enzyme. (Figure 14A).

Structural Comparison of Arachidonic Acid Bound to Native and V349A/W387F PGHS-1

To verify that the two mutations V349A/W387F did not alter the overall integrity of the active site, all atoms of 17 side chains (excluding residues 349 and 387) within the COX active site of native and double mutant were superimposed giving a root mean

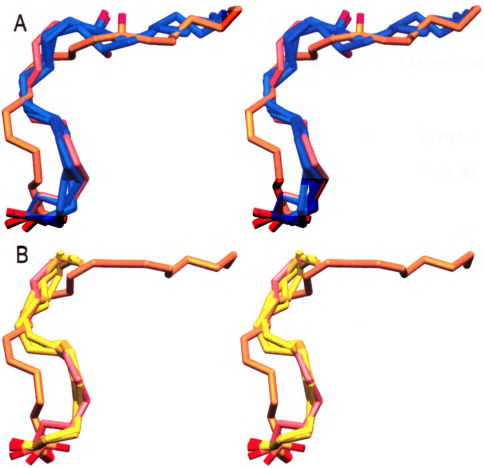

Figure 14 Arachidonic acid conformers obtained from simulated annealing. A. Family of conformers obtained from simulated annealing originated from the starting conformation of AA bound to native oPGHS-1 in the V349A/W387F protein. The starting conformation of AA used in the simulating annealing, shown in *orange*, was used to derive the family of conformers shown in *blue*. For comparison, carbon atoms of AA, which was originally built into the electron density, are shown in *pink*. Oxygens of the carboxylate are colored *red*. Modeled proS hydrogens are shown in *purple*. B. Family of conformers obtained from simulated annealing originating from the starting conformation of AA originally built into observed electron density in the V349A/W387F protein. The family of simulated annealing conformers is showin in *yellow*, the starting conformation used form simulated annealing is shown in *pink*, and for comparison the conformation of AA bound in native oPGHS-1 is shown in *orange*

square deviation of 0.4Å. This indicates that the positions of the active site residues in the crystal structure of the V349A/W387F oPGHS-1 were not significantly perturbed by the presence of the two mutations. The overall binding of AA within the COX active sites of both the native and the double mutant is similar with respect to many of the key ionic and hydrophobic interactions (Table 2).

Although the structure of AA bound to the V349A/W387F mutant is grossly similar to that of AA bound to native enzyme, there are several significant differences. Atoms C3-C6 of AA are shifted into the space created by the Val349Ala substitution (Figure 15). In the native structure, Val349 contacts C3 and C4 (Table 2). In the mutant, these interactions are lost, and C3 and C4 rotate and move into the space created by this mutation. Rotations in this portion of the AA molecule result in large shifts of more rigid regions of AA as evidenced by the significant downward shift of the C5-C6 double bond (Figure 15). The differences in the positions of carbons between AA in the native enzyme versus V349/W387F oPGHS-1 structures are as great as 3.0 Å when taking into account coordinate error of 0.43Å. There is also a significant difference in the location of the C11-C12 double bond of AA, which is moved via rotation about the C9-C10 bond toward the space created by the Trp387Phe mutation. In the native structure, Trp387 makes two contacts with C11 and one with C12 (Table 2). The loss of these contacts in the double mutant contributes to displacement of the C11-C12 bond.

Discussion

Native PGHS-1 forms small amounts of 11*R*-HPETE and 15*R/S*-HPETE in addition to the major product PGG_2. [52, 53]. The monohydroperoxides have little or no biological activity and are considered to be abortive products that result from a failure of

Table 2 Distances between selected side chains atoms of COX active site amino acids and carbons of AA bound to native and V349A/W387F oPGHS-1. The distances listed between the side chain atoms of AA were abstracted from the native oPGHS-1/AA crystal structure (Protein Data Bank 1DIY) [42] or from the distances observed between AA bound to V349A/W387F/AA oPGHS-1 as reported here (Protein Data Bank 1U67). NA, not applicable. The mean coordinate errors of the two structures are both about 0.4Å.

Atom of AA	*Native oPGHS-1 (Residue/atom)*	*Distance (Å)*	*V349A/W387F oPGHS-1 (Residue/Atom)*	*Distance (Å)*
C3	V349/CG1	3.4	A349/CG1	>4
C4	V349/CG1	3.1	A349/CB	>4
C5	I523/CG2	3.3	I523/CG2	>4
C5	V349CB	>4	A349CB	3.0
C6	I523/CG2	3.4	I523/CG2	>4
C6	V349CB	>4	A349CB	3.8
C7	L352/CD2	3.9	L352/CG2	>4
C11	L352/CD2	3.4	L352/CD2	>4
C11	W387/CZ2	4.0	NA	NA
C11	W387/CH2	3.4	NA	NA
C11	NA	NA	F387/CZ	3.7
C11	L352/CD2	3.4	L352/CD2	3.8
C12	L352/CD2	3.9	L352/CD2	>4
C12	Y348/CEZ	3.2	Y348/CEZ	>4
C12	W387/CH2	3.7	NA	NA
C12	NA	NA	F387/CZ	3.7
C12	NA	NA	F387/CE2	3.9

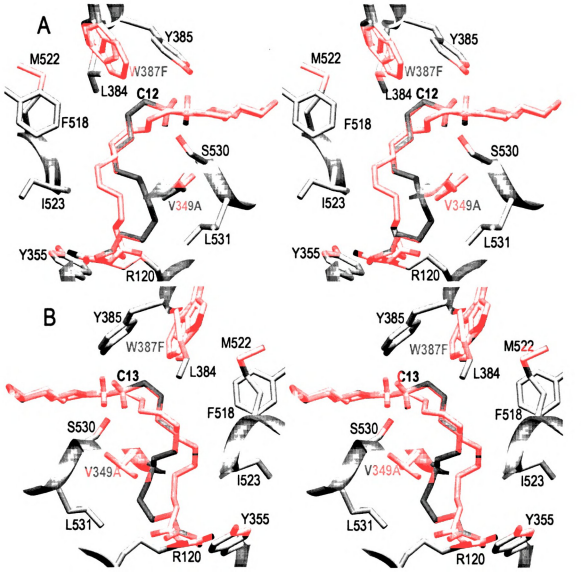

Figure 15 Comparison of AA bound to native and V349A/W387F oPGHS-1. A. stereo view of the superposition of AA bound to the V349A/W387F oPGHS-1 COX site (C1-C12 colored *blue* with the ω end portion ((C-13-C20) obtained from simulated annealing; colored *majenta*) and AA bound to the native oPGHS-1 COX site (colored *orange*). Atoms of amino acids side chains are shown using a color scheme in which carbons are *gray*, nitrogens are *blue*, oxygens are *red*, and sulfur is *yellow*. For clarity only residues Trp^{387} and Val^{349} (both colored *orange*) of the COX active site native PGHS-1 are shown. These latter amino acids were mutated to Phe^{387} and Ala^{349}, respectively, which are shown in *gray*. B. A view of the COX active site rotated 180° with the same color scheme as in A.

the enzyme to form the endoperoxide. In earlier studies, we provided kinetic evidence that the nature of the oxygenated product formed by native PGHS-1 is determined by the conformation of AA when the rate determining step in cyclooxygenase catalysis-abstraction of the 13*proS* hydrogen [25], occurs [52, 53]. We performed the studies reported here as a structural test of this concept. We developed a V349A/W387F mutant of PGHS-1 that forms primarily 11-HPETE, determined the structure of AA in the COX active site of the mutant and finally compared the structures of AA in the native and mutant oPGHS-1.

Previous studies identified Val349 and Trp387 as playing particularly significant roles in guiding formation of the 9,11 endoperoxide group [52, 53, 76]. Substitutions at either site yield mutant enzymes that produce 30-55% 11*R*-HPETE [53]. The fact that the V349A/W387F mutant described here forms mainly 11-HPETE suggests that in native PGHS-1 Val349 and Trp387 function coordinately to facilitate PGG_2 formation.

The structure of AA in the cyclooxygenase site of V349A/W387 oPGHS-1 was observed to be significantly different than that of AA in native PGHS-1. Both AA structures appear to be catalytically competent in that the distances between the phenolic oxygen of Tyr385 and the 13*proS* hydrogen of AA are estimated to be within about 3 Å in both structures; however, it should be noted that the 13- *proS* hydrogen modeled into the AA structure in V349A/W387F oPGHS-1 is more distant than that in the native oPGHS-1:AA complex. Because native and V349A/W387F oPGHS-1 form primarily PGG_2 and 11R-HPETE, respectively, the results of our structural studies are consistent

with the overall model that the product formed by PGHS-1 is determined by the conformation of AA in the cyclooxygenase site when the rate limiting step in the reaction occurs.

Comparisons of the AA structures observed in the native and mutant enzymes and modeling the structure of a putative 11-hydroperoxyl radical into the COX sites suggest how Trp387 and Val349 might participate in forming the endoperoxide group. In the native enzyme there are interactions between Trp387 and both C11 and C12 that are eliminated when Trp387 is mutated to phenylalanine. The interactions between Trp387 and C11 and C12 may (a) constrain the orientation of the C11-C12 bond thereby positioning C11 optimally with respect to C9 and (b) after oxygen insertion at C11, guide rotations of the 11*R*-hydroperoxyl group and the C10-C11 bond to move the hydroperoxyl group towards C9 for an *R* side attack. Mutation of Trp387 to phenylalanine eliminates the steric interactions involving C11 and C12 that direct formation of the endoperoxide group. We suggest that with the mutant enzyme, changes in the rotational freedom about both the C10-C11 bond and the bond between C11 and the peroxyl oxygen allow the 11-hydroperoxyl intermediate to assume unproductive conformations, where the attack by the 11-hydroperoxyl group on C9 is unfavorable and no endoperoxide can be thus formed.

The Val349Ala mutation further contributes to the altered orientation of the C8-C13 portion of AA in the V349A/W387F mutant. Past studies [49, 50, 52, 53, 76] have documented the influence of Val349 on product formation and the stereochemistry of O_2 insertion. The role of Val349 in supporting formation of the endoperoxide group is interesting because the effect is exerted over a relatively long distance. In native oPGHS-

1, Val349 protrudes into the COX channel and the CG1 atom of Val349 contacts C3 and C4 of AA (Table 2) restricting movement of the flexible C1-C5 region at the carboxyl end of AA [42, 53]. When Val349 is mutated to alanine, C3 and C4 of AA rotate into the space created by the mutation and the C5-C6 double bond moves into the newly available space. These results are consistent with the idea that in the native enzyme, Val349 acts as a structural guide to position the carboxyl end of AA [53]. The shifts in the positions of atoms C3-C6 of AA in the V349A/W387F result in a significant change in the final orientation of the C11-C12 bond that, in turn, permits movement of atoms C9-C12 of AA into the extra space created by the Trp387Phe mutation (Figure 15). Thus, in the native enzyme the positioning the carboxyl end of AA by Val349 must facilitate proper positioning of the atoms C8-C13 for hydrogen abstraction and endoperoxide formation.

In summary, residues Val349 and Trp387 in native oPGHS-1 are crucial for ensuring that AA adopts the proper conformation so that the reaction proceeds on course to produce PGG_2 [53]. We have found that V349A/W387F human PGHS-2 also produces predominantly 11-HPETE suggesting that these two residues play similar roles in PGHS-2 (unpublished data). The structural evidence provided by our present study supports the hypothesis that the nature of the products formed in the COX reaction depends on the conformation of AA at the instant of abstraction of the 13*proS* hydrogen. The conformation of AA in the COX site of native oPGHS-1 differs significantly from the conformation of AA in the COX site of V349A/W387F oPGHS-1. This additional, albeit indirect evidence supports the conclusion that the conformation of AA observed in the native enzyme [42, 53] is that which leads to PGG_2 formation.

Acknowledgements

The use of the Advanced Photon Source was supported by the United States Department of Energy, Basic Energy Sciences, Office of Energy Research, under Contract W-31-109-Eng-38. This work was supported in part by Program Project Grant P01 GM57323 and by R01 HL56773-06 and R01 GM68848 from the National Institutes of Health.

[1]This work was previously published in the Journal of Biological Chemistry as an article entitled "Crystal Structure of Arachidonic Acid Bound to a Mutant of Prostaglandin Endoperoxide Synthase-1 That Forms Predominantly 11-Hydroperoxyeicosatetraenoic Acid, Harman, C.A., Rieke, C.J., Garavito, R.M, and Smith, W.L. *J. Biol. Chem.* (2004) 279:42429-42935.

CHAPTER III

MEAD ACID BINDING TO THE COX SITE OF PGHS-1

Introduction

Much of what we know about the substrate specificity of the PGHS enzymes is from kinetic and crystallographic studies with essential fatty acids [52, 56] [42, 49, 50], which are discussed in Chapter I. Essential fatty acids, which include linoleate (18:2, ω6), EPA (20:5, ω3), DHLA (20:3, ω6) and AA (20:4, ω6) must be obtained from dietary means in mammals that lack desaturases capable of incorporating double bonds at positions at or beyond the ω6 position. Thus, fatty acids that possess double bonds at 3 or 6 carbons in from the methyl end (ω-end) of the fatty acid are essential.

Lack of essential fatty acids in the diet leads to a condition called essential fatty acid (EFA) deficiency, which is accompanied by a compensatory accumulation of mead acid (5Z, 8Z, 11Z-eicosatrienoic acid; 20:3, ω9), in cellular membranes. The degree of deficiency can be estimated by the ratio of Mead acid to AA in the phoshoplipids [54, 84, 85]. The pathophysioloical changes associated with EFA deficiency include salt-dependent hypertension [86], inhibition of chronic inflammation [87] and impaired reproductive and epidermal functions [88]. Although these physiological conditions have mainly been attributed to the reduction in the biosynthesis of PGs because of the low availability of AA in the cellular membranes, it has been suspected that Mead acid, a non-essential fatty acid, might act as a substitute for AA [58, 89, 90]. It may therefore be possible that this fatty acid and/or its metabolites contribute to some symptoms of EFA deficiency.

Although Mead acid is a non-essential fatty acid that accumulates in times of EFA deficiency, it is found as the major eicosanoic fatty acid component in normal cartilage [91] and plays a structural role in maintaining necessary membrane fluidity [89]. Despite these mainly structural roles, Mead acid is believed to have a limited metabolic purpose. Interestingly, studies have found that Mead acid can, in fact be metabolized by 5-lipoxygenase to leukotrienes, and by several others enzymes, which include arachionate 12-lipoxygenase, and cytochrome P450, strongly suggesting that Mead acid could substitute for AA [58, 92-94].

The PGHS enzymes have been shown to be capable of utilizing various fatty acids albeit with lower efficiency in vitro [56]. Several studies investigated this possibility with Mead acid as well and found it to be a very poor substrate for the PGHS enzymes; however, trace amounts of products including 11-HETE was shown to be formed from Mead acid by PGHS [58, 90]. The nature of these products demonstrated that Mead acid undergoes a similar reaction mechanism as observed with AA, in which hydrogen abstraction occurs at C13. However, prostaglandin products are not formed from Mead acid. Instead the products resemble that of "abortive" COX reaction products, which suggests that Mead acid cannot support cyclopentane ring formation probably because it lacks the ω6 double bond [90]. This may also explain the low catalytic efficiency observed for Mead acid as substrate for PGHS in that there is no bis-allylic system centered around C13 (missing ω6 double bond), making hydrogen abstraction at C13 more difficult [90, 95]. This is interesting considering that Mead acid is very similar to AA, with the exception of the lack of the ω6 double bond. This highlights the significance of 20-carbon essential fatty acids, which have this crucial ω6

double bond. The majority of the PGHS-1 crystal structures complexed with fatty acids have been with essential fatty acids. These essential fatty acid complexes have exemplified the importance of how the number and position of double bonds result in optimal positioning of the fatty acid for catalysis and thus its ability to be utilized as a substrate. Kinetic and crystallographic studies of PGHS with essential fatty acids have not only shown how these fatty acids bind and undergo oxygenation by PGHS, but also that several of them including DHLA and EPA (both 20 carbons in length) may support endoperoxide formation and cyclopentane ring closure i.e. prostaglandin formation [49, 50, 56, 59]. In an effort to determine why Mead acid, which lacks the ω6 double bond is such as poor substrate for PGHS, we sought to determine a crystal structure of PGHS-1 complexed with Mead acid. This structural study attempts to elucidate whether 1) the lack of the ω6 double bond in Mead acid influences the binding and positioning of mead acid for catalysis, thus making it a poor substrate or 2) the lack of ω6 double bond is more significant in providing the chemical environment for catalysis and cyclization.

Experimental Procedures

Materials

Arachidonic acid and Mead acid were purchased from Cayman Chemical Co. (Ann Arbor, MI). Sf21 insect cells and 100X Antibiotic-Antimycotic were purchased from Invitrogen. Fetal bovine serum and HyQ-SFX insect medium used for cell growth and protein expression of protein used in AA complex were purchased from HyClone (Logan, UT). Ni-NTA superflow resin was purchased from Qiagen, and n-octyl-β-D-glucopyranoside (β-OG) used for crystallization was purchased from Anatrace (Maumee, OH).

Expression of Recombinant Native Ovine PGHS-1 with Cleavable His-Tag

Constructs of PGHS in pFastbac and preparation of baculovirural stocks were previously prepared by Dr. Chong Yuan, in the laboratory of Dr. William Smith. The constructs contained in pFastbac vector have a cDNA encoding native oPGHS-1 and an rTEV (recombinant tobacco etch virus) [96] protease cleavable 8X-histidine tag. DH10Bac cells were transformed with pFastbac vectors to obtain baculoviral DNA, which was then isolated and used to transfect sf21 insect cells to produce recombinant baculovirus. The recombinant baculovirus was amplified, and supernatants of amplifications were used as inoculum stocks. Sf21 insect cells were grown in 1L shaker flasks to an approximate density of 1.7-2.0 $x10^6$ cells/mL in medium containing 1% antibiotic and antimycotic and were then infected with recombinant baculovirus at a multiplicity of infection of 0.1 at 27°C. Three to four days after infection, cells were harvested by centrifugation.

Purification of Recombinant Native Ovine PGHS-1 with Cleavable His-tag and Native Ovine from Ram Seminal Vesicles

Purification of recombinant ovine PGHS-1 from sf21 cells was performed according to a modified procedure developed by Dr. Chong Yuan. Cell pellets from 4L of cells were resuspended in Buffer A (composed of 20 mM Tris-HCl pH 8.0 and 100 mM KCl), homogenized and then lyzed by sonication. To solubilize PGHS from the membranes, $C_{10}E_6$ was added to the lysate up to 0.8% (v/v) which was then incubated at 4° C for 45 min with gentle agitation. Solubilized lysate was centrifuged at 15,000 rpm at 4° C for 20 min, followed by ultracentrifugation at 45,000 rpm at 4°C for 2 hrs. The supernatant was carefully removed and incubated for at least 3 hrs at 4°C with Ni-NTA

resin (Qiagen) equilibrated in Buffer B (composed of 20 mM Tris-HCl, pH 8.0, 300 mM KCl, 5 mM imidazole, 5% glycerol, and 0.1% $C_{10}E_6$). After this incubation period, the mixture of Ni-NTA resin plus supernatant was poured into a column which was washed with four column volumes of Buffer B (composed of 20 mM Tris-HCl, pH8.0, 300 mM KCl, 5 mM imidazole, 5% glycerol, and 0.1% $C_{10}E_6$), Buffer C (composed of 20 mM Tris-HCl pH8.0, 1 M KCl, 20 mM imidazole, 5% glycerol, 20mM galactose, and 0.1% $C_{10}E_6$), and Buffer D (composed of 20 mM Tris-HCl pH8.0, 100 mM KCl, 50 mM imidazole, 5% glycerol, and 0.1% $C_{10}E_6$). The 8X-histidine-tagged PGHS was then eluted with Buffer E (composed of 20 mM Tris-HCl, pH8.0, 100 mM KCl, 250 mM imidazole, 5% glycerol, and 0.1% $C_{10}E_6$). Fractions with the highest specific peroxidase activity [42] were pooled and concentrated using a Millipore Ultrafree -15 spin concentrator (30-kDa molecular weight cut off) to volume 250 μL. To cleave 8X-histidine tag, protein was diluted to 10 mL with Buffer F (composed of 20 mM Tris-HCl, pH8.0, 100 mM KCl, 250 mM imidazole, 5% glycerol, and 0.1 $C_{10}E_6$) to which 2,000 units of rTEV (Invitrogen) was added and allowed to incubate for >12hrs. To remove the rTEV protein and histidine tag from PGHS protein, partially purified mixture was loaded onto a second Ni-NTA, and was washed with two column volumes of Buffer B (composed of 20 mM Tris-HCl, pH 8.0, 300 mM KCl, 5 mM imidazole, 5% glycerol, 0.1% $C_{10}E_6$). PGHS protein lacking the histidine tag was collected in the Buffer B flow thru while the rTEV protein and histidine tag were retained on the column. Purified PGHS was concentrated to ~50 μl and the buffer was exchanged into 1X PBS 0.0.4% β-OG with a final volume being ~100-250 μL of the purifed protein. Protein concentrations were determined using the BCA protein assay (Pierce, Rockford, IL).

Native ovine PGHS-1, which was to be used for crystallization trials was also purified from ram seminal vesicles as previously described [78].

Crystallization and Data Collection of oPGHS-1/MA and oPGHS-1/AA Complexes.

Apo-PGHS-1 obtained from either sf21 cells or ram seminal vesicles was concentrated to least 6-10 mg/mL and prepared for crystallization trials by adding 1.5 molar excess of Co^{3+}-protoporphyrin IX to reconstitute the inactive halo-enzyme. Prior to setting up crystallization experiments, protein was incubated with fatty acid substrates (AA or Mead acid (MA)) at approximately five times the molar concentration of protein. Using the sitting drop vapor diffusion method, 3 μL of protein was mixed with 3 μL of buffer composed of 0.64 M sodium citrate, 0.3-0.9 M LiCl, 0.3% (w/v) β-OG, and 1 mM NaN_3, and equilibrated within reservoir containing 0.68-0.88 M sodium citrate, 0.3-0.6 M LiCl, and 1 mM NaN_3. Crystals appeared within two weeks to several months. Crystals were harvested, briefly soaked in cryosolution containing 1.0 M sodium citrate, 1.0 M LiCl, and 0.5% β-OG and 1M sodium malonate as a cryoprotectant, and then were immediately flash frozen in liquid N_2 (-196°C). Data from both Mead acid and AA protein complexes were collected at beamline 5-ID at COM-cat (Argonne National Lab, Argonne, IL). Data from a single crystal of both complexes were indexed and integrated using DENZO [79] and then scaled with SCALEPACK [79].

Structure Determination and Refinement of oPGHS-1/MA and oPGHS-1/AA Complexes

Both oPGHS-1/MA and oPGHS-1/AA datasets were refined with CNS (version 1.1) [80] in which the protein portion of native oPGHS-1 (Protein Databank entry 1DIY) was used as starting model for rigid body refinement. With each refinement one round of

simulated annealing proceeded rigid body refinement, which was then followed by iterative cycles of minimization, B-factor refinement (bgroup), and model building. Various non-protein portions of the model (i.e. heme, sugars and detergents molecules) were included as the phases improved during the refinement process. Insufficient electron density for Co^{3+}-protoporphyrin and substrate was observed in the oPGHS-1/AA structure, and thus these groups were not included in the refined model. It should be noted that a second dataset of this complex was collected at the same time from the same crystallization experiment. This dataset was also analyzed to see if the electron density for Co^{3+}-protoporphyrin and mead acid improved. Unfortunately, similar results were obtained with this dataset, thus further refinement was not performed.

Minimal electron density for Mead acid in the oPGHS-1/MA structure was observed making it difficult to confidently position Mead acid within the density. As a result Mead acid was not included in the refined model. There was enough electron density for portions of Mead acid, however to conduct simulated annealing experiments described later in this section. Although both models are incomplete, the current R and R_{free} for the oPGHS-1/MA and oPGHS-1/AA complexes are currently 25.1%& 30.1% and 26.6% & 31.0% (Table 3).

Simulated Annnealing Experiments with the oPGHS-1/MA Complex

Because there was enough density observed in the COX active site to indicate some degree of Mead acid binding, several trials of simulated annealing (from CNS version 1.1) were performed in order to obtain conformers that would reasonably fit within the observed electron density. The simulated annealing experiments were

Table 3 Refinement Statistics of oPGHS-1/AA and oPGHS-1/MA Complexes

SCALING	**oPGHS-1/AA**	**oPGHS-1/MA**
Space group	p6522	p6522
Unit cell a=b, c (Å)	183.12, 104.07	182.46, 104.26
# of unique reflections	26,448	24,030
Resolution (Å)	30-2.75	30-2.85
R_{merge}, all data (%; $I > \sigma$)	8.8 (25.3)	8.3 (44.4)
Completeness (%)	97.1 (76.0)[a]	98.5 (81.2)[a]
Average I/σ	15	18.1
REFINEMENT	CNS	CNS
# reflections in refinement	21,301	21462
# of reflections in working set	20293	20422
R & Free R Factor (%) reflections > 1σ on F	26.6 & 31.0	25.1 & 30.1
Included Co^{3+}-protoporhyrin in refinement	no	yes
Included fatty acid substrate in refinement	no	no

[a]Represents values observed in last resolution shell.

performed as follows: Mead acid was placed in the COX active site of the PGHS-1/MA complex and experiments were conducted using the observed structure factors of the oPGHS-1/MA complex. The starting conformation of Mead acid in these experiments

was analogous to the original conformation of AA observed in the native PGHS-1 crystal structure; however, the chemical nature of Mead acid is different in that the ω6 double bond (C14-C15 bond in AA) is missing. Ten trials of simulated annealing were performed creating a comparison of ten separate conformers. Interestingly, the conformers were remarkably different from each other within various regions of Mead acid; in addition, only two of the ten conformers obtained possessed almost identical conformations.

Ki studies of Mead acid with Native oPGHS-1

The K_i of Mead acid was determined by measuring the K_m of AA (concentration curve of 2, 5, 25, 50, 100 μM) at fixed concentrations of 0, 2, 10, and 25 μM of mead acid. Cyclooxygenase assays were performed at 37°C by monitoring the initial O_2 uptake using an oxygen electrode as previously described in [52] and in "Experimental Procedures" of Chapter II. An exception to these procedures was that the enzyme and Mead acid were added together to assay buffer and the reaction was initiated with AA. The apparent K_m of AA at each concentration of Mead acid was calculated from non-linear regression of AA saturation curves and was plotted against mead acid concentration to obtain the K_i of mead acid.

The IC_{50} value for Mead acid was also determined by measuring the rate reduction of PGHS at constant AA concentration with increasing amounts of Mead acid. The experiments were conducted at a constant concentration of 50 μM AA and sequential increasing Mead acid concentrations until an ~50% reduction in the rate was observed.

Results and Discussion

Analysis of the oPGHS-1/AA Complex

Native oPGHS-1/AA structure was determined to 2.75 Å resolution. Well-defined density (contoured to 1σ) was observed for the protein portion in which various side chains and carbonyl groups of the protein backbone were easily distinguishable. In addition, high quality of density was observed for some but not all of the sugar residues, which include two sugars at Asn68, two sugars at Asn144, and two sugars at Asn410. Although these portions of the structure were clearly observed, density for the Co^{3+}-protoporhyrin and AA were not as well defined being only sparingly observed at contour levels below 2.5σ (Figure 16).

In previous structures, significant and well-defined density has been observed for Co^{3+}-protoporphyrin, particularly the Co^{3+} ion; therefore, the lack of density in this region of the structure was surprising and an indication of low occupancy possibly as a result of insufficient reconstitution of Co^{3+}-protoporphyrin. Several reasons could explain the lack of binding of Co^{3+}-protoporphyrin. First, Co^{3+}-protoporphyrin does not bind as well as heme, which is required for PGHS activity. In addition, the Co^{3+}-protoporphyrin stock used for these crystallization studies could have been oxidized therefore, could not bind to PGHS efficiently. The combination of these two possibilities could explain the low occupancy of Co^{3+}-protoporphyrin in this structure. Density in the COX active site, where AA normally binds was also very minimal. As with previous structures, density in the vicinity of Arg120 and Tyr355 was usually observed. In some cases, density originating from the mouth of the active site up into the channel was also

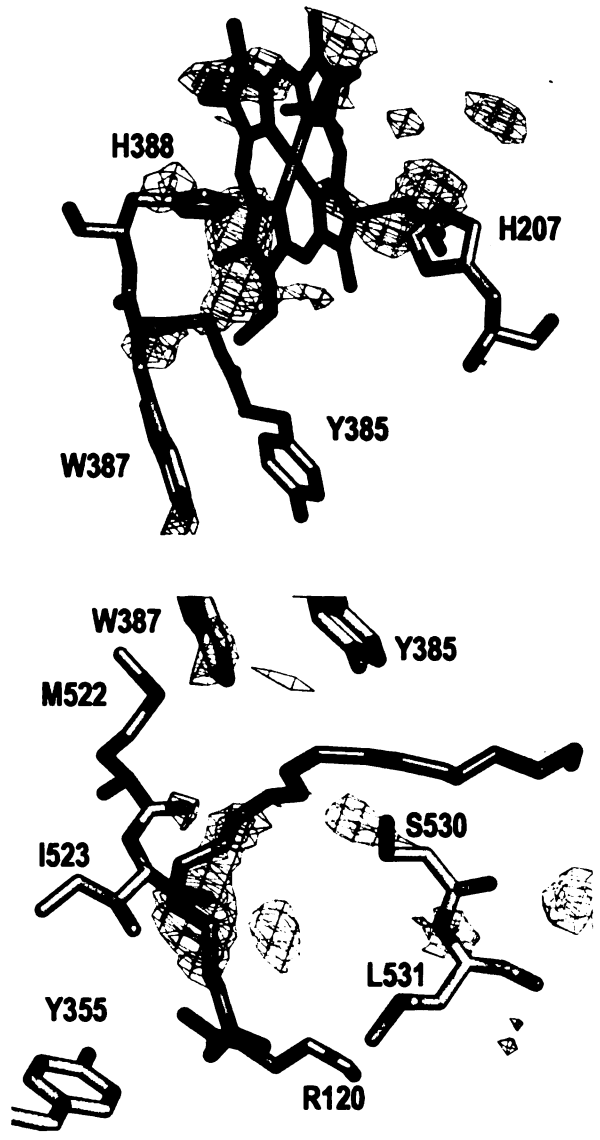

Figure 16 View of electron density observed in the POX and COX site of native PGHS-1. The top figure shows the observed electron density within the POX site at two contour levels of 2.5σ (*green*) and 3.0σ (*magenta*) and superimposed within the site for comparison is the Co^{3+}-protoporphyrin from the original PGHS-1 structure (1diy). Bottom figure shows the electron density observed in the COX site also shown at two contour levels (same as in A). AA from the original native PGHS-1/AA complex (1diy) was superimposed for comparison in the COX active site

observed. In this case, no density was observed near the mouth; however, a slight elongated bulge of density (contoured to 2.5σ) was observed further up in the channel, possibly representing carbons C3-C6 (Figure 16). The lack density for AA again

indicates low occupancy, which is possibly a consequence of insufficiently bound Co^{3+}-protoporphyrin. Studies have indicated that with apo-PGHS-1 there is a lower affinity for ligands as compared to the halo form of PGHS.

Because the electron density for both Co^{3+}-protoporphyrin and AA was insufficient, these two significant portions of the structure were not included; therefore, specific structural information could not be obtained from this structure complex. Although this model could not serve as a comparison to the oPGHS-1/MA structure, there were several major advances made in the process of obtaining this structure with respect to purification and crystallization. This was the first time that crystallization trials were performed with PGHS in which the 8X-histidine tag was removed. In this series of experiments, removal of the histidine tag helped facilitate faster crystallization of PGHS since crystals of PGHS having the histidine tag removed appeared in 1-2 weeks as compared to PGHS still possessing the histidine tag appearing after 2-4 month or longer.

There is the possibility that the reduced time for crystallization could be a result of increased purity of PGHS. This construct of PGHS-1 encoded a longer histidine tag, an 8X-histidine tag, in this case, as compared to the previous constructs with a 6X-histidine tag. A longer histidine tag may be more beneficial in that it can enhance the binding i.e. by binding more tightly, thus allowing a more stringent washing of the column which in turn would more effectively remove impurities before elution of protein. In this case, it would be difficult to determine if the decreased time to grow crystals is a result of more pure protein or removal of the histidine tag. Several experiments thus far suggest that removal of the histidine tag may play the greater role; however, purer protein may also assist in improving conditions for crystal growth.

Analysis of the oPGHS-1/Mead acid Complex

The structure of oPGHS-1/MA complex was determined to 2.85Å. Well-defined density was observed for the protein portion of the structure as well as most of the non-protein substructure including heme and several sugars residues. Unlike the native PGHS-1/AA structure, density for the Co^{3+}-protoporphyrin group in the native PGHS-1/MA complex was complete and very well defined with a large density peak for Co^{3+} ion observable to a contour level up to 5σ indicating Co^{3+}-protoporphyrin is bound with high occupancy. Initial Fo-Fc density contoured to 2.5-3σ within the COX active site indicated the presence of bound Mead acid; however, the density was not continuous up through the COX channel. A large peak of density was observed near the mouth in addition to a second larger elongated peak reaching up into the COX channel to approximately Tyr385 (Figure 17). AA from the original native PGHS-1/AA structure was used as a guide in fitting Mead acid into the density with the carboxylate group being placed into the peak of density observed at the mouth as a starting point fitting the remaining carbon chain into the portion of density observed further up into the channel. Although electron density was observed within the COX active site indicating Mead acid was bound, at best the density only showed possible placement of atoms C1-C10. However, placement of atoms C2-C10 was difficult to do with confidence. This difficulty in placing Mead acid in that density is not unusual given that there are probably many conformers that exist and that all or most of these conformers could reasonably fit the electron density observed for mead acid. To remedy this situation of multiple conformers that would reasonably fit the observed electron density, simulated annealing

experiments similar to those discussed in Chapter II were performed. These experiments provided a means to utilize the x-ray information observed for the carboxylate portion

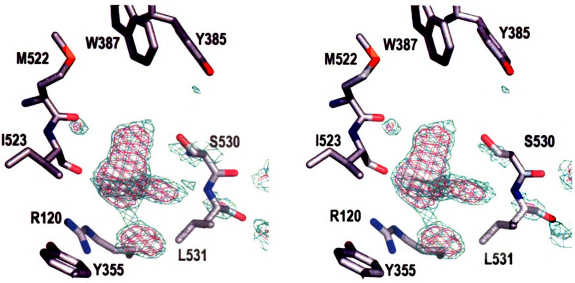

Figure 17 Initial Fo-Fc electron density observed in the COX active site of oPGHS-1/MA complex. Electron density is shown at two contour levels of 2.5σ (*green*) and 3.0σ (*magenta*).

of Mead acid and combine it with molecular dynamics, which would treat the portions of Mead acid having no observed structural information. Ten trials of simulated annealing experiments were performed as described in the "Experimental Procedures" section of this chapter, and ten conformations were obtained. The conformers overall appear to grossly fit the limited electron density; however, some conformers have a better overall fit than others (Figures 18).

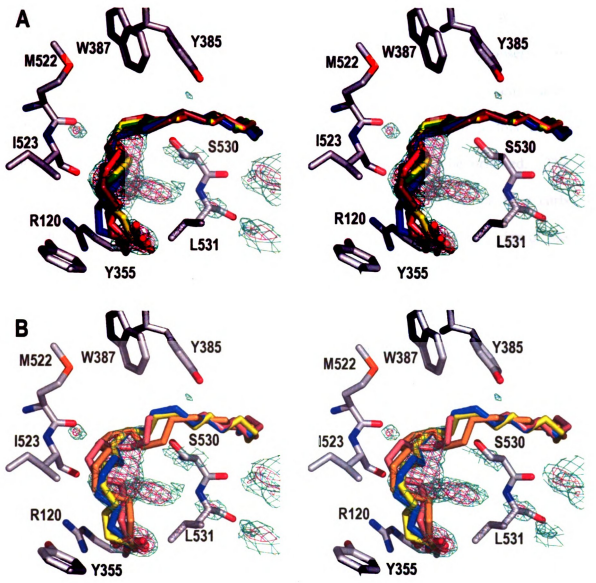

Figure 18 Comparison of catalytically possible and inhibitory conformations of mead acid obtained from simulated annealing. A. Comparisons of the six catalytically possible conformers of mead acid obtained from simulated annealing within Fo-Fc electron density shown at two contour levels 2.5σ (*green*) and 3.0σ (*magenta*). Of the six conformers, two have almost identical conformations (*green* and *yellow*). B. Comparison of the four inhibitory conformers of Mead acid obtained from simulated annealing shown within the Fo-Fc density (same density as shown in A).

There are significant differences observed between the conformers. With all the conformers, the carboxyl group fit well within the small peak of density observed near the mouth of the COX active site; however, extreme deviations start to occur reaching atoms C2-C4, which is one region missing electron density. The trajectory of these atoms is crucial in how the remaining atoms in the chain will be oriented. These simulated annealing experiments reveal that there is much variability in these carbon positions, which may account for the lack of well-defined density for this region of Mead acid. The same may be true for the ω-end (atoms C14-C20) of Mead acid. Mead acid would have more flexibility within its ω-end as compared other fatty acids such as DHLA, which has the C14-C15 double bond, and EPA having an addition double bond at position C17-C18. Interestingly, the mead acid conformers obtained from simulated annealing reflect this concept, in which significant variations occur near or at the C14-C15 bond position resulting in extreme variation in position of the C13 atoms, and its modeled in pro*S* hydrogen. Comparing the position of the modeled pro*S* hydrogens of all the conformers, two groups of conformers were observed as being those in a catalytically possible conformation and those in an inhibitory conformation. Of the ten conformers, six are those of the catalytically possible conformers (including conformers 1, 3, 4, 6, 8, 9), while the remaining four conformers (conformers 2, 5, 7, 10) are considered to be of inhibitory binding mode appearing unable to support the abstraction of the C13 pro*S* hydrogen of mead acid.

In comparing the positions of the modeled pro*S* hydrogens of the catalytically possible conformers, the pro*S* hydrogens, ranging in distances of 2.7-3.2Å from Tyr385, the catalytic residue, appear to be in reasonable positions for potential abstraction (Figure

19). Interestingly, the carboxyl end and ω-end of each of the "catalytically possible" conformers do vary significantly; despite these variations in the carboxyl end of mead acid, the trajectory of the carbon chain up to C13 of each conformer eventually aligns with Tyr385 for the potential abstraction of the pro*S* hydrogen at C13.

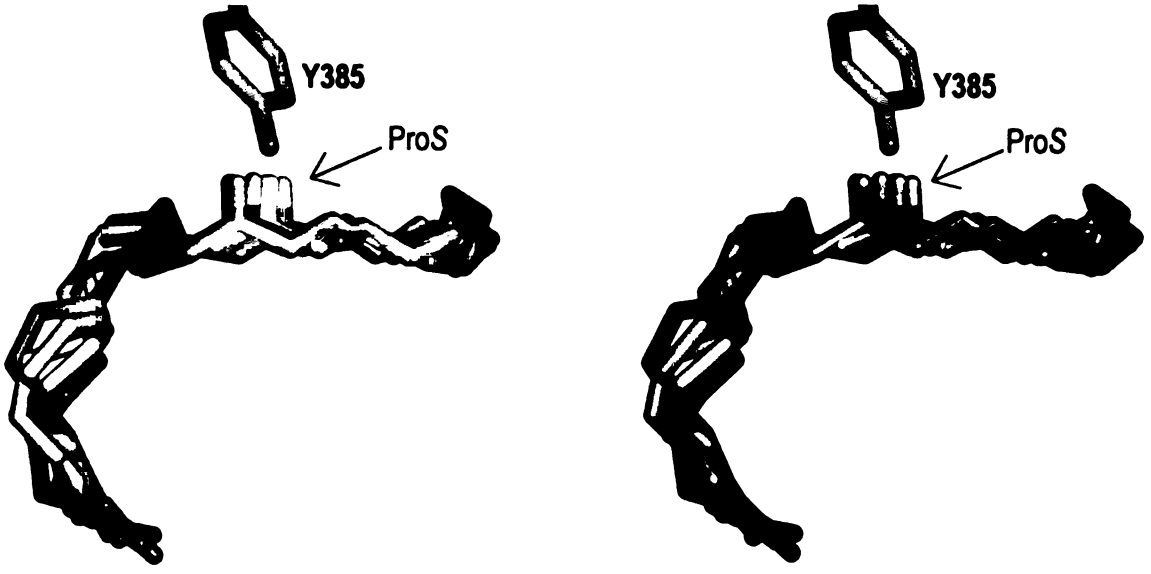

Figure 19 Comparison of the modeled pro*S* hydrogen positions of the catalytically possible conformers obtained from simulated annealing. Despite having significant differences in atom positions within the carboxyl half and ω-end of Mead acid, the pro*S* hydrogens are oriented towards Tyr385 within distances ranging from 2.8-3.3Å.

When comparing how the two groups of conformers fit the observed electron density within the COX site, the catalytically possible group of conformers appears to fit the density better than the inhibitory conformers (Figure 18). The electron density, therefore, seems to reflect an average conformer, which may be more similar to average of the catalytically possible conformers. However, lack of density for atoms near or at atom C13, in addition to there being so much variation observed within the carboxyl end of all the conformers, this suggestion is just speculation.

The inhibitory conformers differ significantly from the catalytically possible conformers particularly in areas near atoms C13-C15 of mead acid. Comparison of the carbon positions between the catalytically possible conformers and the inhibitory conformers reveal that the effects of missing the ω6 double bond (C14-C15 double bond) is more pronounced with the inhibitory conformers being reflected by the extremely altered position of C13. The modeled pro*S* hydrogens at C13 of three of the four inhibitory conformers are positioned in such as way as to not support potential hydrogen abstraction since the pro*S* hydrogens of these conformers are oriented in opposing directions with respect to the position of Tyr385 (Figure 20).

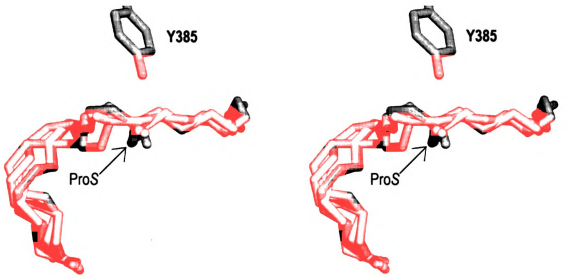

Figure 20 Comparison of the modeled pro*S* hydrogen positions of the inhibitory binding conformers obtained from simulated annealing. The pro*S* hydrogens are shown in very altered positions relative to Tyr385 demonstrating these binding modes are unlikely to support catalysis. Conformer shown in orange (conformer 7) is observed as being significantly different than the other three conformers.

Interestingly, this type of binding mode was captured in the crystal structure of EPA bound to PGHS [49]. Unlike the other inhibitory conformers, the modeled pro*S* hydrogen at C13 of conformer 7 is somewhat oriented up towards Tyr385; however, it is too far removed from the Tyr385 for potential abstraction (Figure 20).

These structural results are consistent with the fact that Mead acid is a poor substrate for PGHS, being that it cannot be metabolized very efficiently. Trace amounts of products are formed and were found to resemble that of abortive COX products such as 11-HETE, thus suggesting that Mead acid undergoes a similar sequence of catalytic steps beginning with the abstraction of the pro*S* hydrogen, the rate limiting step. The simulating annealing experiments reflect this in demonstrating that Mead acid can bind a majority of the time in a conformation such that abstraction of the C13 pro*S* hydrogen is possible. Interestingly, the simulated annealing experiments also revealed that Mead acid could bind in a mode that would not support catalysis (i.e. bind within the active site in an inhibitory conformation). This opened up the possibility that Mead acid could actively compete with AA in binding and may act as an inhibitor of PGHS. EPA is known to be a potent inhibitor of PGHS. This was further evidenced by the crystal structure of the PGHS-1/EPA complex in which EPA was captured bound in an inhibitory manner with the pro*S* hydrogen at C13 being oriented in the opposing direction of Tyr385 making potential abstraction unlikely [49]. The *Ki* of Mead acid was measured to test the ability of Mead acid to act as an inhibitor of PGHS-1. The *Ki* was determined to ~62 μM (Figures 21 & 22), in addition, the IC_{50} of Mead acid was found to be ~100 μM at 50 μM AA. These results indicate that mead acid can compete with AA and inhibit PGHS activity to some degree. However, when comparing the *Ki* of Mead acid to the K_m of AA

determined to be 9 μM with no Mead acid present (Figure 21), in addition to the IC_{50} values ranging from 0.3-50 μM of various NSAIDs [71] and the indomethacin ethanolamides [97] described later in Chapter IV, it appears that Mead acid

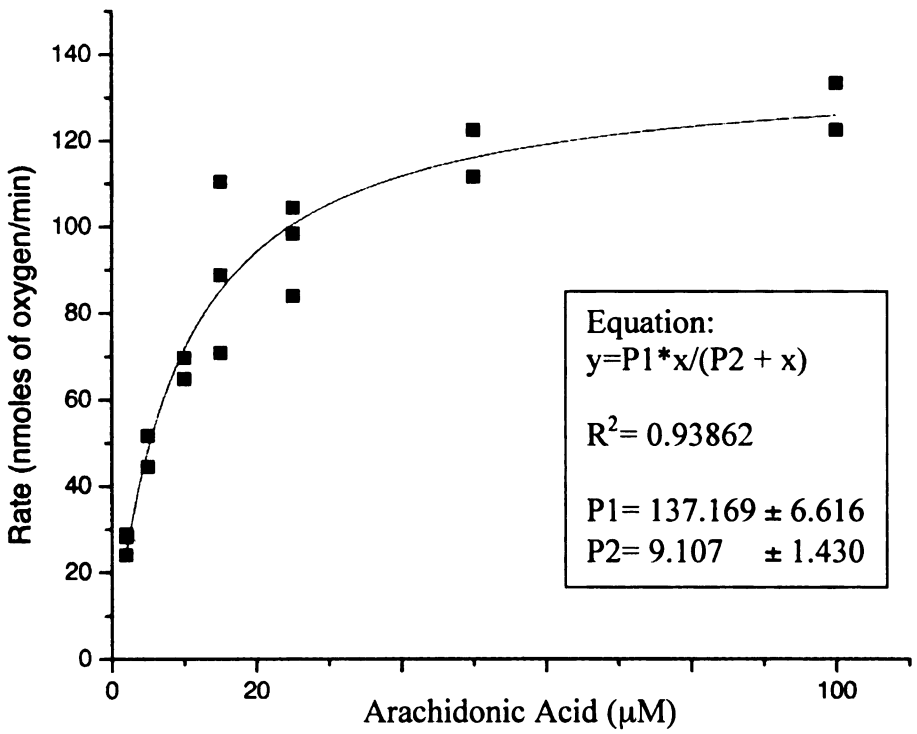

Figure 21 Arachidonic acid saturation curve of PGHS. Shown is one of four non-linear regression fits (from Origin) of an AA saturation curve of PGHS at 0 μM Mead acid. All data, including at least two measurements for each concentration of AA along the curve was included in the non-linear fit. P1 and P2 represent V_{max} and K_m, both of which were varied in the non-linear regression fit (V_{max}=137.2 and K_m=9.1 at zero mead acid concentration). Non-linear regression fits of AA saturation curves of PGHS in the presence of 5, 10, and 25 μM were plotted similarly in Origin. With the regression of each of these plots, the P1 (V_{max}) was fixed at 137.2 while varying P2 (K_m) to obtain the apparent K_m of AA at various Mead acid concentrations. To determine *Ki* of Mead acid the apparent K_m were replotted against Mead acid concentration and results are shown in Figure 22.

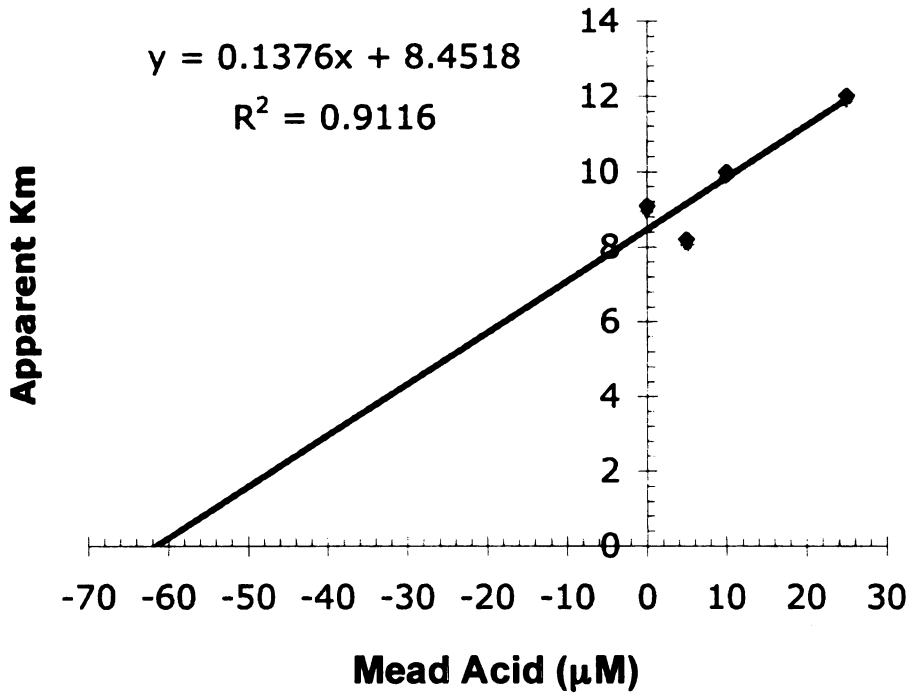

Figure 22 The K_i plot of Mead acid. The apparent K_m values obtained from similar saturation curves shown in Figure 21 were plotted against the Mead acid concentration. The K_i represented by the x-intercept was determined to be ~62 μM. The equation of the regression and correlation coefficient (R^2) are displayed in the graph.

is not a very potent inhibitor of PGHS. This is interesting given that Mead acid, although a poor substrate appears to bind to the COX site so how can it not be a potent inhibitor. One explanation is that Mead acid just does not bind as well as AA. This is evidenced by observing the variability in carbon atoms positions of ten conformers obtained from the simulated annealing experiments. In addition, the limited density observed for mead acid in the COX active site possibly indicates low occupancy of Mead acid within the COX site. As a result of increased flexibility within the ω-end (atoms C14-C20) of Mead acid

as compared to other fatty acids such as EPA or DHLA, a stable binding conformation may not be able to be achieved. The density observed for the carboxylate group of Mead acid near that mouth is shifted from the position of the carboxylate group of AA in PGHS-1/AA complex. The consequence of this difference in the placement of the carboxylate group of Mead acid is a loss of the interaction between the carboxylate group of Mead acid and guanidium of Arg120 being a significant interaction for high affinity binding of AA and other fatty acids as well as various NSAIDs with a free carboxylate. With the loss of this interaction as a result of increased flexibility within the ω-end, Mead acid may not be able to stabilize an interaction with Arg120, thus preventing it from binding as efficiently as AA.

These studies with mead acid demonstrate that the ω6 double bond found in essential fatty acids appears to not only play an important role in the positioning the C13 pro*S* hydrogen of 20 carbon fatty acids with respect to Tyr385, but appears to be significant in achieving high affinity binding of essential fatty acids to PGHS-1. Although six of the ten conformers obtained from simulated annealing indicate that it is possible for Mead acid to bind in a catalytically possible conformation allowing for potential hydrogen abstraction at C13, a combination of the kinetic studies with Mead acid and the limited electron density observed in the COX active site suggest that Mead does not bind as efficiently as the essential fatty acids AA, DHLA, and EPA to PGHS-1, thus may explain why this fatty acid is a poor inhibitor as well as a substrate of PGHS-1.

CHAPTER IV

STRUCTURAL BASIS OF ENANTIOSELECTIVE INHIBITION OF COX-1 BY (S)-α-SUBSTITUTED INDOMETHACIN ETHANOLAMIDES

Introduction

Non-steroidal anti-inflammatory drugs (NSAIDs) provide therapeutic benefit through the direct inhibition of the COX enzymes; however, the anti-inflammatory and analgesic properties of NSAIDs are mainly a result of inhibition of COX-2. Although non-selective inhibition of COX-1 by aspirin can be beneficial in reducing the risk of mortality from cardiovascular disease, the use of aspirin and other NSAIDs has been associated with undesirable gastrointestinal side effects such as stomach ulcers and intestinal bleeding [71, 98]. The predominant role of COX-2 in pain and inflammation spawned the development of selective inhibitors, which target only the COX-2 isoform in order to achieve analgesic and anti-inflammatory properties with minimal associated gastrointestinal toxicity. However, cardiovascular side effects have recently been documented for at least certain COX-2 inhibitors (eg. rofecoxib, valdecoxib).

Structural and functional studies comparing COX-1 and COX-2 have identified some general structural features of NSAIDs binding to the COX active site, in addition to highlighting subtle biochemical differences between the isoforms that have been exploited in the development of COX-2 selective inhibitors [39-41]. The entrance to the COX active site is made up in part by a bundle of four amphipathic helices, which leads to a constriction comprised of residues Arg120, Tyr355, and Glu524. The COX active site then opens into a long hydrophobic channel that extends deep into the core of the

catalytic domain of the protein. Sitting above the constriction and aside the main hydrophobic channel is a smaller, amphipathic region referred to as the "side pocket". A major difference in the active site of the isoforms arises mainly as a result of a valine substitution in COX-2 for isoleucine in COX-1 at position 523. This small change provides enough additional space to allow better access to the side pocket of COX-2. The active site of COX-2 can therefore accommodate the extra bulk of the sulfonamoylphenyl or methylsulfonylphenyl moieties of COX-2 selective inhibitors, particularly those of the diarylhetercyclics (celecoxib, rofecoxib), by placing them in the side pocket.

The potential for interaction between moieties of the drug and residues within the side pocket of COX-2 also seems to be responsible for a phenomenon known as time-dependent inhibition by COX-2 selective NSAIDs. Although diarylheterocycles competitively inhibit COX-2 better than COX-1, their lack of time-dependent inhibition behavior towards COX-1 further enhances their selectivity towards COX-2 [99, 100]. The structural explanation for the lack of time-dependent inhibition towards COX-1 is the extra methyl group of isoleucine at position 523, which restricts access of COX-2 inhibitors to the side pocket in COX-1.

An addition feature of COX-2 selective inhibitors, which may contribute to their low affinity towards COX-1, is that they lack a free carboxylate group. Several crystal structures of COX-1 and COX-2 have shown that NSAIDs with a free carboxylate moiety form an ionic interaction with Arg120, which is located at mouth of the COX active site [39, 41, 42, 101]. This interaction between the carboxylate of acidic NSAIDs and Arg120 appears to be essential for substrate binding to COX-1, as site-directed

mutagenesis studies of COX-1 have demonstrated that the binding of AA and acidic NSAIDs was greatly perturbed when Arg120 is mutated to smaller uncharged residues [67]. In contrast, the equivalent mutations of Arg120 seemed to suggest that electrostatic interactions with this residue in COX-2 were not at all critical for catalysis or NSAID inhibition [68].

Modification of the carboxylate group of the non-selective NSAID indomethacin generates a wide range of ester and amide adducts yielding an array of COX-2 selective inhibitors [102]. The majority of these indomethacin derivatives were shown to be potent and selective for COX-2; however, an exception was observed with the α-substituted indomethacin ethanolamides series of derivatives [97]. The (*R*)/(*S*)-α-substituted indomethacin ethanolamides both demonstrated potent inhibition of COX-2; however, the (*S*)- α-substituted indomethacin ethanolamides inhibited COX-1 as effectively as COX-2. Interestingly, the chiral preference observed with COX-1 inhibition was consistently observed with (*S*) enantiomers across a wide range of α-substitutions (Table 4). Mutagenic studies in COX-2 were unable to identify residues around the COX active site that contributed to the observed chiral selectivity. To understand the structural basis of this chiral discrimination in COX-1, we determined the crystal structures of ovine COX-1 complexed with the α-ethyl substituted enantiomeric pair of these indomethacin ethanolamides. These structures not only provide intriguing insight into the structural basis for the stereo selective binding of the (*S*)-α-substituted indomethacin ethanolamides to COX-1, but also provides an illustration of how COX-1 can bind a non-carboxylate containing inhibitor with high affinity.

Table 4 Comparative inhibition of native COX-1 and COX-2 by various α-substituted indomethacin ethanolamides. Data shown in table was obtained from previously published study by Kozak et al. [97]

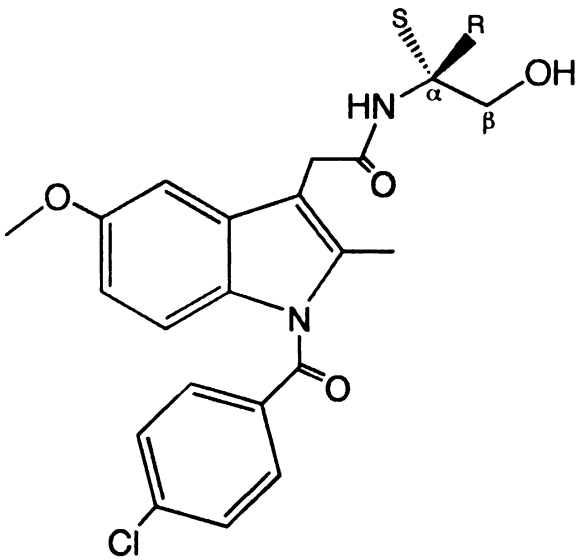

Compound ID	α-substituent	ovine COX-1 IC_{50} (μM)	human COX-2 IC_{50} (μM)
6	(R)-CH_3	33	0.17
7	(S)-CH_3	0.59	0.27
8	(R)-CH_2CH_3	59	0.10
9	(S)-CH_2 CH_3	0.35	0.28
14	(R)-$CH_2CH_2SCH_3$	51	0.25
15	(S)-$CH_2CH_2SCH_3$	2.3	1.0
16	(R)-C_6H_5	47	0.44
17	(S)-C_6H_5	<1.3	0.085

Experimental Procedures

Materials

Detergents $C_{10}E_6$ used for solublization and n-octyl-β-D-glucopyranoside (β-OG) used for purification and crystallization was purchased from Anatrace (Maumee, OH). Hemin was purchased from Sigma (St. Louis, MO). Compound 8 (Indomethacin-(*R*)-α-ethyl-ethanolamide) and compound 9 (Indomethacin-(*S*)-α-ethyl-ethanolamide) used in crystallization experiments were synthesized according to the procedures described in Kozak et al. [97]. The nomenclature as compounds 8 and 9 refers to their earlier designation [97].

Crystallization of native ovine COX-1/inhibitor complexes

COX-1 used for crystallization was purified from ram seminal vesicles as previously described [78]. Protein was prepared for crystallization trials by adding 1.5 molar excess of hemin to reconstitute the protein. Inhibitors at a concentration of 100 μM of either compound 8 or compound 9 were then added to protein and left to incubate for at least 10 min before setting up crystallization experiments. Using the sitting drop vapor diffusion method, 3 μL of protein was mixed with 3 μL of buffer composed of 0.64 M sodium citrate, 0.3-0.9 M LiCl, 0.3% (w/v) β-OG, and 1 mM NaN_3, and equilibrated within reservoir containing 0.68-0.88M sodium citrate, 0.3-0.6 M LiCl, and 1 mM NaN_3. Crystals appeared within 2-3 weeks

Data Collection of oCOX-1/Comp8 and oCOX-1/Comp9 complexes

Crystals were harvested, briefly soaked in a solution containing 1.0 M sodium citrate, 1.0 M LiCl, and 0.15% (w/v) β-OG, and 1 mM sodium malonate as a

cryoprotectant. Crystals were then flash frozen in liquid nitrogen at -165°C. Data collection on crystals of COX-1/drug complexes was performed at beamline 5-ID at COM-cat (Argonne National Lab, Argonne, IL). Data from a single crystal of COX-1/complexed with compound 8 (COX-1/Comp8) was indexed and integrated using DENZO [79] and then scaled with SCALEPACK [79]. Datasets collected from two crystals of COX-1/complexed with compound 9 (COX-1/Comp9) were indexed and integrated separately and then merged together during scaling using SCALEPACK.

Structure Determination and Refinement with CNS

The COX-1 structures complexed with compound 8 or compound 9 were determined using native COX-1 structure (Protein Databank entry 1DIY) as a phasing model for rigid body refinement utilizing CNS version 1.1 [80]. After an initial round of simulated annealing, several iterative cycles of positional and group B-factor refinement and model building in which sections of model including several sugar molecules, detergent molecules, in addition to fitting inhibitors were performed. To further complete the model, water molecules were included and were followed by additional refinement.

Structure Determination and Refinement with REFMAC

The COX-1/Comp9 and COX-1/Comp8 datasets were also refined with REFMAC version 5.0 in the CCP4 program suite [103]. REFMAC refinement for the COX-1/Comp9 dataset started with the protein portion of COX-1/Comp9 structure refined by CNS (Protein Databank entry 1DIY). The COX-1/Comp9 structure was initially put through TLS refinement [104] and then restrained positional refinement. Each round of refinement included 10 cycles of TLS at fixed B-factor of 40, followed by

20 cycles of restrained refinement (which included positional refinement followed by B-factor refinement). A single TLS group consisting of protein residues 33-580 was used for the TLS portion of refinement. Iterative cycles of TLS/restrained refinement were followed by cycles of map calculation and model building. As refinement progressed, the TLS group was expanded to include protein, in addition, to heme, sugars, detergent molecules and compound 9 as they were included in the model. After adding heme, six saccharide groups, and a glucopyranoside head group from β-OG, and approximately 20 waters, the R and R_{free} converged at 23.9% and 29.7%. The same refinement protocol was applied to the COX-1/Comp8 dataset to complete the comparison of the two refinement programs (Table 5).

Result and Discussion

Comparison of CNS vs. REFMAC Refinement for COX-1/inhibitor complexes

There was a significant difference in the R factors obtained from CNS as compared to REFMAC with the COX-1/Comp9 and COX-1/Comp8 structures (Table 5). Although, the crystallographic R factors differ noticeably, the electron density maps obtained from both refinement programs were virtually identical, especially with respect to the electron density observed for the inhibitor in the active site. The shape of the electron density was identical, and the inhibitor orientation determined in CNS refinement fit easily into the density obtained from refinement with REFMAC. The significant difference in the refinement statistics between CNS and REFMAC may not be unusual given that each program utilizes different methods and algorithms to calculate bulk solvent and other

Table 5 Summary of data collection and refinement statistics.

SCALING	COX-1/Comp8		COX-1/Comp9	
Spacegroup	$P6_522$		$P6_522$	
(a) Å	181.72		181.40	
(b) Å	181.72		181.40	
(c) Å	104.09		103.40	
Resolution Å	2.85		2.70	
No. of unique reflections	24,207		28,072	
Completeness	97.4 (82.9)[a]		99.9 (100)[a]	
R_{merge}	7.8 (24.1)[a]		9.7 (33.5)[a]	
REFINEMENT	**CNS**	**REFMAC**	**CNS**	**REFMAC**
No. of used reflections	22932	22275	23511	26478
No. of atoms in refinement	4598	4641	4575[b]	4653[b]
R-factor (%)	24.2	21.7	28.3	24.1
Free R (%)[c]	29.6	26.1	33.5	29.2
Mean positional error (Å)	0.45	0.49	0.54	0.58
r.m.s.d. bond length (Å)	0.008	0.013	0.013	0.014
r.m.s.d. bond angle (°)	1.60	1.78	1.76	1.56
Average B-factor				
protein	68.9	72.6	54.2	49.3
inhibitor	95.3	87.1	87.0	55.2
citrate	73.5	94.7	NA	NA

[a]Values in parentheses represent values in highest resolution shell

[b]The number of atoms included in refinement differ since some atoms were not included in CNS refinement.

[c]Free R was calculated with 5% of reflections set aside as the test set which is

parameters during refinement. This is particularly true for the TLS (translation/libration/screw) refinement procedure in REFMAC [104, 105], which better treats the static and dynamic disorder arising from rigid body displacement than traditional B-factor refinement.

Binding of Compound 8 vs. Compound 9 in the COX site

The electron density maps obtained from both CNS and REFMAC refinement of the COX-1/Comp8 structure shows that compound 8 binds in an orientation that closely resembles the way the parent compound, indomethacin, binds to the enzyme [41, 101]: the chlorobenzyl group is orientated up to the apex of the channel by Y385, the methoxy group of the indole ring points towards the COX-2 side pocket, and the ethanolamide group is positioned towards the mouth of the channel near R120 and Y355 (Figure 23). The hydroxyl group of the ethanolamide moiety of compound 8 makes a hydrogen bond with the guanidinium group of R120 (Figure 23). The electron density for compound 9, the (*S*)-stereoisomer, in the COX-1/Comp9 structure, obtained from refinement with either CNS and REFMAC, clearly shows an elongated stretch of electron density within the side pocket region of the COX active site defined by residues Gln192, His90, L517, Phe518, Ile523 (Figure 24A). This contrasts with what is seen with the COX-1/Comp8 complex. The orientation of compound 9 that best represents the observed electron density is with the chlorobenzyl moiety orientated towards the mouth, the methoxy group points towards the top of the channel by Y385, and the ethanolamide group is positioned in this side pocket region (Figure 24 A&B). The ethanolamide group of compound 9 makes many interactions with the hydrophilic and hydrophobic residues of the side pocket with the hydroxyl group making hydrogen bonds with His90 and Gln192 and several hydrophobic interactions with Phe518 and Ile523 (Figure 24 B). An additional hydrophilic interaction is observed between the guanidium group of Arg120 and the carbonyl group of the chlorobenzyl moiety oriented at the mouth of the active site. The extra density that is observed in the side pocket of the COX-1/Comp9 complex is the

major difference observed in the electron density maps between the two complexes thus indicating two different and contrasting modes of binding for Compound 8 and 9.

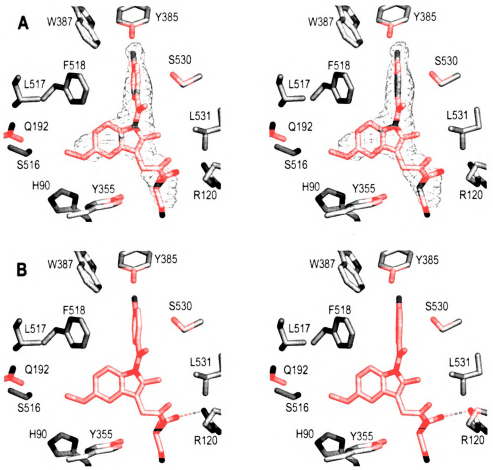

Figure 23 Compound 8 bound in the COX active site. A. Stereo view of compound 8 bound in the COX active site with simulated annealing omit map difference density (*blue*) contoured to 4σ. Various residues within the active site are shown with carbons for compound 8 shown in *orange*, oxygen *red*, nitrogen *blue*, and chlorine *magenta*. B. Stereo representation of compound 8 bound in the COX site in the same manner as the parent compound indomethacin; the chlorobenzyl group oriented up towards the top of the channel, the methoxy group on the indole ring points towards the side pocket (L517, F518, I523, Q192, S516), and the ethanolamide group with *R*-ethyl substitution sits next to R120 and Y355 at the mouth of the active site. Carbons atoms of compound 8 are shown with same color scheme as in (A). The hydroxyl group of ethanolamide group makes a hydrogen bond with R120, while the *R*-ethyl group is positioned just outside the mouth of the active site.

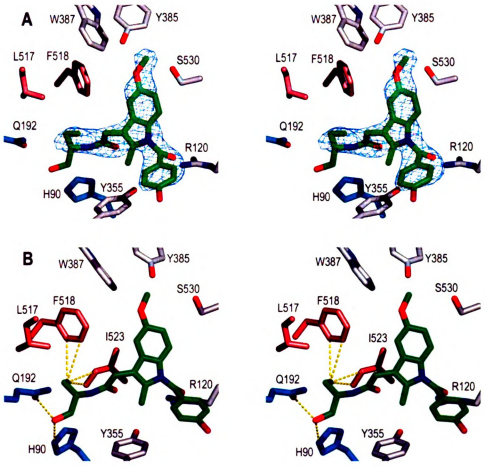

Figure 24 Compound 9 bound in the COX active site. A. Stereo view of compound 9 fitted into simulated annealing omit map difference density (*blue*) coutoured to 4σ. Carbons atoms of compound 9 are colored *green* with heteroatoms colored same as in Figure 23. B. Compound 9 bind much differently than 8: the chlorobenzyl group is oriented towards the mouth of the active site, the methoxy group of indole ring is oriented up into the top of the channel, and the ethanolamide group with the S-ethyl substitution lies within the side pocket region of the channel. The hydroxyl group of the ethanolamide is oriented near the hydrophilic region (*cyan*) of the side pocket making hydrogen bonds with residues Q192 and H90 while the *S*-ethyl group is oriented into the more hydrophobic region (*pink*) of the side pocket making Van der Waals intereactions with I523 and F518.

Evaluation of the Structural Basis for Stereoselectivity

The inhibitor complexes suggest that the distinctly different binding modes for compound 8 and compound 9 arise as a result of the ability of one enantiomer to optimize binding interactions within the side pocket. The ethanolamide moiety of compound 9, which is able to access the side pocket in COX-1, utilizes both the hydrophilic and hydrophobic properties of the COX-1 side pocket; the hydroxyl group of the ethanolamide makes hydrogen bonds to residues Gln192 and His90, while the ethyl group makes several hydrophobic contacts with residues Ile523, Phe518, and Leu517 (Figure 24 B). The binding mode of compound 9 is analogous to the way COX-2 selective inhibitors bind to COX-2 suggesting that the side pocket in COX-1 is accessible depending on the nature of the substitutents present in the inhibitor. Structure-activity studies, which systematically evaluated various substitutions at the α-position of indomethacin ethanolamides, found that altering the hydroxl group influenced the chiral-dependent selectivity towards COX-1 to some degree [97]. When the hydroxyl group was replaced with either a methoxy or methyl group the chiral dependence changes so that the (*R*) enantiomers were more potent against COX-1 than the corresponding (*S*) enantiomers. Collectively, these results suggest that the inability of the (*R*) enantiomers to inhibit COX-1 was not merely due to an increase in unfavorable steric interactions, but also dependent on the loss of favorable binding interactions. This is demonstrated in the crystal structures presented here in that an elaborate network of interactions is needed to favor the more stable binding mode of compound 9. Conversely, the binding mode of compound 8 observed in the crystal structure displays a quite different set of interactions, where none occur within the side pocket. Instead, the ethanolamide moiety of compound

8 is oriented towards the mouth of the active site, making one hydrophilic interaction between the hydroxyl of compound 8 and guanidium group of Arg120 (Figure 23 B).

To visualize why compound 8 does not adopt the same binding mode as compound 9, compound 8 was modeled in COX active site by positioning the ethanolamide moiety within the side pocket (Figure 25 A). With the hydroxyl group of the ethanolamide positioned to make potential ionic interactions with Q192 and H90, the

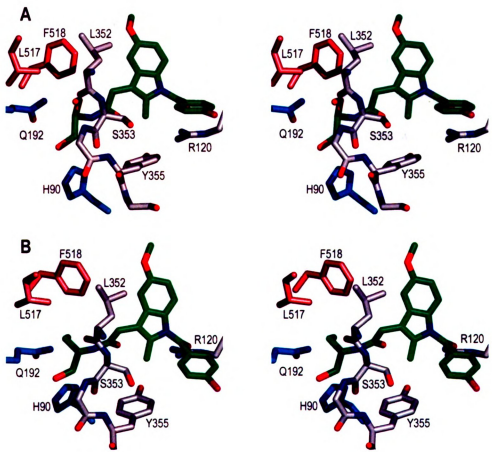

Figure 25 Comparison of the placement of the (*R*)-ethyl vs. (*S*)-ethyl group in COX-1 side pocket. A. Stereo view of compound 8 modeled in the COX active site as compound 9 would bind. The R-ethyl group of 8 (*orange*) is positioned so that the hydroxyl group is in an orientation where it could hydrogen bond with Q192 and H90. B. Stereo of compound 9 bound within the COX active site for comparison of the position of the ethyl group.

R-ethyl group was unable to take advantage of similar hydrophobic interactions observed for compound 9 (Figure 25 B) because the ethyl group is oriented in the opposite direction of the *S*-ethyl group of compound 9. In addition, it became clear that the *R*-stereochemistry made it more difficult to avoid steric clashes particularly with the protein backbone between residues 352 and 355.

Anomalous ligand interactions in the COX-1/Compound 8 Structure

During inspection of the COX-1/Comp8 structure, significant Fo-Fc electron density (contoured to 4σ) was observed near the heme within the peroxidase active site. The shape of the density appeared to resemble citrate, which is present in the crystallization buffer. After including citrate in the model refinement, the refined density from CNS showed that citrate fit well (Figure 26). Citrate is bound with one of its

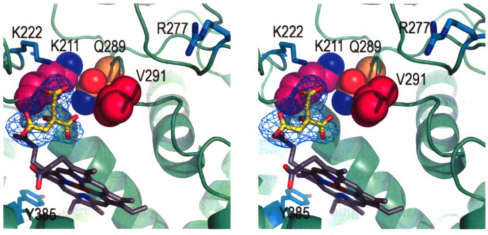

Figure 26 Citrate bound in the POX site. Stereo view of citrate bound in the POX site of the COX-1/Comp8 structure with simulated annealing omit map density (*blue*) contoured to 3σ. Citrate (carbons *yellow*, oxygen *red*) is straddled between heme (carbon *gray*, oxygen *red*, nitrogen *blue*, iron *rust*) and Lys222 (carbon *cyan*, nitrogen *blue*). Residues proposed to interact with PGG_2, the substrate of the peroxidase are shown as spheres. Site of trypsin cleavage is near residue R277.

carboxylate groups interacting with one of the propionate groups of heme. A second interaction involves the amino group of Lys222 interacting with another one of the carboxylate groups of citrate (i.e. citrate is straddled between the heme and Lys222) (Figure 26). An additional hydrophilic interaction occurs with the hydroxyl group of citrate and the same propionate group of the heme. Structure refinement using REFMAC did not improve the electron density around the citrate in the peroxidase active site as markedly as refinement with CNS. Nonetheless, both refinement experiments clearly suggest that citrate weakly binds to the peroxidase active site as suggested by the observed electron density and temperature factors. The potential relevance of citrate binding to the peroxidase active site is that Lys222 is located in the immediate vicinity of several residues (Lys211, Gln289, and Val291) proposed to interact and possibly stabilize binding of PGG_2, the substrate of the peroxidase reaction (Figure 26) [106, 107].

What makes the observation of citrate binding interesting is that it was not observed in the peroxidase site of the COX-1/Comp9 structure, despite the fact that the crystallization conditions and crystal handling protocols were identical in both cases. Thus, are there structural differences in inhibitor binding, which may favor binding of citrate in one case and not the other? Previous studies have shown that binding of inhibitors to the COX site can conribute to stabilizing POX activity [108]. Several crystal structures of different COX-1/ligand complexes (including NSAIDs and fatty acid substrates) were superimposed onto the COX-1/Comp9 and COX-1/Comp8 structures. All of the active site residues displayed only small, and not statistically significant, changes in conformations; however, in the COX-1/Comp8 structure, Arg120 adopts a significantly altered conformation in order to accommodate the binding of compound 8.

Unlike the more extended conformation seen in the COX-1/Comp9 structure and most other COX-1 crystal structures, Arg120 is found in a more kinked configuration in the COX-1/Comp8 structure (Figure 27). This structural readjustment of Arg120 results in a slight widening of the mouth to the COX active site suggesting that the binding of compound 8 may cause local strain, which may, in turn, be manifested in a faster dissociation rate for compound 8. This model for why compound 8 is a weaker inhibitor

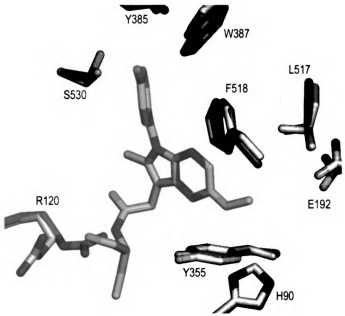

Figure 27 Compound 8 (*orange*) bound in the COX active site after the structures of COX-1 complexes were superimposed. The *green* residues represent the positions observed in the COX-1/Comp9 structure and the *gray* residues show their positions in the COX-1/Comp8 structure. The only residue to show a significantly altered conformation is R120: in the COX-1 complex R120 is extended, while it is kinked in the COX-1/Comp8 complex. This conformational change upon binding of compound 8 may be the result of some local strain. One consequence of this adjustment of R120 conformation is that the mouth of the active site becomes wider, suggesting that compound 8 may have a faster dissociation rate as compared to compound 9.

than compound 9 is currently being tested. The observation of citrate binding to the POX site in the COX-1/Comp8 structure, but not in the COX-1/Comp9 structure makes the altered conformation of Arg120 more intriguing. Past studies have shown that inhibitor binding can protect the COX-1 enzyme from cleavage of an exposed peptide loop located near the POX site by trypsin (Figure 26) [109, 110]. Further studies have revealed there is differential protection from trypsin cleavage depending on the ligand binding in the COX site suggesting that the binding of different ligands may induce different extents of conformation changes, resulting in varying sensitivities to protease cleavage [111]. Thus, we speculate that the strained binding of a weak COX-1 inhibitor, like compound 8, promotes citrate binding to the peroxidase active site, while the tighter binding mode of compound 9 disfavors citrate binding. However, the mechanism for transmitting the subtle structural differences occurring in the POX site arising from ligand binding to the COX active site is unknown.

Summary

The COX-1 complexes of compounds 8 and 9 provide some initial clues about the physical parameters that define the modes of binding and chiral selectivity of these α-substituted indomethacin ethanolamides. Several unanswered questions still remain: (a) why (*S*)-α-substituted ethanolamides with quite bulky R-groups bind just as well as the *S*-stereoisomers with less bulky R-groups, (b) how bulky an R-group can the COX-1 side pocket accommodate, and (c) would the binding mode of the (*S*)-α-substituted compounds shift if the R-group gets too bulky? The crystal structure of the COX-1/Comp9 complex clearly shows there is enough space for the ethyl group, but this may not be the case for larger moieties.

A recent computer modeling study [112] investigated the basis of stereo-selective binding using several indomethacin ethanolamides possessing the larger isopropyl substituent. Although, the binding modes obtained for the (*S*)-series of inhibitors were not similar to that seen in the COX-1/Comp9 structure, they did reveal that the molecule having the *R*-isopropyl group had to maintain a constrained conformation in order to achieve the same binding interactions as the *S*-enantiomer. This directly supports what was observed in the crystal structure in that the binding of compound 8 induces strain within the protein as evidenced by altered conformation of Arg120.

However, the physical basis for the chiral selectivity of COX-1 for a wider range of R-groups may turn out to be much more complicated than simple steric hindrance. For example, the strong interactions between the ethanolamide group of compound 9 compensates for the lack of a strong interaction between a carboxylate group and Arg120 and Tyr355 being necessary for high affinity binding in COX-1. Crystal structures of COX-1 complexed with α-substituted indomethacin ethanolamides having larger R-group substitutions may provide further information about interactions that define the different binding modes within the COX active site.

Acknowledgements

All data presented here was collected at COM-CAT (Sector 32 beamline) at Advanced Photon Sources (Argonne, IL), and thus we would like to thank Joe Brunzelle of LS-CAT for his assistance during our time at COM-CAT. This work was supported in part by the United States Department of Energy, Basic Energy Sciences, Office of Energy Research, under Contract W-31-109-Eng-38 and by grants R01 HL56773, P01 GM57323, and R01CA89450 from the National Institute of Health.

CHAPTER V

FUTURE DIRECTIONS

Structural Studies of PGHS-1

Although there are many reported structures of PGHS-1 that are invaluable in providing an understanding of the catalytic mechanism, product formation, substrate specificity and inhibition, there are still more protein/ligand complexes of PGHS-1 that are of interest for future studies. Several interesting mutants yet to be studied structurally are those favoring formation of 15-HETE, another abortive product that is produced in minor amounts by native PGHS-1 and PGHS-2. Residues within the hydrophobic pocket of the COX site that contact the ω-end of AA appear to be involved in proper positioning of the ω-end of AA thereby influences PGG_2 formation. When these residues are mutated product formation is shifted to favor 15-HETE; therefore, it would be interesting to study these mutant proteins structurally. With the reproductive success of obtaining high quality crystals of native and mutant PGHS complexed with various ligands, this process has shown to be applicable in pursing further structures of AA and other fatty acids bound to mutants of PGHS.

The conformation of arachidonic acid bound to a mutant that make predominantly 15-HETE

We know that native PGHS enzymes are not 100% efficient in forming PGG_2 from AA as observed by formation of minor amounts of the abortive products 11-HETE and 15-HETE, in addition, the conformation of AA at the moment of hydrogen

abstraction will favor a particular product. With a crystal structure of AA bound to a mutant of PGHS that forms predominantly 11-HETE (Chapter II), a different conformation of AA was observed and increased our understanding of how 11-HETE is formed. Mutation studies have revealed that there are residues that when mutated will favor formation of 15-HETE. How PGHS forms 15-HETE is not well understood structurally; however, possible mechanisms explaining 15-HETE formation have been proposed and focus on the positioning of AA in the active site as well as how this influences the stereochemical addition of oxygen at C15.

Oxygen addition at C15 is of much interest because the stereochemistry of oxygen addition at the C15 position has shown to be more variable with mutants of PGHS-1 that favor 15-HETE formation as compared to oxygen addition at C11 with mutants favoring 11-HETE, being exclusively the *R*-enantiomer. Although native PGHS-1 forms exclusively 15S-HETE, various mutations have not only influenced the products formed but also the stereochemistry in which a mixture of *R/S* 15-HETE is formed with the 15*S*-HETE enantiomer being the predominant enantiomer. Understanding the stereochemistry of oxygen addition a C15 in PGHS-1 is even more intriguing when considering the case of aspirin acetylated PGHS-2, in which the 15*R*-HETE enantiomer is formed exclusively [70, 113]. Thus, alterations of particular residues within the COX active of both isoforms result in not only favoring the formation of 15-HETE, but can also change the stereochemistry of oxygenation at this position of AA.

Although many elegant experiments have led to a basic understanding of the residues involved in influencing the shift from PGG_2 to 15-HETE in both PGHS-1 [53] and PGHS-2 [76, 113, 114], the structural basis of how oxygenation first occurs at C15

and how these residues influence the stereochemistry is not clear in either PGHS-1 or PGHS-2. There are two single mutations in PGHS-1 that have been shown to shift the product profile to favor formation of 15-HETE from AA having both the *R/S* stereochemistry. These mutations include L534A, favoring formation of ~50% 15*S*-HETE and V349L, favoring formation of ~30% 15-HETE with 70% *S* to 30% *R* [53]. Potentially, a V349l/L534A mutant of PGHS-1 may form predominantly 15-HETE, and therefore, could be used for structural studies. A crystal structure of AA bound to this mutant could demonstrate the adopted conformation AA that leads to 15-HETE, in addition to gaining some structural information about the influence of residues on the stereochemistry of oxygen addition at C15 of AA.

Arachidonic acid binding to G533A PGHS-1

The residue G533 lies at the distal end of the cycloxygenase channel where the Cα carbon abuts up against the last two carbons of the ω end of AA [42]. Mutation of G533 to alanine in ovine PGHS-1 and human PGHS-2 result in loss of COX activity; however, POX activity is retained [53]. Interestingly, this same mutant in murine PGHS-2 still has both COX and POX activity [115]. Residue G533 having a drastic effect on catalysis when mutated is far removed from the site of catalysis, thus it is thought from structural analysis that this residue influences the positioning of the ω-end of AA allowing for optimal placement of C13 for abstraction. However, it is unclear if catalysis is lost as result of a misalignment of C13 upon binding of AA or if the mutation at G533 simply prevents binding of AA. A crystal structure of AA bound to oPGHS-1 G533A mutant would be of major interest for two reasons. This structure would not only demonstrate that AA is binding to the G533A mutant, but could also show the binding

conformation of AA and in turn show the significance in positioning of the ω-end and how this would effect catalysis.

Indomethacin Ethanolamides/PGHS-1 crystal structures

Chapter IV revealed the structural basis of how the stereochemistry of the indomethacin ethanolamides can affect how these novel inhibitors bind and ultimately effect the degree of inhibition of PGHS-1. Although some knowledge was gained from crystal structures of an enantiomeric pair of these inhibitors, questions still remain as to the physical basis for chiral selectivity of COX-1 with indomethacin ethanolamides with a wider range of R-group substituents. The side pocket of COX-1 can accommodate an ethyl substitution (Table 4, Compound 9), but possibly not larger R-groups (Table 4, Compounds 14-17), thus is there may be a shift in binding modes that would explain how these inhibitors with bulkier R-groups would bind. The results obtained from Chapter IV do provide testable conclusions and hypotheses. Mutating residues that have been shown to interact with the inhibitors, particularly Phe518, Leu517, and Gln192 could highlight their roles in stabilizing the binding modes of compound 9 via hydrogen bonding and hydrophobic interactions. In addition, more detailed binding experiments comparing the association/dissociation rates of compound 8 and 9 could clarify chiral selectivity based on the binding dynamics of these inhibitors. Lastly, as mentioned in Chapter IV, a crystal structure of an α-substituted indomethacin ethanolamide having a larger R-group substitution bound to COX-1 could demonstrate a shift in binding modes when the R-group gets too bulky for the side pocket. A good candidate R-group substitution for a structure complex would be a phenyl group substitution (Table 4, Compound 17). This

group would be a good representative because of its larger size and limited flexibility, thus electron density could be easily recognized within the active site.

Structural Studies of PGHS-2

There are have several structures of PGHS-1 bound to various fatty acids that have been significant in elucidating the structural basis of binding and oxygenation of these various fatty acids; however, there is very little known structurally about how these fatty acids bind to PGHS-2. There have been at least two published crystal structures of AA bound to PGHS-2; however, these structures have provided no clear structural understanding of fatty acid binding because the AA was bound in an unproductive conformation [116, 117]. The reason as to why AA was captured in this conformation is interesting and may predict a future problem in obtaining fatty acid complexes with PGHS-2, nonetheless, further structures are needed to understand the differences in substrate specificity of the two isoforms.

Crystallization of human PGHS-2 complexed with fatty acids

Crystallization of human PGHS-1 has s been a very difficult task; however, several recent approaches have been successful in obtaining diffraction quality crystals of human PGHS-2. Several constructs of PGHS-2 have been made (Dr. Chong Yuan in the lab of Dr. Smith) in order to 1) obtain highly purified protein and 2) increase ability of protein to crystallize. The range of constructs made so far include an rTEV cleavable N-terminus 8X-histidine tag, and an rTEV cleavable 8X-histidine tag located just before 18-amino acid (aa) cassette at C-terminus of PGHS-2. Another construct of interest is a native PGHS-2 with a histidine-tag inserted just before the 18-aa cassette thus allowing

simultaneously cleavage of the histidine-tag and the C-terminus using the endogenous trypsin cleavage site located near to the 18-aa cassette region of PGHS-2. The benefit of these constructs is to use the histidine-tag for purification and then cleave off the histidine tag to reduce possible problems in crystallization arising from the presence of the histidine tag. In addition, the 18-aa cassette of PGHS-2, which is not crucial to catalytic activity of PGHS, has never been observed crystallographically possibly because it is very flexible and therefore may be a problem in crystallization. Thus, removal of the 18-aa insert may improve the chances of obtaining crystals.

Recently, crystals have been obtained of a PGHS-2 construct having both the his-tag and 18-aa cassette removed (Figure 28) from crystallization conditions that had previously been know to crystallize PGHS-2 [118]. The crystals, being extremely fragile diffracted to approximately 5-6Å and currently a preliminary space group is being determined. Future work will include reproducing these crystals and optimizing conditions to reduce the time to grow and possibly increase the stability of the crystals so that multiple substrate and inhibitor complexes can be obtained consistently.

Figure 28 Crystal of human PGHS-2 grown in the presence of AA.

Structures of human PGHS-2 with various fatty acid

Most of the structural information of fatty acid binding to PGHS was obtained with PGHS-1 mostly because of the robustness of PGHS-1 crystallization. Thus, once reproducible crystallization conditions are established for PGHS-2 mirror structures of various substrate complexes with PGHS-2 can be obtained for comparison.

Interesting differences in substrate specificity between the two isoforms have yet to be understood on a structural level. As mentioned previously, only one crystal structure of PGHS-2, the murine form, with the substrate bound has been reported. This structure captures AA bound in an unproductive conformation in which the carboxylate group was oriented up into the hydrophobic channel. The observation that AA was captured in a "backwards" configuration within the COX active site of PGHS-2 might indicate the difficulty in capturing a catalytically competent conformation of the substrate. PGHS-2 is known to be the more promiscuous of the isoforms in utilizing various fatty acids. PGHS-2 was able to selectively oxygenate 2-arachidonyl glycerol, an endocannabinoid, with similar efficiency as AA while PGHS-1 was not. The fatty acid, 2-arachidonyl glycerol, in comparison to AA, has a glycerol group in place of carboxylate group (C1 attached via the 2 position of glycerol). This increases the size of this fatty acid, thus it is suggested that PGHS-2 can utilize this fatty acid more efficiently than PGHS-1 because it can bind within the larger PGHS-2 active site. Interestingly, this substrate may prove to be useful. The extra bulk of the glycerol group, may force a binding orientation most likely a productive conformation within the PGHS-2 active site. Therefore, a productive conformation of a fatty acid may be obtained and at the same time show how this interesting fatty acid binds within the PGHS-2 active site.

Crystal structures of PGHS-2 with indomethacin ethanolamides

With preliminary structural results of how this compounds bind to PGHS-1, comparative structures with PGHS-2 would be very interesting. The crystal structures of indomethacin ethanolamides bound to PGHS-1 described in Chapter IV reveal two binding modes as a result of a separate set of binding interactions, which apparently stabilize the inhibitors. Comparing the binding of these inhibitors, which inhibit PGHS-2 with similar and better efficiency could emphasize and validate similarities of binding between PGHS-2 and PGHS-1. Specifically, it could provide a clearer understanding of the binding mode of Compound 9 in PGHS-1 as well as understanding the binding mode of Compound 8 in PGHS-2 and how it would compare to PGHS-1.

REFERENCES

1. Smith, W. L., Garavito, R. M. & DeWitt, D. L. (1996) Prostaglandin endoperoxide H synthases (cyclooxygenases)-1 and -2, *J Biol Chem. 271*, 33157-33160.

2. Marnett, L. J., Rowlinson, S. W., Goodwin, D. C., Kalgutkar, A. S. & Lanzo, C. A. (1999) Arachidonic acid oxygenation by COX-1 and COX-2 - Mechanisms of catalysis and inhibition, *J Biol Chem. 274*, 22903-22906.

3. Smith, W. L., DeWitt, D. L. & Garavito, R. M. (2000) Cyclooxygenases: Structural, Cellular, and Molecular Biology, *Annu Rev Biochem. 69*, 149-182.

4. Smith, W. L. & Murphy, R. C. (2002) The eicosanoids: cyclooxygenase, lipooxygenase, and epoxgenase pathways in *Biochemistry of Lipids, Lipoproteins, and Membranes* (Vance, D. E. & Vance, J. E., eds), Elsevier Science B.V., Amsterdam.

5. Oates, J. A., Fitzgerald, G. A., Branch, R. A., Jackson, E. K., Knapp, H. R. & Roberts, L. J. (1988) Clinical Implications of Prostaglandin and Thromboxane A-2 Formation 2, *New Engl J Med. 319*, 761-767.

6. Oates, J. A., Fitzgerald, G. A., Branch, R. A., Jackson, E. K., Knapp, H. R. & Roberts, L. J. (1988) Clinical Implications of Prostaglandin and Thromboxane-A2 Formation 1, *New Engl J Med. 319*, 689-698.

7. Smith, W. L. & Marnett, L. J. (1991) Prostaglandin Endoperoxide Synthase - Structure and Catalysis, *Biochim Biophys Acta. 1083*, 1-17.

8. Katori, M. & Majima, M. (2000) Cyclooxygenase-2: its rich diversity of roles and possible application of its selective inhibitors, *Inflamm Res. 49*, 367-392.

9. Kargman, S. L. & al., e. (1995) Expression of Prostaglandin G/H synthase-1 and -2 protein in human colon cancer, *Cancer Res. 55*, 2556-2559.

10. Kino, Y., Kojima, F., Kiguchi, K., Igarashi, R., Ishizuka, B. & Kawai, S. (2005) Prostaglandin E2 production in ovarian cancer cell lines is regulated by cyclooxygenase-1 not cyclooxygenase-2, *Prostaglandins, Leukot Essent Fatty Acids. 73*, 103-111.

11. Fletcher, B. S., Kujubu, D. A., Perrin, D. M. & Herschman, H. R. (1992) Structure of the mitogen-inducible TIS10 gene and demonstration that the TIS10-encoded protein is a functional prostaglandin G/H synthase, *J Biol Chem. 267*, 4338-4344.

12. Dietz, R., Nastainczyk, W. & Ruf, H. (1988) Higher oxidation states of prostaglandin H synthase. Rapid electronic spectroscopy detected two spectral intermediates during the peroxidase reaction with prostaglandin G2, *Eur J Biochem. 171*, 321-328.

13. Tsai, A. L., Wu, G., Palmer, G., Bambai, B., Koehn, J. A., Marshall, P. J. & Kulmacz, R. J. (1999) Rapid kinetics of tyrosyl radical formation and heme redox state changes in prostaglandin H synthase-1 and-2, *J Biol Chem. 274*, 21695-21700.

14. Kujubu, D. A., Fletcher, B. S., Varnum, B. C., Lim, R. W. & Herschman, H. R. (1991) TIS10, a Phorbol Ester Tumor Promoter-inducible mRNA from Swiss 3T3 Cells, Encodes a Novel Prostaglandin Synthase/Cyclooxygenase Homologue, *J Biol Chem. 266*, 12866-12872.

15. Murakami, M., Kambe, T., Shimbara, S. & Kudo, I. (1999) Functional coupling between various phospholipase A(2)s and cyclooxygenases in immediate and delayed prostanoid biosynthetic pathways, *J Biol Chem. 274*, 3103-3115.

16. Fitzpatrick, F. A. & Soberman, R. (2001) Regulated formation of eicosanoids, *J Clin Invest. 107*, 1347-1351.

17. Smith, W. L. & Langenbach, R. (2001) Why there are two cyclooxygenase isozymes, *J Clin Invest. 107*, 1491-1495.

18. Schuster, V. L. (1998) Molecular mechanisms of prostaglandin transport, *Annu Rev Physiol. 60*, 221-242.

19. Nishio, T. & al., e. (2000) Molecular identification of a rat novel organic anion transporter moat1, which transports prostaglandin D(2), leukotriene C(4), and taurocholate, *Biochem Biophys Res Commun. 275*, 831-838.

20. Chan, B. S., Bao, Y. & Schuster, V. L. (2002) Role of conserved transmembrane cationic amino acids in the prostaglandin transporter PGT, *Biochemistry. 41*, 9215-9221.

21. Boie, Y. & al., e. (1997) Molecular cloning and characterization of the four rat prostaglandin E2 prostanoid receptor subtypes, *Eur J Biochem. 340*, 227-41.

22. Wise, H. (1999) Characterization of chimeric prostacyclin/prostaglandin D(2) receptors, *Eur J Biochem. 386*, 89-96.

23. Sarrazin, P. & al., e. (2001) Characterization of the prostaglandin receptors in human osetoblasts in culture, *Prostaglandins Leukot Essent Fatty Acids. 64*, 203-210.

24. Negishi, M., Sugimoto, Y. & Ichikawa, A. (1995) Molecular mechanism of diverse actions of prostanoid receptors, *Biochim Biophys Acta. 1259*, 109-119.

25. Hamberg, M. & Samuelsson, B. (1967) On the mechanism of the biosynthesis of prostaglandins E-1 and F-1-alpha, *J Biol Chem. 242*, 5336-5343.

26. Hamberg, M. & Samuelsson, B. (1967) Oxygenation of unsaturated fatty acids by the vesicular gland of sheep, *J Biol Chem. 242*, 5344-5354.

27. Shimokawa, T., Kulmacz, R. J., DeWitt, D. L. & Smith, W. L. (1990) Tyrosine 385 of prostaglandin endoperoxide synthase is required for cyclooxygenase catalysis, *J Biol Chem. 265*, 20073-20076.

28. Tsai, A. L., Hsi, L. C., Kulmacz, R. J., Palmer, G. & Smith, W. L. (1994) Characterization of the tyrosyl radicals in ovine prostaglandin H synthase-1 by isotope replacement and site-directed mutagenesis, *J Biol Chem. 269*, 5085-5091.

29. Tsai, A. L., Kulmacz, R. J. & Palmer, G. (1995) Spectroscopic Evidence for Reaction of Prostaglandin H Synthase-1 Tyrosyl Radical with Arachdionic Acid, *J Biol Chem. 270*, 10503-10508.

30. Wu, G., Wei, C. H., Kulmacz, R. J., Osawa, Y. & Tsai, A. L. (1999) A mechanistic study of self-inactivation of the peroxidase activity in prostaglandin H synthase-1, *J Biol Chem. 274*, 9231-9237.

31. Smith, W. L. & Lands, W. E. M. (1972) Oxygenation of Polyunsaturated Fatty-Acids during Prostaglandin Biosynthesis by Sheep Vesicular Gland, *Biochemistry. 11*, 3276-&.

32. Hemler, M. E. & Lands, W. E. M. (1980) Evidence for a Peroxide-Initiated Free-Radical Mechanism of Prostaglandin Biosynthesis, *J Biol Chem. 255*, 6253-6261.

33. Markey, C. M., Alward, A., Weller, P. E. & Marnett, L. J. (1987) Quantitative Studies of Hydroperoxide Reduction by Prostaglandin-H Synthase - Reducing Substrate-Specificity and the Relationship of Peroxidase to Cyclooxygenase Activities, *J Biol Chem. 262*, 6266-6279.

34. Marshall, P. J. & Kulmacz, R. J. (1988) Prostaglandin H synthase: distinct binding sites for cyclooxygenase and peroxidase substrates, *Arch Biochem Biophys. 266*, 162-170.

35. Song, I., Ball, T. M. & Smith, W. L. (2001) Different Suicide Inactivation Processes for the Peroxidase and Cyclooxygenase Activities of Prostaglandin Endoperoxide H Synthase-1, *Biochem Biophys Res Commun. 289*, 869-875.

36. Garavito, R. M., Malkowski, M. G. & DeWitt, D. L. (2002) The structures of prostaglandin endoperoxide H synthases-1 and -2, *Prostaglandins Other Lipid Mediat. 68-69*, 129-152.

37. Otto, J. C., DeWitt, D. L. & Smith, W. L. (1993) N-glycosylation of prostaglandin endoperoxide synthases-1 and -2 and their orientations in the endoplasmic reticulum, *J Biol Chem. 268*, 18234-18242.

38. Barnett, J., Chow, J., Ives, D., Chiou, M., Mackenzie, R., Osen, E. & al., e. (1994) Purification, characterization and selective inhibition of human prostaglandin G/H synthase 1 and and expressed in the bacuolvirus system, *Biochim Biophys Acta. 1209*, 130-139.

39. Picot, D., Loll, P. J. & Garavito, R. M. (1994) The X-Ray Crystal-Structure of the Membrane-Protein Prostaglandin-H(2) Synthase-1, *Nature. 367*, 243-249.

40. Luong, C., Miller, A., Barnett, J., Chow, J., Ramesha, C. & Browner, M. F. (1996) Flexibility of the NSAID binding site in the structure of human cyclooxygenase-2, *Nature Struct Biol. 3*, 927-933.

41. Kurumbail, R. G., Stevens, A. M., Gierse, J. K., McDonald, J. J., Stegeman, R. A., Pak, J. Y., Gildehaus, D., Miyashiro, J. M., Penning, T. D., Seibert, K., Isakson, P. C. & Stallings, W. C. (1996) Structural basis for selective inhibition of cyclooxygenase-2 by anti-inflammatory agents, *Nature. 384*, 644-648.

42. Malkowski, M. G., Ginell, S. L., Smith, W. L. & Garavito, R. M. (2000) The productive conformation of arachidonic acid bound to prostaglandin synthase, *Science. 289*, 1933-1937.

43. Spencer, A. G., Woods, J. W., Arakawa, T., Singer, I. I. & Smith, W. L. (1998) Subcellular localization of prostaglandin endoperoxide H synthases-1 and -2 by immunoelectron microscopy, *J Biol Chem. 273*, 9886-9893.

44. McGeer, P. L. & McGeer, E. G. (1999) Inflammation of the brain in Alzheimer's diease: implications for therapy, *J Leuko Biol. 65*, 409-415.

45. Patrignani, P. & al., e. (1994) Biochemical and pharmacological characterization of the cylcooxygenase activity of human blood prostaglandin endoperoxide synthases, *J Pharmacol Exp. Ther. 271*, 1705-1712.

46. Patrono, C. (1994) Aspirin as an antiplatelet drug, *New Engl J Med. 330*, 1287-1294.

47. Shitashige, M., Morita, I. & Murota, S. (1998) Different substrate utilization between prostaglandin endoperoxide H synthase-1 and -2 in NIH3T3 fibroblasts, *Biochim Biophys Acta. 1389*, 57-66.

48. Chen, W., Pawelek, T. R. & Kulmacz, R. J. (1999) Hydroperoxide dependence and cooperative cyclooxygenase kinetics in prostaglandin H synthase-1 and-2, *J Biol Chem. 274*, 20301-20306.

49. Malkowski, M. G., Thuresson, E. D., Lakkides, K. M., Rieke, C. J., Micielli, R., Smith, W. L. & Garavito, R. M. (2001) Structure of Eicosapentaenoic and Linoleic Acids in the Cyclooxygenase Site of Prostaglandin Endoperoxide H Synthase-1, *J Biol Chem. 276*, 37547-37555.

50. Thuresson, E. D., Malkowski, M. G., Lakkides, K. M., Rieke, C. J., Mulichak, A. M., Ginell, S. L., Garavito, R. M. & Smith, W. L. (2001) Mutational and X-ray crystallographic analysis of the interaction of dihomo-gamma -linolenic acid with prostaglandin endoperoxide H synthases, *J Biol Chem. 276*, 10358-10365.

51. Gund, P. & Shen, T. Y. (1977) Model for Prostaglandin Synthetase Cyclo-Oxygenation Site and Its Inhibition by Antiinflammatory Arylacetic Acids, *J Med Chem. 20*, 1146-1152.

52. Thuresson, E. D., Lakkides, K. M. & Smith, W. L. (2000) Different catalytically competent arrangements of arachidonic acid within the cyclooxygenase active site of prostaglandin endoperoxide H synthase-1 lead to the formation of different oxygenated products, *J Biol Chem. 275*, 8501-8507.

53. Thuresson, E. D., Lakkides, K. M., Rieke, C. J., Sun, Y., Wingerd, B. A., Micielli, R., Mulichak, A. M., Malkowski, M. G., Garavito, R. M. & Smith, W. L. (2001) Prostaglandin endoperoxide H synthase-1: the functions of cyclooxygenase active site residues in the binding, positioning, and oxygenation of arachidonic acid, *J Biol Chem. 276*, 10347-10357.

54. Willis, A. L. (1987) in *CRC Handbook of Eicosanoids: Prostaglandins and Related Lipids* (Willis, A. L., ed) pp. 3-46, CRC Press, Inc., Boca Raton, FL.

55. Lands, W. E. M. & Samuelsson, B. (1968) Phospholipid Precursors of Prostaglandins, *Biochim Biophys Acta. 164*, 426-&.

56. Laneuville, O., Breuer, D. K., Xu, N. X., Huang, Z. H., Gage, D. A., Watson, J. T., Lagarde, M., Dewitt, D. L. & Smith, W. L. (1995) Fatty-Acid Substrate Specificities of Human Prostaglandin Endoperoxide-H Synthase-1 and Synthase-2 - Formation of 12-Hydroxy-(9Z,13E/Z,15Z)-Octadecatrienoic Acids from Alpha-Linolenic Acid, *J Biol Chem. 270*, 19330-19336.

57. Larsen, L. N., Dahl, E. & Bremer, J. (1996) Peroxidative oxidation of leuco-dichlorofluorescein by prostaglandin H synthase in prostaglandin biosynthesis from polyunsaturated fatty acids, *Biochim Biophys Acta-Lipids Lipid Meta. 1299*, 47-53.

58. Oliw, E. H., Hornsten, L., Sprecher, H. & Hamberg, M. (1993) Oxygenation of 5,8,11-Eicosatrienoic Acid by Prostaglandin Endoperoxide Synthase and by Cytochrome-P450 Monooxygenase - Structure and Mechanism of Formation of Major Metabolites, *Arch Biochem Biophys. 305*, 288-297.

59. Needleman, P., Whitaker, M. O., Wyche, A., Watters, K., Sprecher, H. & Raz, A. (1980) Manipulation of Platelet-Aggregation by Prostaglandins and Their Fatty-Acid Precursors - Pharmacological Basis for a Therapeutic Approach, *Prostaglandins. 19*, 165-181.

60. Knapp, H. R. (1990) Prostaglandins in Human Semen during Fish Oil Ingestion - Evidence for Invivo Cyclooxygenase Inhibition and Appearance of Novel Trienoic Compounds, *Prostaglandins. 39*, 407-423.

61. Kaduce, T. L., Figard, P. H., Leifur, R. & Spector, A. A. (1989) Formation of 9-Hydroxyoctadecadienoic Acid from Linoleic-Acid in Endothelial-Cells, *J Biol Chem. 264*, 6823-6830.

62. Lands, W. E. M., LeTellier, P. R., Rome, L. H. & Vanderhoek, J. Y. (1973) Inhibition of prostaglandin biosynthesis, *Adv Biosci. 9*, 15-28.

63. Kozak, K. R., Rowlinson, S. W. & Marnett, L. J. (2000) Oxygenation of the endocannabinoid, 2-arachidonylglycerol, to glyceryl prostaglandins by cyclooxygenase-2, *J Biol Chem. 275*, 33744-33749.

64. Kozak, K. R., Crews, B. C., Ray, J. L., Tai, H., Morrow, J. D. & Marnett, L. J. (2001) Metabolism of Prostaglandin Gycerol Esters and Prostaglandin Ethanolamides in Vitro and in Vivo, *J Biol Chem. 276*, 36993-36998.

65. Kozak, K. R., Crews, B. C., Morrow, J. D., Wang, L. H., Ma, Y. H., Weinander, R., Jakobsson, P. J. & Marnett, L. J. (2002) Metabolism of the Endocannabinoids, 2-Arachidonlyglycerol and Anandamide, into Prostaglandin, Thromboxane, and Prostacyclin Glycerol Esters and Ethanolamides, *J Biol Chem. 277*, 44877-44885.

66. Rome, L. H. & Lands, W. E. M. (1975) Structural requirements for time-dependent inhibition of prostaglandin biosynthesis by anti-inflammatory drugs, *Proc Natl Acad Sci USA. 72*, 4863-4865.

67. Bhattacharyya, D. K., Lecomte, M., Rieke, C. J., Garavito, R. M. & Smith, W. L. (1996) Involvement of arginine 120, glutamate 524, and tyrosine 355 in the binding of arachidonate and 2-phenylpropionic acid inhibitors to the cyclooxygenase active site of ovine prostaglandin endoperoxide H synthase-1, *J. Biol. Chem. 271*, 2179-2184.

68. Rieke, C. J., Mulichak, A. M., Garavito, R. M. & Smith, W. L. (1999) The role of arginine 120 of human prostaglandin endoperoxide H synthase-2 in the interaction with fatty acid substrates and inhibitors, *J Biol Chem. 274*, 17109-17114.

69. O'Neill, G. P., Mancini, J. A., Kargman, S., Yergey, J., Kwan, M. Y., Falgueyret, J.-P., Abramovitz, M., Kennedy, B. P., Ouellet, M., Cromlish, W., Culp, S., Evans, J. F., Ford-Hutchinson, A. W. & Vickers, P. J. (1993) Overexpression of Human Prostaglandin G/H Synthase-1 and -2 by Recombinant Vaccinia Virus: Inhibition by Nonsteroidal Anit-Inflammatory Drugs and Biosythesis of 15-Hydroxyeicosatraenoic acid, *Mol Pharm. 45*, 245-254.

70. Lecomte, M., Laneuville, O., Ji, C., DeWitt, D. L. & Smith, W. L. (1994) Acetylation of human prostaglandin endoperoxide synthase-2 (cyclooxygenase-2) by aspirin, *J Biol Chem. 269*, 13207-13215.

71. Dewitt, D. L. (1999) Cox-2-selective inhibitors: The new super aspirins, *Mol Pharm. 55*, 625-631.

72. Gierse, J. K., McDonald, J. J., Hauser, S. D., Rangwala, S. H., Koboldt, C. M. & Seibert, K. (1996) A single amino acid difference between cyclooxygenase-1 (COX-1) and -2 (COX-2) reverses the selectivitiy of COX-2 specific inhibitors, *J Biol Chem. 271*, 15810-15814.

73. Marnett, L. J. & DuBois, R. N. (2002) COX-2: a target for colon cancer prevention, *Annu Rev Pharmacol Toxicol. 42*, 55-80.

74. van der Donk, W. A., Tsai, A.-L. & Kulmacz, R. J. (2002) The cyclooxygenase reaction mechanism, *Biochemistry. 41*, 15451-15458.

75. Garavito, R. M. & Mulichak, A. M. (2003) The structure of mammalian cyclooxygenases, *Ann Rev Biophys Biomol Struct. 32*, 183-206.

76. Schneider, C., Boeglin, W. E., Prusakiewicz, J. J., Rowlinson, S. W., Marnett, L. J., Samel, N. & Brash, A. R. (2002) Control of prostaglandin stereochemistry at the 15-carbon by cyclooxygenases-1 and -2. A critical role for serine 530 and valine 349, *J Biol Chem. 277*, 13354-13360.

77. Spencer, A. G., Thuresson, E. A., Otto, J. C., Song, I., Smith, T., DeWitt, D. L., Garavito, R. M. & Smith, W. L. (1999) The membrane binding domains of prostaglandin endoperoxide H synthase-1 and -2: Peptide mapping and mutational analysis, *J Biol Chem. 274*, 32936-32942.

78. Malkowski, M. G., Theisen, M. J., Scharmen, A. & Garavito, R. M. (2000) The formation of stable fatty acid substrate complexes in prostaglandin H-2 synthase-1, *Arch Biochem Biophys. 380*, 39-45.

79. Otwinowski, Z. & Minor, W. (1997) Processing of X-ray diffraction data collected in oscillation mode, *Macromol Crystallogr, Pt A. 276*, 307-326.

80. Brunger, A. T., Adams, P. D., Clore, G. M., DeLano, W. L., Gros, P., Grosse Kunstleve, R. W., Jiang, J. S., Kuszewski, J., Nilges, M., Pannu, N. S., Read, R. J., Rice, L. M., Simonson, T. & Warren, G. L. (1998) Crystallography & NMR system: A new software suite for macromolecular structure determination, *Acta Crystallogr D. 54*, 905-921.

81. Sack, J. S. (1988) Chain – A Crystallographic Modeling Program, *J Mol Graphics. 6*, 224-225.

82. Laskowski, R. A., MacArthur, M. W., Moss, D. S. & Thornton, J. M. (1993) PROCHECK: a program to check the stereochemical quality of protein structures, *J Appl Cryst. 26*, 283-291.

83. Evans, S. V. (1993) SETOR: hardware-lighted three-dimensional solid model representations of macromolecules, *J Mol Graphics. 11*, 134-138.

84. Mead, J. F. & Slaton, W. H. (1956) Metabolism of Essential Fatty Acids.3. Isolation of 5,8,11-Eicosatrienoic Acid from Fat-Deficient Rats, *J Biol Chem. 219*, 705-709.

85. Lefkowith, J. B., Flippo, V., Sprecher, H. & Needleman, P. (1985) Paradoxical Conservation of Cardiac and Renal Arachidonate Content in Essential Fatty-Acid Deficiency, *J Biol Chem. 260*, 5736-5744.

86. Cox, J. W., Rutecki, G. W., Francisco, L. L. & Ferris, T. F. (1982) Studies of the Effects of Essential Fatty-Acid Deficiency in the Rat, *Cir Res. 51*, 694-702.

87. Bonta, I. L., Chrispij, H., Noordhoe, J. & Vincent, J. E. (1974) Reduction of Prostaglandin-Phase in Hind-Paw Inflammation and Partial Failure of Indomethacin to Exert Antiinflammatory Effect in Rats on Essential Fatty-Acid Deficient Diet, *Prostaglandins. 5*, 495-503.

88. Burr, G. O. & Burr, M. M. (1930) On the nature and role of the fatty acids essential in nutrition, *J Biol Chem. 86*, 587-621.

89. Elliott, W. J., Morrison, A. R., Sprecher, H. & Needleman, P. (1986) Calcium-Dependent Oxidation of 5,8,11-Icosatrienoic Acid by the Cyclooxygenase Enzyme-System, *J Biol Chem. 261*, 6719-6724.

90. Oliw, E. H., Hornsten, L. & Sprecher, H. (1997) Oxygenation of 5,8,11-eicosatrienoic acid by prostaglandin H synthase-2 of ovine placental cotyledons: Isolation of 13-hydroxy-5,8,11-eicosatrienoic and 11-hydroxy-5,8,12-eicosatrienoic acids, *J Chromatogr B. 690*, 332-337.

91. Adkisson, H. D., Risener, F. S., Zarrinkar, P. P., Walla, M. D., Christie, W. W. & Wuthier, R. E. (1991) Unique Fatty-Acid Composition of Normal Cartilage - Discovery of High-Levels of N-9 Eicosatrienoic Acid and Low-Levels of N-6 Polyunsaturated Fatty-Acids, *FASEB J. 5*, 344-353.

92. Nugteren, D. H. & Christhazelhof, E. (1987) Naturally-Occurring Conjugated Octadecatrienoic Acids Are Strong Inhibitors of Prostaglandin Biosynthesis, *Prostaglandins. 33*, 403-417.

93. Hammarstrom, S. (1981) Conversion of 5,8,11-Eicosatrienoic Acid to Leukotriene-C3 and Leukotriene-D3, *J Biol Chem. 256*, 2275-2279.

94. Lagarde, M., Burtin, M., Rigaud, M., Sprecher, H., Dechavanne, M. & Renaud, S. (1985) Prostaglandin-E2-Like Activity of 20-3N-9 Platelet Lipoxygenase End-Product, *FEBS Lett. 181*, 53-56.

95. Porter, N. A., Caldwell, S. E. & Mills, K. A. (1995) Mechanisms of Free-Radical Oxidation of Unsaturated Lipids, *Lipids. 30*, 277-290.

96. Kapust, R. B., Tozser, J., Fox, D., Anderson, D. E., Cherry, S., Copeland, T. D. & Waugh, D. S. (2001) Tobacco etch virus protease: mechanism of autolysis and rational design of stable mutants with wild-type catalytic proficiency, *Protein Eng. 14*, 993-1000.

97. Kozak, K. R., Prusakiewicz, J. J., Rowlinson, S. W. & Marnett, L. J. (2002) Enantiospecific, selective cyclooxygenase-2 inhibitors, *Bioorg Med Chem Lett. 12*, 1315-1318.

98. Garavito, R. M. & DeWitt, D. L. (1999) The cyclooxygenase isoforms: structural insights into the conversion of arachidonic acid to prostaglandins, *Biochim Biophys Acta. 1441*, 278-287.

99. Walker, M. C., Kurumbail, R. G., Kiefer, J. R., Moreland, K. T., Koboldt, C. M., Isakson, P. C., Seibert, K. & Gierse, J. K. (2001) A three-step kinetic mechanism for selective inhibition of cyclo-oxygenase-2 by diarylheterocyclic inhibitors, *Biochem J. 357*, 709-718.

100. Gierse, J. K., Koboldt, C. M., Walker, M. C., Seibert, K. & Isakson, P. C. (1999) Kinetic basis for selective inhibition of cyclo-oxygenases, *Biochem J. 339*, 607-614.

101. Loll, P. J., Picot, D., Ekabo, O. & Garavito, R. M. (1996) Synthesis and use of iodinated nonsteroidal antiinflammatory drug analogs as crystallographic probes of the prostaglandin H-2 synthase cyclooxygenase active site, *Biochemistry. 35*, 7330-7340.

102. Kalgutkar, A. S., Crews, B. C., Rowlinson, S. W., Marnett, A. B., Kozak, K. R., Remmel, R. P. & Marnett, L. J. (2000) Biochemically based design of cyclooxygenase-2 (COX-2) inhibitors: Facile conversion of nonsteroidal antiinflammatory drugs to potent and highly selective COX-2 inhibitors, *Proc Natl Acad Sci USA. 97*, 925-930.

103. 4, C. C. P. N. (1994) The CCP4 Suite: Programs for Protein Crystallography, *Acta Crystallogr D. 50*, 760-763.

104. Winn, M. D., Isupov, M. N. & Murshudov, G. N. (2001) Use of TLS parameters to make ansiotropic displacments in macromolecular refinement, *Acta Crystallogr. D. 57*, 122-133.

105. Winn, M. D., Murshudov, G. N. & Papiz, M. Z. (2003) Macromolecular TLS Refinement in REFMAC at Moderate Resolutions, *Methods in Enzymol. 374*, 300-321.

106. Garavito, R. M. (2001) Prostaglandin endoperoxide H synthase-1 and -2 in *Handbook of Metalloproteins* (K. Wieghardt, R. H., T. L. Poulos, and A. Messerschmidt, ed) pp. 245-63, John Wiley, Sussex.

107. Seibold, S. A., Smith, W. L. & Cukier, R. I. (2004) Peroxidase site of prostaglandin endoperoxide H synthase-1: Docking and molecular dynamics studies with a prostaglandin endoperoxide analog, *J Phys Chem B. 108*, 9297-9305.

108. Seibold, S. A., Ball, T., Hsi, L. C., Mills, D. A., Abeysinghe, R. D., Micielli, R., Rieke, C. J., Cukier, R. I. & Smith, W. L. (2003) Histidine 386 and its role in cyclooxygenase and peroxidase catalysis by prostaglandin-endoperoxide H synthases, *J Biol Chem. 278*, 46163-46170.

109. Kulmacz, R. J. (1989) Topography of Prostaglandin-H Synthase - Antiinflammatory Agents and the Protease-Sensitive Arginine-253 Region, *J Biol Chem. 264*, 14136-14144.

110. Chen, Y. N., Bienkowski, M. J. & Marnett, L. J. (1987) Controlled Tryptic Digestion of Prostaglandin H-Synthase - Characterization of Protein-Fragments and Enhanced Rate of Proteolysis of Oxidatively Inactivated Enzyme, *J Biol Chem. 262*, 16892-16899.

111. Kalgutkar, A. S., Crews, B. C. & Marnett, L. J. (1996) Kinetics of the interaction of nonsteroidal antiinflammatory drugs with prostaglandin endoperoxide synthase-1 studied by limited proteolysis, *Biochemistry. 35*, 9076-9082.

112. Moth, C. W., Prusakiewicz, J. J., Marnett, L. J. & Lybrand, T. P. (2005) Stereoselective Binding of Indomethacin Ethanolamides Derivatives to Cyclooxygenase-1, *J Med Chem. 48*, 3613-3620.

113. Xiao, G., Tsai, A. L., Palmer, G., Boyar, W. C., Marshall, P. J. & Kulmacz, R. J. (1997) Analysis of Hydroperoxide-Induced Tyrosyl Radicals and Lipoxygenase Activity in Aspirin-Treated Human Prostaglandin H Synthase-2, *Biochemistry. 36*, 1836-1846.

114. Mancini, J. A., Oneill, G. P., Bayly, C. & Vickers, P. J. (1994) Mutation of Serine-516 in Human Prostaglandin G/H Synthase-2 to Methionine or Aspirin Acetylation of This Residue Stimulates 15-R-HETE Synthesis, *FEBS Lett. 342*, 33-37.

115. Rowlinson, S. W., Crews, B. C., Lanzo, C. A. & Marnett, L. J. (1999) The binding of arachidonic acid in the cyclooxygenase active site of mouse prostaglandin endoperoxide synthase-2 (COX-2) - A putative L-shaped binding conformation utilizing the top channel region, *J Biol Chem. 274*, 23305-23310.

116. Kiefer, J. R., Pawlitz, J. L., Moreland, K. T., Stegeman, R. A., Hood, W. F., Gierse, J. K., Stevens, A. M., Goodwin, D. C., Rowlinson, S. W., Marnett, L. J., Stallings, W. C. & Kurumbail, R. G. (2000) Structural insights into the stereochemistry of the cyclooxygenase reaction, *Nature. 405*, 97-101.

117. Kurumbail, R. G., Kiefer, J. R. & Marnett, L. J. (2001) Cyclooxygenase enzyme: catalysis and inhibition, *Curr Opin Struct Biol. 11*, 752-760.

118. Marco, S. D., Priestle, J. P., Grutter, M. G., Wennogle, L. P. & Boyar, W. (1997) Characterization, crystallization and preliminary crystallographic analysis of human recombinant cyclooxygenase-2, *Acta Crystallogr D. 53*, 224-226.